BioMed Research International

Biotechnology and Green Chemistry

Guest Editors: Bernardo Dias Ribeiro, Isabel Marrucho, Luciana Gonçalves, and Maria Alice Z. Coelho

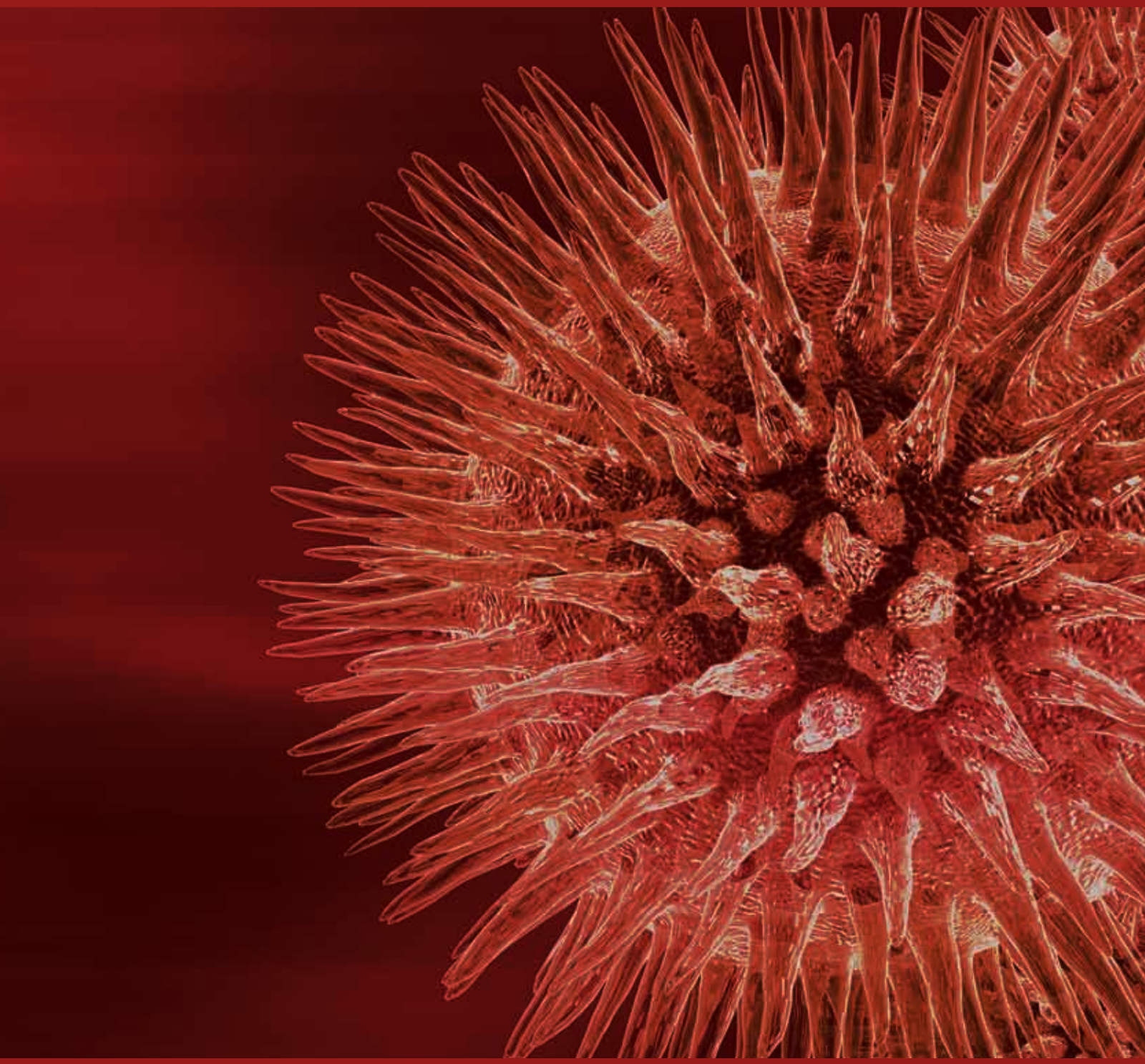

Biotechnology and Green Chemistry

BioMed Research International

Biotechnology and Green Chemistry

Guest Editors: Bernardo Dias Ribeiro, Isabel Marrucho, Luciana Gonalves, and Maria Alice Z. Coelho

Contents

Hindawi Publishing Corporation
BioMed Research International
Volume 2014, Article ID 590586, 2 pages
http://dx.doi.org/10.1155/2014/590586

Editorial
Biotechnology and Green Chemistry

Bernardo Dias Ribeiro,[1] Isabel Marrucho,[2] Luciana Gonçalves,[3] and Maria Alice Z. Coelho[1]

[1] *Escola de Química, Universidade Federal Rio de Janeiro, 21941-902 Rio de Janeiro, RJ, Brazil*
[2] *Instituto de Tecnologia Química e Biológica, Universidade Nova de Lisboa, 2780-157 Oeiras, Portugal*
[3] *Departamento de Engenharia Química, Universidade Federal do Ceará, 60455-760 Fortaleza, CE, Brazil*

Correspondence should be addressed to Maria Alice Z. Coelho; alice@eq.ufrj.br

Received 5 January 2014; Accepted 5 January 2014; Published 12 March 2014

White biotechnology can be regarded as applied biocatalysis, with enzymes and microorganisms, aiming at industrial production of bulk and fine chemicals to food and animal feed additives. In its turn biocatalysis has many attractive features in the context of greenchemistry: mild reaction conditions (physiological pH and temperature); environmentally compatible catalysts and solvent (often water) combined with high activities; and chemo-, regio-, and stereoselectivities in multifunctional molecules. This affords processes which are shorter, generate less waste, and are, therefore, both environmentally and economically more attractive than conventional routes.

This special issue includes aspects involving the use of white biotechnology (enzymes, microorganisms, and plant tissues) within the green chemistry concept, concerning the use of alternative solvents (supercritical fluids, pressurized gases, ionic liquids, and micellar systems) and energies (microwaves and ultrasound); sustainable approaches for production of fine and bulk chemicals (aromas, polymers, pharmaceuticals, and enzymes); use of renewable resources or agroindustrial residues; biocatalysts recycling; and waste minimization.

This special issue contains six papers, where three are related to green synthesis of nanoparticles and one paper covers biological pretreatment for enzymatic hydrolysis and bioethanol production. Two papers regard the use of alternative reaction systems. In the first paper entitled *"Green synthesis of silver nanoparticles using Pinus eldarica bark extract,"* S. Iravani and B. Zolfaghari present the optimization of the biosynthesis production of silver nanoparticles through the evaluation of *Pinus eldarica* bark extract quantity, substrate concentration, temperature, and pH on the formation of such material. The preparation of nanostructured silver particles using *P. eldarica* bark extract provides an environmentally friendly option, as compared to currently available chemical and/or physical methods.

The second paper, *"Green and rapid synthesis of anticancerous silver nanoparticles by Saccharomyces boulardii and insight into mechanism of nanoparticle synthesis,"* by A. Kaler et al. describes an ecofriendly method for the synthesis of silver nanoparticles (AgNPs) by cell free extract (CFE) of *Saccharomyces boulardii*. In addition to the optimization of relevant synthesis parameters as culture age, cell mass concentration, temperature, and reaction time, the paper presents particles characterization by UV-Visible spectroscopy, EDX (energy dispersive X-Rays) analysis, transmission electron microscopy, and zeta potential, as well as the elucidation of proteins/peptides role in nanoparticles formation and stability and their anticancer activity. The method therein described a method that does not require tedious downstream processing and it may be scaled up to develop a viable technology for the Ag-nanoparticle synthesis.

In the third paper, *"Biosynthesis, antimicrobial and cytotoxic effect of silver nanoparticles using a novel Nocardiopsis sp. MBRC-1,"* P. Manivasagan et al. present another green approach for biosynthesis of nanoparticles using the culture supernatant of *Nocardiopsis* sp. MBRC-1 to achieve the reduction of silver ions from a silver nitrate solution. The obtained nanoparticles were characterized by UV-visible, TEM, FE-SEM, EDX, FTIR, and XRD spectroscopy. The prepared silver nanoparticles exhibited strong antimicrobial activity against bacteria and fungi. Cytotoxicity of biosynthesized AgNPs

against *in vitro* human cervical cancer cell line (HeLa) showed a dose-response activity.

In the fourth paper, *"Biological pretreatment of rubberwood with Ceriporiopsis subvermispora for Enzymatic hydrolysis and bioethanol production,"* F. Nazarpour et al. investigate a novel feedstock for enzymatic hydrolysis and bioethanol production using biological pretreatment: rubberwood (*Hevea brasiliensis*). To improve ethanol production, rubberwood was pretreated with white rot fungus *Ceriporiopsis subvermispora* to increase fermentation efficiency. The fungal pretreatment provides a cost-effective method for reducing the recalcitrance of rubberwood with high selectivity of lignin degradation rate and minimal cellulose loss for enzymatic hydrolysis and bioethanol production.

In the fifth paper, the research of G. D. Yadav and S. Devendran entitled *"Microwave assisted enzymatic kinetic resolution of (±)-1-phenyl-2-propyn-1-ol in non-aqueous media,"* proposes a kinetic resolution of 1-phenyl-2-propyn-1-ol, an important chiral synthon, through esterification with acyl acetate. The authors investigate synergism between microwave irradiation and enzyme catalysis. The lipase (Novozym 435) catalyzed kinetic resolution under microwave irradiation. The maximum conversion of 48.78% was obtained in 2 h using 10 mg enzyme loading with equimolar concentration of alcohol and ester at 60°C under microwave irradiation. From the progress curve analysis, it was found that reaction followed the ping-pong bi-bi mechanism with dead end inhibition of alcohol. Beside the previous papers herein described, the preparation of chiral secondary alcohols using lipase catalyzed kinetic resolution is mild and clean as compared to chemical process.

In the seventh paper entitled *"Demonstration of redox potential of Metschnikowia koreensis for stereoinversion of secondary alcohols/1,2-diols,"* by V. S. Meena et al. reports the *Metschnikowia koreensis*-catalyzed one-pot deracemization of secondary alcohols/1,2-diols and their derivatives with *in vivo* cofactor regeneration. This ecofriendly method afforded the product in high yield (88%) and excellent optical purity (>98% ee), minimizing the requirement of multistep reaction and expensive cofactor.

Bernardo Dias Ribeiro
Isabel Marrucho
Luciana Gonçalves
Maria Alice Z. Coelho

Hindawi Publishing Corporation
BioMed Research International
Volume 2014, Article ID 482678, 9 pages
http://dx.doi.org/10.1155/2014/482678

Research Article

Microwave Assisted Enzymatic Kinetic Resolution of (±)-1-Phenyl-2-propyn-1-ol in Nonaqueous Media

Saravanan Devendran and Ganapati D. Yadav

Department of Chemical Engineering, Institute of Chemical Technology, Matunga, Mumbai 400 019, India

Correspondence should be addressed to Ganapati D. Yadav; gdyadav@yahoo.com

Received 12 April 2013; Revised 20 October 2013; Accepted 2 December 2013; Published 23 February 2014

Academic Editor: Luciana Rocha Barros Gonçalves

Kinetic resolution of 1-phenyl-2-propyn-1-ol, an important chiral synthon, was studied through trans-esterification with acyl acetate to investigate synergism between microwave irradiation and enzyme catalysis. Lipases from different microbial origins were employed for the kinetic resolution of (R/S)-1-phenyl-2-propyn-1-ol, among which *Candida antarctica* lipase B, immobilized on acrylic resin (Novozym 435), was found to be the best catalyst in *n*-hexane as solvent. Vinyl acetate was the most effective among different acyl esters studied. The effect of various parameters was studied in a systematic manner. Definite synergism between microwave and enzyme was observed. The initial rate was improved around 1.28 times under microwave irradiation than conventional heating. Under optimum conditions, maximum conversion (48.78%) and high enantiomeric excess (93.25%) were obtained in 2 h. From modeling studies, it is concluded that the reaction follows the Ping-Pong bi-bi mechanism with dead end alcohol inhibition. Kinetic parameters were obtained by using nonlinear regression. This process is green, clean, and easily scalable as compared to the chemical process.

1. Introduction

Enantiomeric pure chemicals are needed for synthesis of optically active compounds that have significant market values across a variety of industries [1], among which chiral secondary alcohols have several applications in pharmaceutical and chemical industries, such as chiral auxiliaries, and they can be easily derivatized with different functional groups [2]. In comparison with classical chemical methods such as preferential crystallization, diastereomerization, chromatographic separation, and asymmetric reduction by chiral metal oxides, biocatalytic processes are broadly accepted as good options to prepare optically pure secondary alcohols [3]. Biocatalysts score over chemical processes because they often possess high stereo-, chemo-, and regio-selectivity. Biocatalytic systems can be operated at mild operating conditions that reduce byproduct formations and are recyclable and easily adoptable in nonaqueous and neoteric solvents. Biocatalytic processes are reported as simple and cost effective for the synthesis of single enantiomeric compounds. However, the major drawback of these processes is the fact that they are slow in nature and need to be intensified in order to meet industrial requirements [4–6].

Among various biocatalytic paths, lipase catalyzed kinetic resolution of racemic mixtures have been favored for preparing the optically active secondary alcohols through hydrolysis and transesterification reactions. Lipases have inherent ability to accept a broad range of substances and do not require expensive cofactors like NAD(P)H. Lipases are readily available from animal, plant, and microbial sources and remain active in both organic and neoteric solvents like ionic liquids and supercritical carbon dioxide ($scCO_2$). However, alcohol dehydrogenases catalyzed asymmetric reduction requires expensive cofactors for its catalytic activity and is also less adoptable to nonaqueous media [7, 8].

In recent years, microwave irradiation, a green and clean alternative energy source, has been employed to enhance the reaction rates and selectivities for organic synthesis as well as materials production [9, 10]. In the conventional heating, the rate of heat transfer from external heating source to reaction system depends on the thermal conductivity of reaction vessel, which might lead to higher temperature at

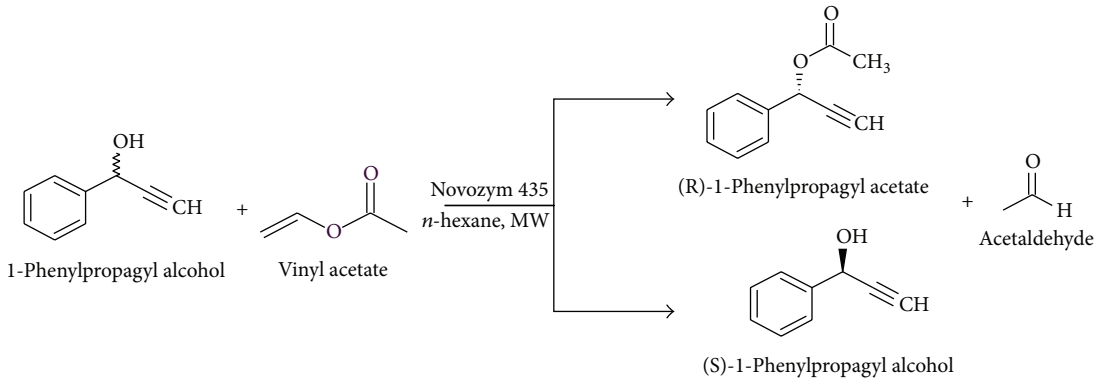

Scheme 1: Lipase catalysed transesterification of (R/S)-1-phenylpropagyl alcohol with vinyl acetate under microwave irradiation.

vessel surface than the reaction mixture. Hence, it requires longer equilibrium time and is difficult to control. On the contrary, microwave irradiation results in efficient internal heating by direct coupling of microwave energy with polar molecules such as solvents, reagents, or catalysts in the vessel. Microwaves pass through the wall of reactor and are converted into heat directly in bulk mass of material in the vessel. It is irrespective of the thermal conductivity of vessel material. The temperature gradient observed in microwave heating is exactly opposite to that in conventional heating. Thus, it reduces the reaction time [11]. The synergism with microwave irradiation is found to enhance the reaction rate in enzymatic reactions [12]. The rate of lipase catalyzed reaction is enhanced to several folds as compared to conventional heating and the lipase is quite stable under microwave irradiation [13, 14].

Optically active 1-phenyl-2-propyn-1-o1 and its substituted derivatives are important precursors for synthesis of enantiomeric pure natural compounds and biologically active molecules such as eicosanoids and macrolides antibiotics [15]. They can also be used as starting materials for stereoselective synthesis of polyhydroxylated compounds, allenes, benzo[*b*]furan (1-benzofuran), and derivatives [16, 17]. There are a few studies reported on the synthesis of the single enantiomer of 1-phenyl-2-propyn-1-o1 by asymmetric hydrolysis by using microbes, asymmetric chemical catalysis, or lipase catalyzed kinetic resolution under conventional heating [18–23]. All these processes require either longer reaction time or high enzyme loading and there is no information on kinetics of the reaction, which is required for reactor design and scale-up. In the current work, microwave assisted lipase catalyzed transesterification of (R/S)-1-phenyl-2-propyn-1-o1 was undertaken with vinyl acetate in nonaqueous media (Scheme 1). The effect of various parameters such as different commercially available immobilized lipases, acyl donors, solvents, agitation speed, temperature, catalyst loading, and acyl donor concentration was studied systematically by varying one parameter at a time. Finally, the mechanism was proposed and kinetics were developed. All results are novel and useful to scale up this process.

2. Materials and Methods

2.1. Enzymes. The following enzymes were received as gift samples from M/s Novozymes A/S (Bagsvaerd, Denmark): (i) Novozym 435: Lipase B from *Candida antarctica*, supported on a macroporous acrylic resin with a water content of 1-2% (w/w) and enzyme activity 10,000 PLU/g, (ii) Lipozyme RM-IM: Lipase from *Rhizomucor miehei*, supported on a macroporous anion exchange resin with a water content of 2-3% (w/w) and enzyme activity 6 BAU/g, and (iii) Lipozyme TL IM: Lipase from *Thermomyces lanuginosus*, supported on porous silica granulates with water content 1-2% and enzyme activity 175 IU/g.

2.2. Chemicals. Hexane, toluene, cyclohexane, isopropyl ether, vinyl acetate, and other analytical and HPLC grade reagents were purchased from M/s S.D. Fine Chemicals Pvt. Ltd., Mumbai, India. (±)-1-Phenyl-2-propyn-1-ol, vinyl butyrate and vinyl laurate were purchased from Sigma-Aldrich India Pvt. Ltd., Bangalore, India. All chemicals and enzymes were used without any further modification/purification.

2.3. General Experimental Setup

2.3.1. Conventional Heating. The experimental setup consisted of a 3 cm i.d. mechanically agitated glass reactor of 50 cm^3 capacity, equipped with four baffles and a six-bladed turbine impeller. The entire reactor assembly was immersed in a thermostatic water bath, which was maintained at a predetermined temperature with an accuracy of ±1°C. A typical reaction mixture consisted of 0.001 mol racemic alcohol and 0.001 mol vinyl ester diluted to 15 cm^3 with *n*-hexane as a solvent. The reaction mass was agitated at 60°C for 15 min at a speed of 300 rpm and then 10 mg of enzyme was added to initiate the reaction.

2.3.2. Microwave Heating. The studies were carried out in a commercial microwave reactor assembly (Discover,

CEM-SP1245 model, CEM Corp., Matthews, NC, USA) at the desired temperature. The reactor was a 100 mL capacity, 4.5 cm i.d. cylindrical glass vessel with a provision for mechanical stirring. A standard six-blade-pitched turbine impeller of 1.5 cm diameter was used for agitation. However, the actual reactor volume exposed to the microwave irradiation was 45 mL with 5.5 cm height. The temperature in the reactor was computer controlled. The quantities of reactant and enzyme used for microwave reaction procedure were identical to those used for conventional heating.

2.4. Analysis. Reaction progress and enantiomeric excess (ee) were monitored by periodic withdrawal of clear liquid samples from the reaction mixture which were analyzed by high performance liquid chromatography (HPLC) (1260 infinity series, Agilent technologies, CA, USA) equipped with chiralpak- IB analytical column (250 × 4.6 mm ID) (Daicel Corporation, Japan and; particle size 5 μm). Samples (10 μL) were injected via autosampler. The mobile phase consisted of *n*-hexane and isopropyl alcohol (90 : 10) and the flow rate was maintained at 1 mL·min^{-1}. A DAD detector was used at a wavelength of 220 nm. Retention time of (S), (R)-1-phenyl-2-propyn-1-ol, and (R)-ester were 7.6 min, 6.5 min, and 4.4 min, respectively.

The enantioselectivity ratio (E) and conversion (c, %) were calculated from the enantiomeric excess of the substrate (ee$_s$, %) and product (ee$_p$, %) based on the following:

$$E = \frac{\ln\left[(1-c)\left(1-\mathrm{ee}_s\right)\right]}{\ln\left[(1-c)\left(1+\mathrm{ee}_s\right)\right]}, \quad (1)$$

where

$$c = \frac{\mathrm{ee}_s}{\mathrm{ee}_s + \mathrm{ee}_p},$$

$$\mathrm{ee}_s = \frac{B_{(S)} - B_{(R)}}{B_{(S)} + B_{(R)}}, \quad (2)$$

$$\mathrm{ee}_p = \frac{Q_{(S)} - Q_{(R)}}{Q_{(S)} + Q_{(R)}},$$

where $B_{(R)}$, $B_{(S)}$, $Q_{(R)}$, and $Q_{(S)}$ denote area under the curve of (R)-1-phenyl-2-propyn-1-ol, (S)-1-phenyl-2-propyn-1-ol, and their corresponding esters, respectively.

3. Results and Discussion

3.1. Comparison of Microwave Irradiation and Conventional Heating. In order to compare the effect of microwave irradiation and conventional heating, the enzymatic resolution of (±)-1-phenyl-2-propyn-1-ol was performed in both modes using vinyl acetate as the model acyl donor and identical reaction conditions. It was observed that the reaction rate was increased about 1.28-fold from 1.16×10^{-5} mol·dm^{-3}·s^{-1} to 1.49×10^{-5} mol·dm^{-3}·s^{-1} under microwave irradiation. The E and ee$_s$ under microwave irradiation increased by 1.61- and 1.27-fold, respectively. The final conversion of 48.78%, with E and ee$_s$ of 334 and 93.25%, respectively, was obtained within 2 h under microwave irradiation. While, in conventional heating, a conversion of 42.85% with E and ee$_s$ of 207 and 73.33%, respectively, was obtained. Under microwave irradiation, the ions or dipole of the reactants align in the applied electric field. As the applied field oscillates, the dipole or ion field tries to realign itself with the alternating electric field and, in the process, energy is released in the form of heat through molecule collisions and dielectric loss [24]. The quantity of heat released is directly related to the ability of the matrix to align itself with the frequency of the applied field. Microwave irradiation leads to efficient in situ heating, resulting in uniform distribution of temperature throughout the reaction mass. It is thus likely that minor conformational alterations in enzyme structure can also improve access of reactant to the active site, as compared to conventional heating [25]. A control experiment in the absence of enzyme did not show any conversion which indicated that there must be a definite synergism between enzyme catalysis and microwave irradiation. Thus, all further studies were carried out using microwave irradiation.

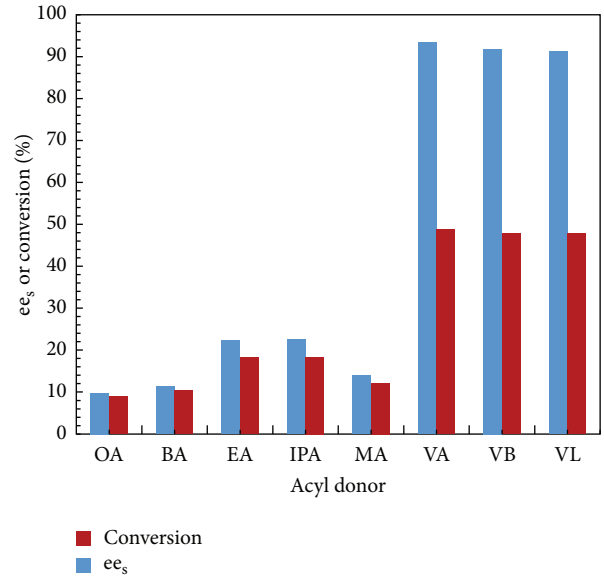

Figure 1: Effect of acyl donor. (Reaction condition: 1-phenyl-2-propyn-1-ol—0.001 mol; acyl donor—0.001 mol; *n*-hexane up to 15 cm^3; speed of agitation—300 rpm; catalyst loading—10 mg; temperature—60°C, OA—Octyl acetate, BA—Butyl acetate, IPA—Isopropyl acetate, EA—Ethyl acetate, MA—Methyl acetate, VA—Vinyl acetate, VB—Vinyl butyrate, and VL—Vinyl laurate).

3.2. Effect of Different Catalysts. In order to compare the activities of three different commercially available immobilized lipases such as Novozym 435 (*Candida antarctica* lipase B), Lipozyme RMIM (*Rhizomucor miehei* lipase), and Lipozyme TLIM (*Thermomyces lanuginosus* lipase) for resolution of (±)-1-phenyl-2-propyn-1-ol under microwave irradiation, transesterification reaction was performed using vinyl acetate as the model acyl donor under similar conditions (Figure 1). It was observed that Novozym 435 showed highest activity among the different catalyst employed in this

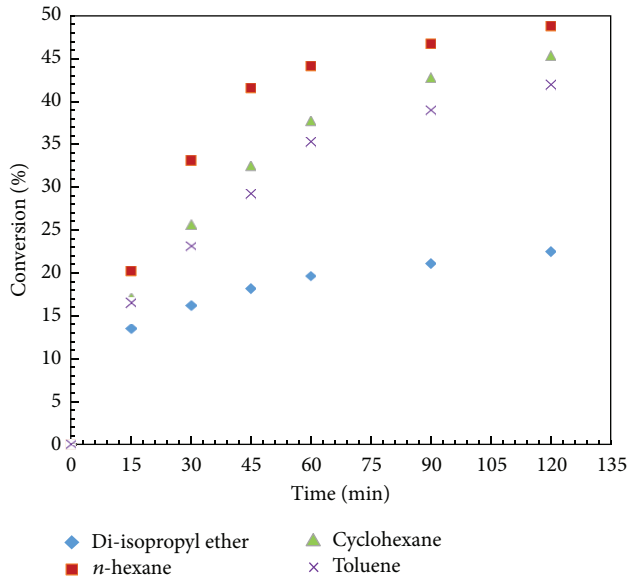

FIGURE 2: Effect of solvent. (Reaction condition: 1-phenyl-2-propyn-1-ol—0.001; vinyl acetate—0.001 mol; solvent up to 15 cm^3; speed of agitation—300 rpm; catalyst loading—10 mg; temperature—60°C).

reaction. With Novozym 435, 48.78% conversion and 93.3% ee_s were obtained. While Lipozyme RMIM and Lipozyme TLIM gave conversions of only 6.37% and 4.4%, respectively. It is reported that both Lipozyme RM IM and Lipozyme TL IM are mainly used to interesterify bulk molecules such as fatty acid derivatives and they have less activity in the resolution of racemic molecules [26]. Hence, further study was carried out using Novozym 435 as the catalyst.

3.3. Effect of Acyl Donors. Acyl donors have the ability to change the enzyme activity and selectivity in nonaqueous medium [27, 28]. Effect of different acyl donors was studied by using 1 : 1 mole ratio of racemic alcohol to acyl donor, with 10 mg enzyme loading at 60°C in *n*-hexane as solvent for 2 h. The liquid phase volume was made up to 15 cm^3 under microwave irradiation (Figure 2). The acyl donors were methyl acetate (MA), ethyl acetate (EA), isopropyl acetate (IPA), butyl acetate (BA), octyl acetate (OA), vinyl acetate (VA), vinyl butyrate (VB), and vinyl laurate (VL). It was observed that both enantioselectivity and conversion increased with increase in alcoholic carbon chain length of alkyl ester from methyl to isopropyl acetate, whereas further increase in alcoholic chain length from C4 to C8 led to decrease in conversion and enantioselectivity of reaction. As compared to alkyl esters, vinyl esters gave good conversion and enantioselectivity. Vinyl alcohol produced during reaction is instantaneously and irreversibly tautomerized to acetaldehyde, which escapes due to its low boiling point and thus there is no inhibition by the coproduct vinyl alcohol. Increasing the chain length of vinyl esters has not shown any significant differences in conversion and enantioselectivity of reaction. Maximum conversion (48.78%) and enantioselectivity (93.25%) were obtained with vinyl acetate vis-a-vis other vinyl esters. Thus, further studies were conducted by using vinyl acetate as the acyl donor.

3.4. Effect of Reaction Media. A proper selection of organic media is necessary for any enzymatic reaction. It has been well reported that organic solvents have the ability to alter the enzyme conformational structure that leads to changes in their activity and also regio-, and stereo-selectivity. Thus, proper selection of solvent is the most important parameter for lipase catalyzed reactions [29]. A number of experiments were performed to study the effect of solvents such as hexane ($\log P = 3.6$), cyclohexane ($\log P = 3.2$), toluene ($\log P = 2.5$), and diisopropyl ether ($\log P = 2$) under similar conditions (Figure 2). Highest conversion (48.78%) and enantiomeric excess ($ee_s = 93.25\%$) were observed when *n*-hexane was employed as the solvent whereas low conversion (22.45%) and enantiomeric excess ($ee_s = 28.96\%$) were observed in di-isopropyl ether, which has the lowest $\log P$ value among the solvents used in this study. On the contrary, conversions of 45.37% and 41.93% were obtained with cyclohexane and toluene, respectively. It has been reported that a tiny water layer around the enzyme particle is necessary to maintain its structure and activity. Solvents having high $\log P$ are hydrophobic in nature but do not strip the water layer around enzyme particle and its structure is not altered [30]. Thus, they show high enzyme activity. Further work was carried out using n-hexane as the solvent.

3.5. Effect of Speed of Agitation. In immobilized enzyme catalyzed reactions, the reactants have to transport from bulk mixture into enzyme active site in the porous particle through convection and diffusion processes [31]. The magnitudes of external mass transfer resistance and intraparticle diffusion limitation play a crucial role in these processes. External mass transfer resistance can be overcome by choosing appropriate speed of agitation. A number of experiments were performed in the range of 100 to 400 rpm by taking 0.001 mol racemic alcohol and vinyl acetate each and 10 mg Novozym 435 made up to 15 cm^3 with *n*-hexane at 60°C (Figure 3). Both the conversion and rate of reaction increased with an increase of agitation speed from 100 to 300 rpm. There was a marginal change in conversion and rate of reaction at 400 rpm. This indicated that there was no external mass transfer limitation above 300 rpm. The external mass transfer and intraparticle diffusion rates were further evaluated by comparing the time constants for reaction (t_r) and diffusion (t_d) using theoretical calculations. These are defined as follows: $t_r = C_0/r(C_0)$ and $t_d = D_S/(k_{SL})^2$, if $t_r \gg t_d$ means that the reaction was not mass transfer controlled [32]. Both C_0 and $r(C_0)$ were determined experimentally and their values were obtained as 0.06667 $mol{\cdot}dm^{-3}$ and 1.4916×10^{-5} $mol{\cdot}dm^{-3}{\cdot}s^{-1}$. Diffusivity of racemic alcohol at 60°C was calculated using Wilke-Chang equation as 5.1063×10^{-5} $cm^2\,s^{-1}$ [33]. The average diameter of the support particle was taken as 0.06 cm since the particle size ranged between 0.03 and 0.09 cm. The value of mass transfer coefficient of liquid phase was calculated, by using Sherwood number of 2, to be 0.5301 $cm{\cdot}s^{-1}$. From these values, the calculated time constants for reaction and

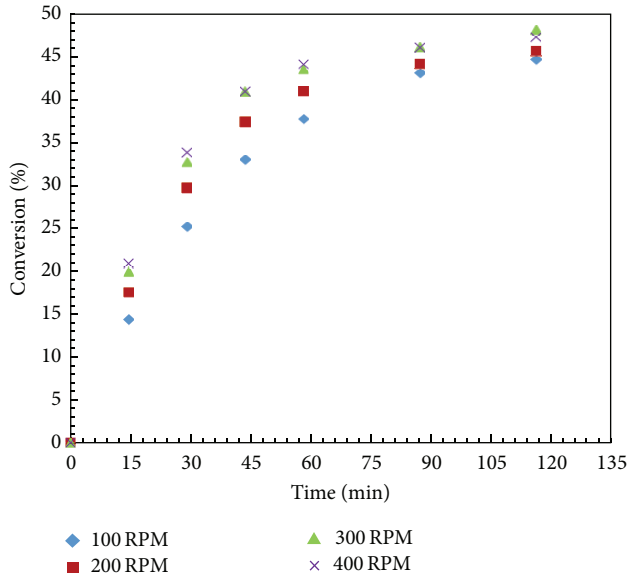

Figure 3: Effect of agitation speed. (Reaction condition: 1-phenyl-2-propyn-1-ol—0.001; vinyl acetate—0.001 mol; *n*-hexane up to 15 cm^3; speed of agitation 100–400 rpm; catalyst loading—10 mg; temperature—60°C).

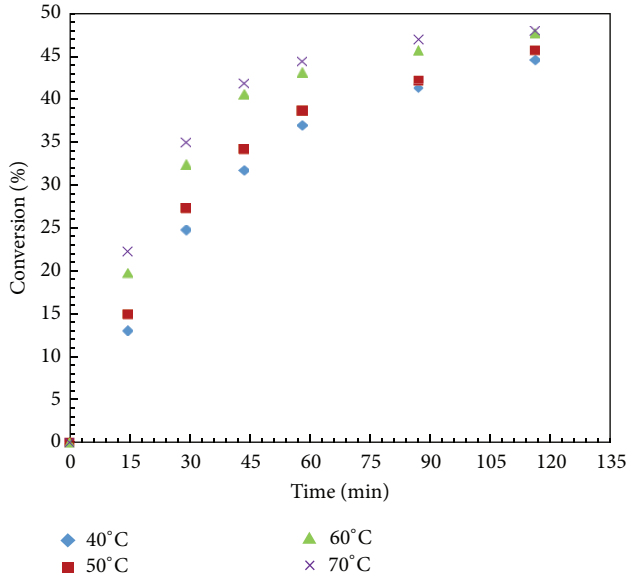

Figure 4: Effect of temperature. (Reaction condition: 1-phenyl-2-propyn-1-ol—0.001; vinyl acetate—0.001 mol; *n*-hexane up to 15 cm^3; speed of agitation 300 rpm; catalyst loading—10 mg; temperature—40–70°C).

diffusion were 4.469×10^3 s and 1.817×10^{-4} s. The time constant for the reaction was much higher than diffusion indicating that there was no external mass transfer resistance.

Further, it is necessary to rule out the intraparticle diffusion limitation. It could be done by comparing the rate of substrate diffusion per unit interfacial area ($k_{SL}C_0$) with the reaction rate per unit area ($\varphi r_0/a$), where φ is the phase volume ratio and "a" is the interfacial area per unit volume of organic phase [32]. Assuming the particle was spherical, $\varphi/a = R_p/3$, where R_p is the radius of the particle. It was found that the value of $k_{SL}C_0 = 0.0353\ \text{mol}\cdot\text{cm}^{-2}\cdot\text{s}^{-1}$ and $\varphi r_0/a = 1.492 \times 10^{-7}\ \text{mol}\cdot\text{cm}^{-2}\cdot\text{s}^{-1}$. It indicated that the rate of substrate diffusion per unit interfacial area was much higher than the reaction rate per unit area. This suggested that there was no intraparticle diffusion limitation. Thus, the reaction was controlled by intrinsic enzyme kinetics. Therefore, further experiments were performed at a speed of 300 rpm.

3.6. Effect of Temperature. It has been reported in most of the literature that temperature plays a critical role in any enzyme catalyzed reaction. It will have an effect on the enzyme activity, enantioselectivity, and rate of reaction because temperature has pronounced effect on viscosity, solubility, and diffusivity of reactants and products. However, at high temperature, the changes in conformation of protein structure will affect their activity and selectivity [34]. Several experiments were performed in the range of 40 to 70°C under similar conditions (Figure 4). It was observed that both conversion and rate of reaction increased with increase in temperature up to 60°C beyond which there was no change in conversion. The enzyme particles may either get denatured or intraparticle diffusion resistance sets in. Further, Arrhenius plot was obtained by plotting the ln (initial rate) versus $1/T$ for both modes of heating and activation energies obtained for microwave and conventional heating were 17.39 $\text{kJ}\cdot\text{mol}^{-1}$ and 15.93 $\text{kJ}\cdot\text{mol}^{-1}$, respectively. These values are similar to those reported for most of the enzymatic reactions [35]. In the case of enantioselectivity, it was observed that the E value increases as temperature increased from 40 to 70°C. It has been reported that enantioselectivity is dependent on reaction temperature and is controlled by enthalpy and entropy of reaction [36]. The following equations were used to relate these terms:

$$\ln E = -\frac{\Delta_{R-S}\Delta H^{\ddagger}}{R} \cdot \frac{1}{T} + \frac{\Delta_{R-S}\Delta S^{\ddagger}}{R}, \qquad \Delta_{R-S}\Delta G^{\ddagger} = -RT \ln (E)\,. \tag{3}$$

The enthalpy and entropy values were calculated by plotting the ln(E) values against the reciprocal reaction temperature (Figure 5). The values of enthalpy and entropy obtained were 9.406 $\text{kJ}\cdot\text{mol}^{-1}$ and 75.93 $\text{J}\cdot\text{mol}^{-1}\cdot\text{K}^{-1}$, respectively. The difference in transition state energy of both enantiomers ($\Delta_{R-S}\Delta G^{\ddagger}$) is −15.88 kJ mol^{-1}. From these values, it was observed that the entropy value was much higher than enthalpy of system and it favors the maximum enantioselectivity at high temperature [37]. Since E value was found to be the highest at 60°C while maintaining a higher enzyme activity, 60°C was selected as the optimum temperature. Thus, further experiments were conducted at this temperature.

3.7. Effect of Enzyme Loading. To select the appropriate amount of enzyme loading, several experiments were performed in the range from 5 to 15 mg enzyme loading under

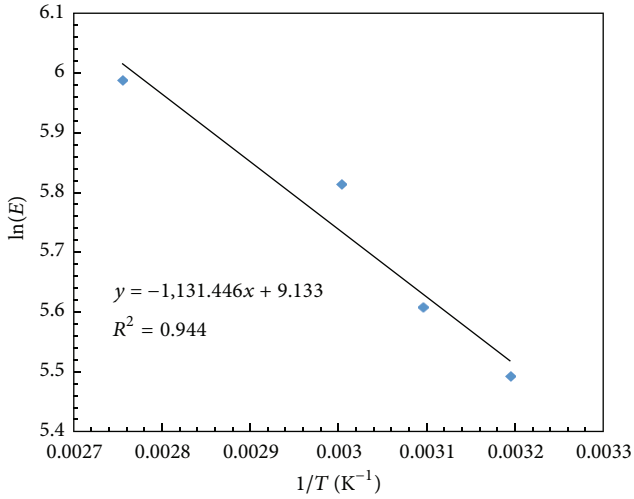

Figure 5: Graphical determination of $\Delta_{R-S}\Delta H^{\ddagger}$ and $\Delta_{R-S}\Delta S^{\ddagger}$.

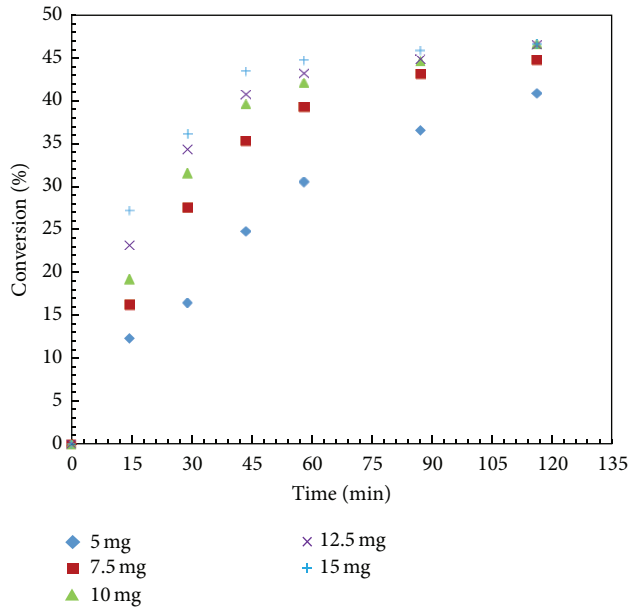

Figure 6: Effect of enzyme loading. (Reaction condition: 1-phenyl-2-propyn-1-ol—0.001; vinyl acetate—0.001 mol; *n*-hexane up to 15 cm^3; speed of agitation 300 rpm; catalyst loading—5–15 mg; temperature—60°C).

similar conditions. The conversion and rate of reaction increased with increase in enzyme loading up to 10 mg; above this loading value, there were no substantial changes in conversion and rate (Figure 6). This would suggest that further addition of enzyme has no effect and it indicated that external mass transfer had limited the rate [29]. Further we observed that the initial rate increased linearly with enzyme loading up to 10 mg which clearly indicated that the reaction was kinetically controlled. Thus, further experiments were carried out at 10 mg as optimum enzyme loading.

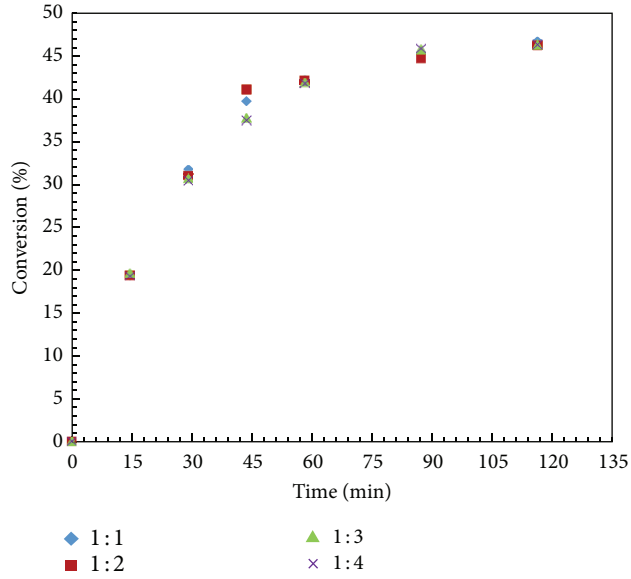

Figure 7: Effect of acyl donor concentration. (Reaction condition: 1-phenyl-2-propyn-1-ol—0.001; vinyl acetate—0.001–0.004 mol; n-hexane up to 15 cm^3; speed of agitation 300 rpm; catalyst loading—10 mg; temperature—60°C).

3.8. Effect of Acyl Donor Concentration. A number of experiments were carried out to analyze the effect of acyl donor concentration on the rate and conversion in the resolution of (±)-1-phenyl-2-propyn-1-ol at 60°C with 10 mg of enzyme loading in n-hexane. The concentration of (±)-1-phenyl-2-propyn-1-ol was kept constant (0.001 mol), and vinyl acetate concentration varied from 0.001 to 0.004 mol; the mixture volume was kept constant at 15 cm^3 by adjusting the amount of *n*-hexane addition. It was found that there were insignificant changes in conversion and rate of reaction with increase concentration of vinyl acetate (Figure 7). It might be possible that, at high concentration, the interaction between acyl donor and enzyme active site increases which leads to reversible competition with alcohol at the active site. Thus further reactions were conducted with 0.001 mole of vinyl acetate.

3.9. Catalyst Reusability. After completion of each run, the catalyst particles were filtered using a membrane filter. Multiple washes were given to the catalyst with fresh solvent (*n*-hexane), dried at room temperature for 12 h, and reused. It was found that there was a marginal decrease in conversion from 48.78 to 45.22% after three reuses, which was due to loss of enzyme during filtration (~2-3%) and drying. No make-up quantity was added. Thus, the enzyme was reusable. When the make-up quantity was added, almost the same conversion was obtained.

3.10. Kinetic Model. Several mechanisms have been proposed for lipase catalyzed reactions (e.g., ordered bi-bi mechanism, ping-pong bi-bi mechanism). However, ping-pong bi-bi mechanism was well adopted for most of the lipases catalyzed

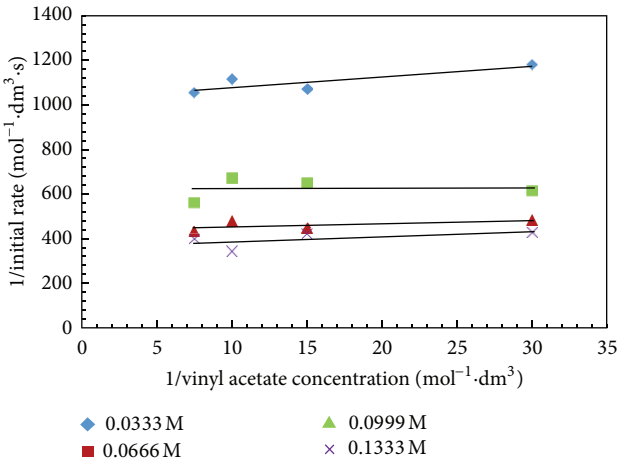

Figure 8: Lineweaver-Burk plot. (Reaction condition: 1-phenyl-2-propyn-1-ol—0.0333–0.1333 M; vinyl acetate—0.0333–0.1333 M; n-hexane up to 15 cm^3; speed of agitation 300 rpm; catalyst loading—10 mg; temperature—60°C).

reactions. The first step of this mechanism is formation of an acyl-enzyme intermediate and the product is released between additions of substrates [38]. In the ordered bi-bi mechanism, the enzyme forms a ternary complex with both substrates and subsequently releases the products [26]. Thus, it was desirable to investigate the mechanism for enantioselective transesterification of (±)-1-phenyl-2-propyn-1-ol with vinyl acetate. For determination of initial rates, a number of experiments were carried out by changing the concentrations of both alcohol (0.0005–0.002 M) and vinyl acetate (0.0005–0.002 M) over a wide range under similar conditions. Initial rates were calculated systematically from the linear portion of the concentration-time profiles. The Lineweaver-Burk plots of reciprocal rate versus reciprocal concentration of vinyl acetate were made (Figure 8). From the plot, it is observed that there are no crossings of lines which rules out the possibility of ternary mechanism. At low concentrations of substrates, the slope of the lines is not influenced by the concentration of the fixed substrate. This is indicative of a mechanism that requires the dissociation of one product before the association of the second substrate to the enzyme-substrate complex. The curved shape at higher concentrations of 1-phenyl-2-propyn-1-ol can be used as an indication for formation of enzyme dead end complex with alcohol. The proposed mechanism is as follows:

$$
\begin{aligned}
E + A &\underset{k_{-1}}{\overset{k_1}{\rightleftarrows}} EA,\\
EA &\underset{k_{-2}}{\overset{k_2}{\rightleftarrows}} P + E',\\
E' + B &\underset{k_{-3}}{\overset{k_3}{\rightleftarrows}} E'B,\\
E'B &\underset{k_{-4}}{\overset{k_4}{\rightleftarrows}} EQ,\\
EQ &\xrightarrow{K_p} Q + E.
\end{aligned}
\tag{4}
$$

Table 1: Values of kinetic parameters for transesterification reaction.

Kinetic parameter	Value
V_m (mol·dm^{-3}·s^{-1})	2.508×10^{-2}
K_{mA} (mol·dm^{-3})	0.0019
K_{mB} (mol·dm^{-3})	0.8863
K_i (mol·dm^{-3})	0.00265

Inhibition steps by 1-phenyl-2-propyn-1-ol

$$
E + B \underset{}{\overset{k_i}{\rightleftarrows}} E_iB. \tag{5}
$$

From these observations, a ping-pong bi-bi mechanism with dead end alcohol inhibition was postulated. These assumptions are used to develop a reaction mechanism which is depicted in Cleland's notation, as shown in Figure 10.

By analogy to the classical mechanism of lipase catalysis, it is assumed that vinyl acetate (A) binds first to the free enzyme (E) and forms a noncovalent enzyme acetate complex (EA), which releases the first product, aldehyde (P) and (E') modified enzyme. The second substrate alcohol (B) reacts with activated enzyme (E') to give the complex ($E'B$) which gives the product ester (Q) and free enzyme (E). Along with this, alcohol (B) also forms the dead end complex (E_iB) by binding to free enzyme (E). Here, B is the R-isomer.

The kinetic representing this model for initial reaction rate can be expressed as

$$
v = \frac{v_m [A] [B]}{K_{mB} [A] + K_{mA} [B] \left(1 + \left([B] / K_i\right)\right) + [A] [B]}, \tag{6}
$$

whereas v is the rate of reaction, v_m the maximum rate of reaction, $[A]$ the initial concentration of vinyl acetate, $[B]$ the initial concentration of (R)-1-phenyl-2-propyn-1-ol, and K_{mA} the Michaelis constant for vinyl acetate, as (S)-enantiomer of alcohol remains unreacted during the reaction, changes in concentration of (S)-enantiomer is neglected. K_{mB} the Michaelis constant for (R)-1-phenyl-2-propyn-1-ol, and K_i the inhibition constant for (R)-1-phenyl-2-propyn-1-ol. The initial rate data were used to determine the kinetic parameters of above mechanism by nonlinear regression analysis using the software package Polymath 5.1 (Table 1). The initial rates of reaction for different reactant concentration were simulated using above equation to verify the proposed kinetic model. The parity plot between simulated rate and experimental rate suggested that the proposed mechanism was valid for this reaction (Figure 9).

4. Conclusion

In this work, lipase catalyzed kinetic resolution of 1-phenyl-2-propyn-1-ol using vinyl acetate as acyl donor was studied under microwave irradiation. Among the employed catalysts, Novozym 435 was found to be the most effective catalyst in n-hexane as solvent. There was synergism between microwave irradiation and lipase. Both conversion and rate of reaction were increased under microwave as compared to conventional heating. Microwave irradiation leads to

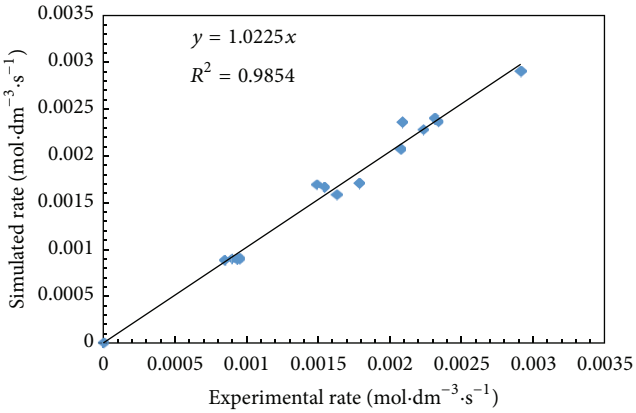

Figure 9: Parity plot of experimental versus simulated rates.

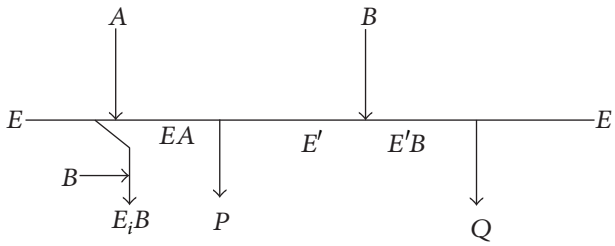

Figure 10

increase the affinity of the substrate toward the active site of lipase. Further, microwaves enhance the collision frequency of reactant molecules that leads to increase in entropy of the system. The effect of various parameters was studied on conversion and rate of reaction. The maximum conversion of 48.78% was obtained in 2 h using 10 mg enzyme loading with equimolar concentration of alcohol and ester at 60°C under microwave irradiation. From the progress curve analysis, it was found that the reaction followed the ping-pong bi-bi mechanism with dead end inhibition of alcohol. The kinetic parameters were refined by using nonlinear regression. There was a good fit between experimental and simulated rates. The preparation of chiral secondary alcohols using lipase catalyzed kinetic resolution is mild and clean as compared to chemical process.

Nomenclature

A: Initial concentration of vinyl acetate, mol·dm^{-3}
B: Initial concentration of (R)-1-phenyl-2-propyn-1-ol, mol·dm^{-3}
E: Free enzyme
EA: Enzyme-acyl complex with A
$E'B$: Modified enzyme-alcohol complex
E_iB: Dead end enzyme-alcohol complex
K_i: Inhibition constant for (R)-1-phenyl-2-propyn-1-ol, mol·dm^{-3}
K_{mA}: Michaelis constant for vinyl acetate, mol·dm^{-3}
K_{mB}: Michaelis constant for (R)-1-phenyl-2-propyn-1-ol, mol·dm^{-3}
P: Acetaldehyde
Q: Ester
v: Rate of reaction, mol·dm^{-3}·s^{-1}
v_m: Maximum rate of reaction, mol·dm^{-3}·s^{-1}
$\Delta_{R-S}\Delta H^{\ddagger}$: Differential activation enthalpy
$\Delta_{R-S}\Delta S^{\ddagger}$: Differential activation entropy
$\Delta_{R-S}\Delta G^{\ddagger}$: Difference in transition state energy of both enantiomers
T: Temperature (K)
R: Gas constant (J·mol^{-1}·K^{-1})
E: Enantiomeric ratio
ee_s: Enantiomeric excess for substrate
ee_p: Enantiomeric excess for product
c: Conversion.

Conflict of Interests

The authors declare that there is no conflict of interests regarding the publication of this paper.

Acknowledgment

Saravanan Devendran received JRF from UGC under its Meritorious Fellowship BSR programme (CAS in Food Engineering and Technology). Ganapati D. Yadav received support from R. T. Mody Distinguished Professor Endowment and J. C. Bose National Fellowship of Department of Science and Technology, Government of India. The authors are thankful to Novo Nordisk, Denmark, for providing lipases as gift sample.

References

[1] R. A. Sheldon, *Chirotechnology: Industrial Synthesis of Optically Active Compounds*, Marcel Dekker, New York, NY, USA, 1993.

[2] R. N. Patel, "Biocatalytic synthesis of chiral pharmaceutical intermediates," *Food Technology and Biotechnology*, vol. 42, no. 4, pp. 305–325, 2004.

[3] A. Ghanem and H. Y. Aboul-Enein, "Lipase-mediated chiral resolution of racemates in organic solvents," *Tetrahedron*, vol. 15, no. 21, pp. 3331–3351, 2004.

[4] G. D. Yadav and K. M. Devi, "Enzymatic synthesis of perlauric acid using Novozym 435," *Biochemical Engineering Journal*, vol. 10, no. 2, pp. 93–101, 2002.

[5] G. D. Yadav and S. Devendran, "Lipase catalyzed synthesis of cinnamyl acetate via transesterification in non-aqueous medium," *Process Biochemistry*, vol. 47, no. 3, pp. 496–502, 2012.

[6] G. D. Yadav, A. D. Sajgure, and S. B. Dhoot, "Enzyme catalysis in fine chemical and pharmacuetical industries," in *Enzyme Mixtures and Complex Biosynthesis*, S. K. Bhattacharya, Ed., pp. 79–108, Landes Biosciences, Austin, Tex, USA, 2007.

[7] J. Durand, E. Teuma, and M. Gómez, "Ionic liquids as a medium for enantioselective catalysis," *Comptes Rendus Chimie*, vol. 10, no. 3, pp. 152–177, 2007.

[8] R. A. Sheldon, "Green solvents for sustainable organic synthesis: state of the art," *Green Chemistry*, vol. 7, no. 5, pp. 267–278, 2005.

[9] B. L. Hayes, *Microwave Synthesis: Chemistry at the Speed of Light*, CEM, Matthews, NC, USA, 2002.

[10] A. Loupy, Ed., *Microwaves in Organic Synthesis*, Wiley-VCH, Weinheim, Germany, 2002.

[11] G. D. Yadav and P. R. Sowbna, "Modeling of microwave irradiated liquid-liquid-liquid (MILLL) phase transfer catalyzed green synthesis of benzyl thiocyanate," *Chemical Engineering Journal*, vol. 179, pp. 221–230, 2012.

[12] D. Yu, H. Wu, A. Zhang et al., "Microwave irradiation-assisted isomerization of glucose to fructose by immobilized glucose isomerase," *Process Biochemistry*, vol. 46, no. 2, pp. 599–603, 2011.

[13] B. Réjasse, S. Lamare, M.-D. Legoy, and T. Besson, "Stability improvement of immobilized *Candida antarctica* lipase B in an organic medium under microwave radiation," *Organic & Biomolecular Chemistry*, vol. 2, no. 7, pp. 1086–1089, 2004.

[14] G. D. Yadav and P. S. Lathi, "Synergism between microwave and enzyme catalysis in intensification of reactions and selectivities: transesterification of methyl acetoacetate with alcohols," *Journal of Molecular Catalysis A*, vol. 223, no. 1-2, pp. 51–56, 2004.

[15] W. R. Roush and R. J. Sciotti, "Enantioselective total synthesis of (−)-chlorothricolide," *Journal of the American Chemical Society*, vol. 116, no. 14, pp. 6457–6458, 1994.

[16] X. Ariza, J. Garcia, Y. Georges, and M. Vicente, "1-phenylprop-2-ynyl acetate: a useful building block for the stereoselective construction of polyhydroxylated chains," *Organic Letters*, vol. 8, no. 20, pp. 4501–4504, 2006.

[17] S. Peng, L. Wang, and J. Wang, "Iron-catalyzed ene-type propargylation of diarylethylenes with propargyl alcohols," *Organic & Biomolecular Chemistry*, vol. 10, no. 2, pp. 225–228, 2012.

[18] B. I. Glänzer, K. Faber, and H. Griengl, "Enantioselective hydrolyses by baker's yeast—III: microbial resolution of alkynyl esters using lyophilized yeast," *Tetrahedron*, vol. 43, no. 24, pp. 5791–5796, 1987.

[19] S.-K. Kang, T. Yamaguchi, S.-J. Pyun, Y.-T. Lee, and T.-G. Baik, "Palladium-catalyzed arylation of α-allenic alcohols with hypervalent iodonium salts: synthesis of epoxides and diol cyclic carbonates," *Tetrahedron Letters*, vol. 39, no. 15, pp. 2127–2130, 1998.

[20] C. Waldinger, M. Schneider, M. Botta, F. Corelli, and V. Summa, "Aryl propargylic alcohols of high enantiomeric purity *via* lipase catalyzed resolutions," *Tetrahedron*, vol. 7, no. 5, pp. 1485–1488, 1996.

[21] D. Xu, Z. Li, and S. Ma, "Novozym-435-catalyzed enzymatic separation of racemic propargylic alcohols. A facile route to optically active terminal aryl propargylic alcohols," *Tetrahedron Letters*, vol. 44, no. 33, pp. 6343–6346, 2003.

[22] C. Raminelli, J. V. Comasseto, L. H. Andrade, and A. L. M. Porto, "Kinetic resolution of propargylic and allylic alcohols by *Candida antarctica* lipase (Novozyme 435)," *Tetrahedron*, vol. 15, no. 19, pp. 3117–3122, 2004.

[23] P. Chen and X. Zhu, "Kinetic resolution of propargylic alcohols via stereoselective acylation catalyzed by lipase PS-30," *Journal of Molecular Catalysis B*, vol. 97, pp. 184–188, 2013.

[24] G. D. Yadav and S. Devendran, "Lipase catalyzed kinetic resolution of (±)-1-(1-naphthyl) ethanol under microwave irradiation," *Journal of Molecular Catalysis B*, vol. 81, pp. 58–65, 2012.

[25] P. Mazo, L. Rios, D. Estenoz, and M. Sponton, "Self-esterification of partially maleated castor oil using conventional and microwave heating," *Chemical Engineering Journal*, vol. 185-186, pp. 347–351, 2012.

[26] G. D. Yadav and P. Sivakumar, "Enzyme-catalysed optical resolution of mandelic acid via *RS*(∓)-methyl mandelate in non-aqueous media," *Biochemical Engineering Journal*, vol. 19, no. 2, pp. 101–107, 2004.

[27] T. Ema, S. Maeno, Y. Takaya, T. Sakai, and M. Utaka, "Significant effect of acyl groups on enantioselectivity in lipase-catalyzed transesterifications," *Tetrahedron: Asymmetry*, vol. 7, no. 3, pp. 625–628, 1996.

[28] T. Miyazawa, S. Kurita, S. Ueji, T. Yamada, and S. Kuwata, "Resolution of mandelic acids by lipase-catalysed transesterifications in organic media: inversion of enantioselectivity mediated by the acyl donor," *Journal of the Chemical Society, Perkin Transactions 1*, no. 18, pp. 2253–2255, 1992.

[29] K. Nakamura, Y. Takebe, T. Kitayama, and A. Ohno, "Effect of solvent structure on enantioselectivity of lipase-catalyzed transesterification," *Tetrahedron Letters*, vol. 32, no. 37, pp. 4941–4944, 1991.

[30] L. A. S. Gorman and J. S. Dordick, "Organic solvents strip water off enzymes," *Biotechnology and Bioengineering*, vol. 39, no. 4, pp. 392–397, 1992.

[31] G. D. Yadav and A. H. Trivedi, "Kinetic modeling of immobilized-lipase catalyzed transesterification of *n*-octanol with vinyl acetate in non-aqueous media," *Enzyme and Microbial Technology*, vol. 32, no. 7, pp. 783–789, 2003.

[32] R. H. Perry and D. W. Green, Eds., *Perry's Chemical Engineers' Handbook*, McGraw-Hill, New York, NY, USA, 1984.

[33] C. R. Wilke and P. Chang, "Correlation of diffusion coefficients in dilute solutions," *AIChE Journal*, vol. 1, no. 2, pp. 264–270, 1955.

[34] Y. Yasufuku and S.-I. Ueji, "Effect of temperature on lipase-catalyzed esterification in organic solvent," *Biotechnology Letters*, vol. 17, no. 12, pp. 1311–1316, 1995.

[35] I. H. Segel, *Enzyme Kinetics: Behavior and Analysis of Rapid Equilibrium and Steady State Enzyme Systems*, Wiley-Interscience, New York, NY, USA, 1975.

[36] R. S. Phillips, "Temperature effects on stereochemistry of enzymatic reactions," *Enzyme and Microbial Technology*, vol. 14, no. 5, pp. 417–419, 1992.

[37] J. Ottosson, J. C. Rotticci-Mulder, D. Rotticci, and K. Hult, "Rational design of enantioselective enzymes requires considerations of entropy," *Protein Science*, vol. 10, no. 9, pp. 1769–1774, 2001.

[38] S. H. Krishna and N. G. Karanth, "Lipase-catalyzed synthesis of isoamyl butyrate: a kinetic study," *Biochimica et Biophysica Acta*, vol. 1547, no. 2, pp. 262–267, 2001.

Hindawi Publishing Corporation
BioMed Research International
Volume 2014, Article ID 410530, 5 pages
http://dx.doi.org/10.1155/2014/410530

Research Article

Demonstration of Redox Potential of *Metschnikowia koreensis* for Stereoinversion of Secondary Alcohols/1,2-Diols

Vachan Singh Meena, Linga Banoth, and U. C. Banerjee

Department of Pharmaceutical Technology (Biotechnology), National Institute of Pharmaceutical Education and Research (NIPER), Sector 67, S. A. S. Nagar, Punjab 160 062, India

Correspondence should be addressed to U. C. Banerjee; ucbanerjee@niper.ac.in

Received 30 April 2013; Revised 13 November 2013; Accepted 24 November 2013; Published 27 January 2014

Academic Editor: Bernardo Dias Ribeiro

The present work reports the *Metschnikowia koreensis*-catalyzed one-pot deracemization of secondary alcohols/1,2-diols and their derivatives with in vivo cofactor regeneration. Reaction is stereoselective and proceeds with sequential oxidation of (*R*)-secondary alcohols to the corresponding ketones and the reduction of the ketones to (*S*)-secondary alcohols. Method is applicable to a repertoire of racemic aryl secondary alcohols and 1,2-diols establishing a wide range of substrate specificity of *M. koreensis*. This ecofriendly method afforded the product in high yield (88%) and excellent optical purity (>98% *ee*), minimizing the requirement of multistep reaction and expensive cofactor.

1. Introduction

Enantiomerically pure secondary alcohols are used as pharmaceuticals, flavors, agricultural chemicals, synthetic intermediates, chiral auxiliaries, and analytical reagents [1]. These enantiopure alcohols can be obtained by kinetic resolution, asymmetric reduction of ketones, oxidation of olefines, ring opening of glycidol with phenol, or stereoinversion of racemic alcohols [2–20]. Among these various methods, stereoinversion is the most promising technique which offers a 100% conversion from racemate to the enantiopure product [21–24].

Sequential chemical oxidation reduction with one or two biocatalysts has been reported in the literature for stereoinversion of racemic alcohols [21, 25–32]. However, the chemical process needs harsh reaction conditions. Combination approach of transition metal catalyst and biocatalyst for stereoinversion of secondary alcohols was also used by various workers [33]. The whole cell biocatalytic stereoinversion is an efficient method for obtaining chiral secondary alcohols [34–37]. Hummel and Riebel detailed the stepwise route to synthesize enantiomerically pure alcohols from the corresponding racemates by employing two stereo complementary alcohol dehydrogenases [38]. The stereoinversion of sec-alcohols by oxidoreductases has also been reported [23]. However, the external addition of the cofactors and the use of isolated or commercially purified enzymes, specific substrates, and moderate substrate concentrations are the limitations of these protocols [36]. Comparing with the above-mentioned approaches, the application of the whole cell biocatalysts for stereoinversion seems to be the more favorable approach in the context of reaction conditions, enzyme stability, and cofactor regeneration. There are only limited reports on the stereoinversion of secondary alcohols using whole cell biocatalysts, such as sec-alcohols and 1,2-diols [30, 36, 39–41]. Obtaining an enantiomerically pure isomer in a one-pot process is currently a hot topic and of great industrial demand [42, 43].

2. Material and Methods

2.1. Chemicals. (±)-Phenyl glycidyl ether, (±)-1-phenyl ethanol, (*R*)/(*S*) 1-phenyl ethanol, and acetophenone were purchased from Sigma (Steinheim, Germany). (*RS*) (±)-3-phenoxy-1,2-propanediol and (*S*)-3-phenoxy-1,2-propanediol were synthesized chemically from phenyl glycidyl ether by the reported procedure [44]. Solvents

required for the synthesis and extraction were acquired from commercial sources and they were either of analytical or commercial grades obtained from Rankem (Mumbai, India) and Merck Ltd (Whitehouse Station, NJ, USA). Growth media components were obtained from Hi-Media Inc. (Mumbai, India). Various HPLC grade solvents *n*-hexane, 2-propanol and acetonitrile were obtained from J. T. Baker (Phillipsburg, NJ, USA). Membrane filters of 0.22 μM were purchased from MDI Pvt. Ltd. (Ambala, India). All other chemicals used were of analytical grade and obtained from standard companies.

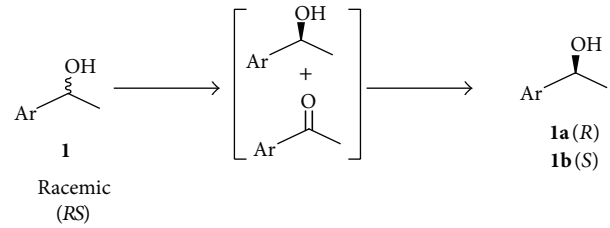

Scheme 1: Concurrent oxidation and reduction for the stereoinversion of racemic secondary alcohols.

2.2. Microorganism and Cultivation Conditions. *Metschnikowia koreensis* MTCC-5520 was used in this study. The strain was isolated in our laboratory, identified by Microbial Type Culture Collection and Gene Bank, Institute of Microbial Technology, Chandigarh, India.

Culture on Agar Plate. The stock culture was maintained at 4°C on agar plate containing YPD medium. The composition of YPD medium was yeast extract (5 g/L), peptone (5 g/L), and dextrose (10 g/L).

Preculture. A single colony from the agar plate was aseptically inoculated into 25 mL YPD medium and grown at 25°C (200 rpm) for 24 h.

Growth of Cellmass. Five milliliters of preculture was transferred in 100 mL YPD medium in a 500 mL shake flask and incubated at 25°C (200 rpm) for 2 days. The cells were harvested by centrifugation at 10,000 g for 10 min and thoroughly washed. The cells were suspended in Tri-HCl buffer (pH 8) and directly used for biotransformation reaction.

2.3. Biotransformation Conditions

2.3.1. Concurrent Oxidation-Reduction of Secondary Alcohols. Typical procedure for deracemization of racemic secondary alcohols to single enantiomer (*S*) with tandem biocatalysts was optimized. one gram wet cellmass of *M. koreensis* was suspensioned in 5 mL Tris-HCl buffer (50 mM; pH 8.0). Racemic secondary alcohols were added into the cell mass suspension to make the final concentration 5 mM in the reaction mixture and reaction was carried out for up to 3 days. The reaction mixture was incubated for fixed time at 30°C (200 rpm). The cells were removed by centrifugation at 10,000 ×g for 10 min and aqueous phase was subjected to reversed phase chiral HPLC analysis for quantifying the reactant and product concentrations.

2.3.2. Reaction Temperature. In order to optimize temperature [45], reaction was performed at different temperatures ranging from 20 to 40°C. Cellmass suspension (150 mg/mL) was prepared in Tris-HCl buffer pH 8, 50 mM and added to the reaction mixture. The stereoinversion was carried out with 5 mM (±)-3-phenoxy-1,2-propanediol as substrate and incubated at various temperatures (200 rpm). The final reaction volume was 15 mL. The reaction was continued for up to 3 days and aliquot (1 mL) was withdrawn at a regular time interval (24 h) and checked for the conversion and enantiomeric excess in chiral-HPLC.

2.3.3. Cellmass Concentration. In order to study the effect of cellmass concentration [45] on stereoinversion, various cellmass concentrations ranging from 100 to 300 mg/mL were used. All other parameters are kept at their optimal values and checked for stereoinversion by performing the reaction in Tris-HCl buffer (pH 8, 50 mM) with 5 mM (±)-3-phenoxy-1,2-propanediol. The final reaction volume was 15 mL. The reaction was continued for up to 3 days and aliquot (1 mL) was withdrawn at a regular time interval (24 h) and checked for the conversion and enantiomeric excess in chiral-HPLC.

2.3.4. Substrate Concentration. In order to find out the optimum substrate concentration [45], various substrate concentrations ranging from 5 to 20 mM in the reaction mixture were added. Cellmass (250 mg/mL) suspended in Tris-HCl buffer (pH 8, 50 mM) was used to perform this experiment. The reaction was carried out at a final volume of 15 mL at 30°C. The reaction was continued for up to 3 days and aliquot (1 mL) was withdrawn at a regular time interval (24 h) and checked for the conversion and enantiomeric excess in chiral-HPLC.

2.4. Analytical Methods. Quantitative formation of single enantiomer of 3-phenoxy-1,2-propanediol, 1-phenyl ethanol, and their corresponding ketones was estimated by High Performance Liquid Chromatography (HPLC, Shimadzu 10AD VP, Kyoto, Japan), equipped with UV detector using a Lux cellulose-1 chiral (4.6 mm × 250 mm, 5 μm, phenomenex, USA) column at 25°C. Elution was carried out by acetonitrile and water (35 : 65) at a flow rate of 0.5 mL/min and detected at 254 nm and 215 nm, respectively.

3. Result and Discussion

In this paper, a single whole cell biocatalyst (one pot) was successfully demonstrated for stereoinversion of aryl secondary alcohols (Scheme 1) and 1,2-diols (Scheme 2) to enantiopure (*S*)-alcohols in excellent yield and enantioselectivity. The present work is an attempt to combine the multienzyme reactions into single-step reactions, while minimizing the conventional drawbacks of catalysis.

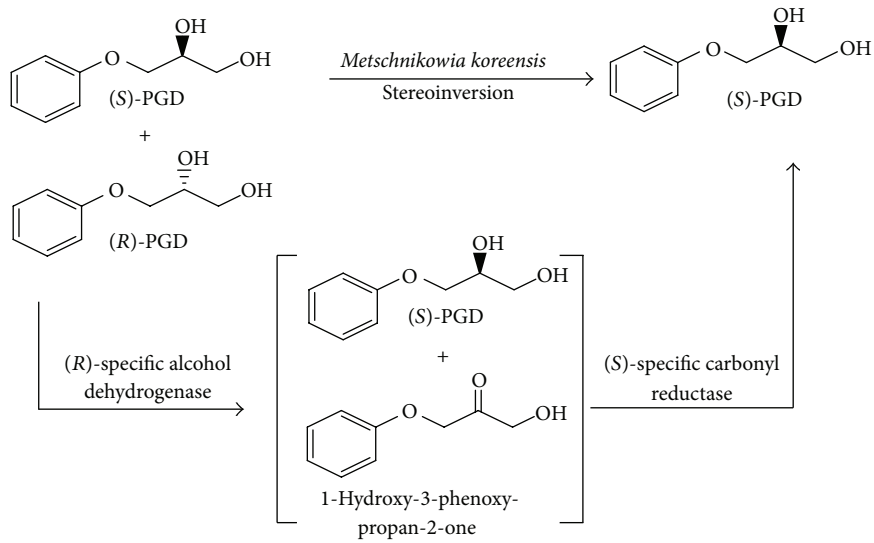

Scheme 2: Stereoinversion of 3-aryloxy-1,2-propanediols by the whole cells of *Metschnikowia koreensis*.

Table 1: Results of the deracemization of secondary alcohols[a].

Entry	Substrate	Yield (%)[b]	*ee* (%)[b]
1	R = H	96	>99
2	R = Me	96	>98
3	R = OMe	88	>98
4	R = NO_2	92	>98
5	R = F	94	>98

[a]Reactions were carried out with different substrates (5 mM, each) using resting cells (250 mg/mL). [b]Yield and *ee* were determined by chiral HPLC with Phenomenex Lux cellulose-1 (250 × 4.6 mm) column.

M. koreensis was examined for its ability to catalyze the stereoinversion process of 1-phenylethanol and 3-aryloxy-1,2-propanediol. The racemic alcohols/diol was converted into single enantiomer, indicating the stereoinversion process catalyzed by redox enzyme. Similar findings were also reported in the literature [41]. It was observed that the whole cells of *M. koreensis* showed good stereoinversion. Sufficiently convinced with the microbial potential of stereoinversion, a detailed systematic optimisation study of various reaction parameters was carried out. The optimum temperature for the stereoinversion process was found to be 30°C. Below and above this temperature, the conversion and enantiomeric excess suffered. The results indicated good enzyme stability and activity at 30°C. Buffers of various pHs ranging from 5 to 8 were tested and it was found that Tris-HCl buffer of pH 8 gave the best results, while keeping the other reaction parameters constant. The optimized cell-mass and substrate concentration were found to be 250 mg/mL and 5 mM, respectively. A mixing rate of 250 rpm was selected as optimum. To study the time course of the *M. koreensis*-catalyzed stereoinversion process, the reaction mixture of racemic 1-phenylethanol was subjected to chiral chromatography at different time intervals. A maximum yield of 98%, with 99% *ee* of (*S*)-after 18 h, was achieved. To investigate mechanistic details of the stereoinversion process, the ketone was used as a model substrate for *M. Koreensis*. The production of (*S*)-alcohol was observed from this reaction [46, 47]. This study suggested a cascade of events that included the initial oxidation of (*R*)-alcohol to ketone in a highly selective reaction leaving (*S*)-alcohol as such. This process is followed by the reduction of ketone to (*S*)-alcohol in higher enantiomeric excess and yield (Table 1).

The biocatalytic stereoinversion behaviour of the 1-phenylethanol derivatives by other microorganisms was also reported in the literature [22, 37]. The encouraging outcome of this study prompted us to test the applicability of this biocatalyst for the stereoinversion of other derivatives of 1-phenylethanol and 3-aryloxy-1,2-propanediol. Impressive results were obtained in each case. Various functional group-substituted alcohols underwent a clean deracemization process and produced (*S*)-isomer with excellent yield and enantiomeric excess (Table 1).

Extrapolation of a similar biocatalytical condition to *M. koreensis*-mediated stereoinversion of (*S*)-3-aryloxy-1,2-propanediol proved the excellent redox potential of this organism towards a diverse array of substrates. It is noted that microbes gave a higher chemical yield with excellent stereoinversion after 3 days of incubation. An overall view of the deracemization process of 3-aryloxy-1,2-propanediol is presented in Table 2.

4. Conclusion

In conclusion, we have identified and demonstrated the redox potential of *Metschnikowia koreensis* for the stereoinversion process of secondary alcohols/1,2-diols. Further research

Table 2: Biocatalytic deracemization of 3-aryloxy-1,2-propanediol by stereoselective oxidation reduction using whole cells of *M. koreensis*[a].

Entry	Substrate	Yield (%)[b]	*ee* (%)[b]	Configuration
1	R = H	98	>99	*S*
2	R = Me	97	>98	*S*

[a]Reactions were carried out with two substrates (5 mM, each) using the resting cells (250 mg/mL). [b]Yield and *ee* were determined by chiral HPLC with Phenomenex Lux cellulose-1 (250 × 4.6 mm) column.

may be initiated on finding out the detailed mechanistic investigation, isolation of probable enzymes, and substrate diversification on the application of this stereoinversion process.

Conflict of Interests

The authors declare that there is no conflict of interests regarding the publication of this paper.

Acknowledgment

Vachan Singh Meena and Linga Banoth would like to thank the Department of Biotechnology, Government of India, for providing senior research fellowship to carry out this work.

References

[1] K. Faber, *Biotransformations in Organic Chemistry*, Springer, Berlin, Germany, 1997.

[2] C. Zhu, G. Yuan, X. Chen, Z. Yang, and Y. Cui, "Chiral nanoporous metal-metallosalen frameworks for hydrolytic kinetic resolution of epoxides," *Journal of the American Chemical Society*, vol. 134, no. 19, pp. 8058–8061, 2012.

[3] X. Hong, M. Mellah, F. Bordier, R. Guillot, and E. Schulz, "Electrogenerated polymers as efficient and robust heterogeneous catalysts for the hydrolytic kinetic resolution of terminal epoxides," *ChemCatChem*, vol. 4, pp. 1115–1121, 2012.

[4] Y. Liu, Y. Wang, Y. Wang, J. Lu, V. Piñón, and M. Weck, "Shell cross-linked micelle-based nanoreactors for the substrate-selective hydrolytic kinetic resolution of epoxides," *Journal of the American Chemical Society*, vol. 133, no. 36, pp. 14260–14263, 2011.

[5] Z. Maugeri, W. Leitner, and P. D. D. María, "Practical separation of alcohol-ester mixtures using Deep-Eutectic-Solvents," *Tetrahedron Letters*, vol. 53, pp. 6968–6971, 2012.

[6] P. B. Brondani, N. M. A. F. Guilmoto, H. M. Dudek, M. W. Fraaije, and L. H. Andrade, "Chemoenzymatic approaches to obtain chiral-centered selenium compounds," *Tetrahedron*, vol. 68, pp. 10431–10436, 2012.

[7] W. Bai, Y.-J. Yang, X. Tao, J.-F. Chen, and T.-W. Tan, "Immobilization of lipase on aminopropyl-grafted mesoporous silica nanotubes for the resolution of (R, S)-1-phenylethanol," *Journal of Molecular Catalysis B*, vol. 76, pp. 82–88, 2012.

[8] C. Aubert, C. Dallaire, G. Pepe, E. Levillain, G. Felix, and M. Gingras, "Multivalent, sulfur-rich PyBox asterisk ligands in asymmetric metal catalysis," *European Journal of Organic Chemistry*, vol. 2012, pp. 6145–6154, 2012.

[9] S. Elias, K. Goren, and A. Vigalok, "Asymmetric transfer hydrogenation of ketones catalyzed by rhodium block copolymer complexes in aqueous micelles," *Synlett*, vol. 23, pp. 2619–2622, 2012.

[10] A. Hernández-Ortega, P. Ferreira, P. Merino, M. Medina, V. Guallar, and A. T. Martínez, "Stereoselective hydride transfer by aryl-alcohol oxidase, a member of the GMC superfamily," *ChemBioChem*, vol. 13, no. 3, pp. 427–435, 2012.

[11] I. Schnapperelle, W. Hummel, and H. Gröger, "Formal asymmetric hydration of non-activated alkenes in aqueous medium through a 'chemoenzymatic catalytic system'," *Chemistry*, vol. 18, no. 4, pp. 1073–1076, 2012.

[12] N. A. Salvi and S. Chattopadhyay, "*Rhizopus arrhizus*-mediated asymmetric reduction of arylalkanones: unusual anti-Prelong products with benzyl alkyl ketones," *Tetrahedron Asymmetry*, vol. 22, no. 14-15, pp. 1512–1515, 2011.

[13] N. G. Khalig, "Investigation of the catalytic activity of poly(4-vinylpyridine) supported iodine as a new, efficient and recoverable catalyst for regioselective ring opening of epoxides," *RSC Advances*, vol. 2, no. 8, pp. 3321–3327, 2012.

[14] A. D. Worthy, X. K. L. Sun, and J. Tan, "Site-selective catalysis: toward a regiodivergent resolution of 1, 2-Diols," *Journal of the American Chemical Society*, vol. 134, pp. 7321–7324, 2012.

[15] T. Aral, M. Karakaplan, and H. Hoşgören, "Asymmetric organocatalytic efficiency of synthesized chiral β-amino alcohols in ring-opening of glycidol with phenols," *Catalysis Letters*, vol. 142, pp. 794–802, 2012.

[16] V. Köhler, J. Mao, T. Heinisch et al., "OsO4•streptavidin: a tunable hybrid catalyst for the enantioselective cis-dihydroxylation of olefins," *Angewandte Chemie*, vol. 50, no. 46, pp. 10863–10866, 2011.

[17] K.-I. Fujita, S. Umeki, M. Yamazaki, T. Ainoya, T. Tsuchimoto, and H. Yasuda, "Magnetically recoverable osmium catalysts for dihydroxylation of olefins," *Tetrahedron Letters*, vol. 52, no. 24, pp. 3137–3140, 2011.

[18] K. I. Fujita, S. Umeki, M. Yamazaki, T. Ainoya, T. Tsuchimoto, and H. Yasuda, "Acid-induced conformational alteration of cis-preferential aromatic amides bearing N-methyl-N-(2-pyridyl) moiety," *Tetrahedron*, vol. 66, pp. 8536–8543, 2010.

[19] T. Matsuda, R. Yamanaka, and K. Nakamura, "Recent progress in biocatalysis for asymmetric oxidation and reduction," *Tetrahedron Asymmetry*, vol. 20, no. 5, pp. 513–557, 2009.

[20] R. N. Patel, "Biocatalysis: synthesis of chiral intermediates for drugs," *Current Opinion in Drug Discovery and Development*, vol. 9, no. 6, pp. 741–764, 2006.

[21] H. Stecher and K. Faber, "Biocatalytic deracemization techniques: dynamic resolutions and stereoinversions," *Synthesis*, no. 1, pp. 1–16, 1997.

[22] G. R. Allan and A. J. Carnell, "Microbial deracemization of 1-Aryl and 1-heteroaryl secondary alcohols," *Journal of Organic Chemistry*, vol. 66, no. 19, pp. 6495–6497, 2001.

[23] T. Tanaka, N. Iwai, T. Matsuda, and T. Kitazume, "Utility of ionic liquid for Geotrichum candidum-catalyzed synthesis of optically active alcohols," *Journal of Molecular Catalysis B*, vol. 57, no. 1–4, pp. 317–320, 2009.

[24] J. H. Schrittwieser, J. Sattler, V. Resch, F. G. Mutti, and W. Kroutil, "Recent biocatalytic oxidation-reduction cascades," *Current Opinion in Chemical Biology*, vol. 15, no. 2, pp. 249–256, 2011.

[25] Y. Shimada, Y. Miyake, H. Matsuzawa, and Y. Nishibayashi, "Ruthenium-catalyzed sequential reactions: deracemization of secondary benzylic alcohols," *Chemistry*, vol. 2, no. 3, pp. 393–396, 2007.

[26] L. Ou, Y. Xu, D. Ludwig, J. Pan, and J. H. Xu, "Chemoenzymatic deracemization of chiral secondary alcohols: process optimization for production of (R)-1-indanol and (R)-1-phenylethanol," *Organic Process Research and Development*, vol. 12, no. 2, pp. 192–195, 2008.

[27] N. Bouzemi, L. Aribi-Zouioueche, and J.-C. Fiaud, "Combined lipase-catalyzed resolution/Mitsunobu esterification for the production of enantiomerically enriched arylalkyl carbinols," *Tetrahedron Asymmetry*, vol. 17, no. 5, pp. 797–800, 2006.

[28] G. R. A. Adair and J. M. J. Williams, "A novel ruthenium catalysed deracemisation of alcohols," *Chemical Communications*, no. 44, pp. 5578–5579, 2005.

[29] G. Fantin, M. Fogagnolo, P. P. Giovannini, A. Medici, and P. Pedrini, "Combined microbial oxidation and reduction: a new approach to the high-yield synthesis of homochiral unsaturated secondary alcohols from racemates," *Tetrahedron*, vol. 6, no. 12, pp. 3047–3053, 1995.

[30] S. M. Mantovani, C. F. F. Angolini, and A. J. Marsaioli, "Chiral organoselenium-transition-metal catalysts in asymmetric transformations," *Tetrahedron*, vol. 20, pp. 2635–2638, 2009.

[31] C. V. Voss, C. C. Gruber, K. Faber, T. Knaus, P. Macheroux, and W. Kroutil, "Orchestration of concurrent oxidation and reduction cycles for stereoinversion and deracemisation of sec-alcohols," *Journal of the American Chemical Society*, vol. 130, no. 42, pp. 13969–13972, 2008.

[32] T. Utsukihara, O. Misumi, K. Nakajima et al., "Highly efficient and regioselective production of an erythorbic acid glucoside using cyclodextrin glucanotransferase from Thermoanaerobacter sp. and amyloglucosidase," *Journal of Molecular Catalysis B*, vol. 51, pp. 19–23, 2008.

[33] B. A. Persson, A. L. E. Larsson, M. Le Ray, and J. E. Bäckvall, "(S)-selective dynamic kinetic resolution of secondary alcohols by the combination of subtilisin and an aminocyclopentadienylruthenium complex as the catalysts," *Journal of the American Chemical Society*, vol. 121, pp. 1645–1650, 1999.

[34] N. J. Turner, "Deracemisation methods," *Current Opinion in Chemical Biology*, vol. 14, no. 2, pp. 115–121, 2010.

[35] Y. Nie, Y. Xu, T. F. Lv, and R. Xiao, "Enhancement of Candida parapsilosis catalyzing deracemization of (R,S)-1-phenyl-1, 2-ethanediol: agitation speed control during cell cultivation," *Journal of Chemical Technology and Biotechnology*, vol. 84, no. 3, pp. 468–472, 2009.

[36] C. V. Voss, C. C. Gruber, and W. Kroutil, "Deracemization of secondary alcohols through a concurrent tandem biocatalytic oxidation and reduction," *Angewandte Chemie*, vol. 47, no. 4, pp. 741–745, 2008.

[37] K. Nakamura, M. Fujii, and Y. Ida, "The use of chiral BINAM NHC-Rh (III) complexes in enantioselective hydrosilylation of 3-oxo-3-arylpropionic acid methyl or ethyl esters," *Tetrahedron*, vol. 12, pp. 3147–3153, 2001.

[38] W. Hummel and B. Riebel, "Chiral alcohols by enantioselective enzymatic oxidation," *Annals of the New York Academy of Sciences*, vol. 799, pp. 713–716, 1996.

[39] L. S. Chen, S. M. Mantovani, L. G. de Oliveira, M. C. T. Duarte, and A. J. Marsaioli, "1,2-Octanediol deracemization by stereoinversion using whole cells," *Journal of Molecular Catalysis B*, vol. 54, no. 1-2, pp. 50–54, 2008.

[40] Q. Hu, Y. Xu, and Y. Nie, "Enhancement of Candida parapsilosis catalyzing deracemization of (R,S)-1-phenyl-1,2-ethanediol to its (S)-enantiomer by a highly productive "two-in-one" resin-based in situ product removal strategy," *Bioresource Technology*, vol. 101, no. 21, pp. 8461–8463, 2010.

[41] C. C. Gruber, I. Lavandera, K. Faber, and W. Kroutil, "From a racemate to a single enantiomer: deracemization by stereoinversion," *Advanced Synthesis and Catalysis*, vol. 348, no. 14, pp. 1789–1805, 2006.

[42] E. Ricca, B. Brucher, and J. H. Schrittwieser, "Multi-enzymatic cascade reactions: overview and perspectives," *Advanced Synthesis and Catalysis*, vol. 353, no. 13, pp. 2239–2262, 2011.

[43] M. L. Ji, Y. Na, H. Han, and S. Chang, "Cooperative multi-catalyst systems for one-pot organic transformations," *Chemical Society Reviews*, vol. 33, no. 5, pp. 302–312, 2004.

[44] P. Salehi, M. Dabiri, M. A. Zolfigol, and M. A. B. Fard, "Silica sulfuric acid; an efficient and reusable catalyst for regioselective ring opening of epoxides by alcohols and water," *Phosphorus, Sulfur and Silicon and the Related Elements*, vol. 179, no. 6, pp. 1113–1121, 2004.

[45] S. M. Amrutkar, L. Banoth, and U. C. Banerjee, "One-pot synthesis of (R)-1-(1-naphthyl)ethanol by stereoinversion using Candida parapsilosis," *Tetrahedron Letters*, vol. 54, pp. 3274–3277, 2013.

[46] A. Singh, Y. Chisti, and U. C. Banerjee, "Stereoselective biocatalytic hydride transfer to substituted acetophenones by the yeast Metschnikowia koreensis," *Process Biochemistry*, vol. 47, pp. 2398–2404, 2012.

[47] A. Singh, Y. Chisti, and U. C. Banerjee, "Production of carbonyl reductase by Metschnikowia koreensis," *Bioresource Technology*, vol. 102, no. 22, pp. 10679–10685, 2011.

Hindawi Publishing Corporation
BioMed Research International
Volume 2013, Article ID 872940, 8 pages
http://dx.doi.org/10.1155/2013/872940

Research Article

Green and Rapid Synthesis of Anticancerous Silver Nanoparticles by *Saccharomyces boulardii* and Insight into Mechanism of Nanoparticle Synthesis

Abhishek Kaler,[1] Sanyog Jain,[2] and Uttam Chand Banerjee[1]

[1] *Department of Pharmaceutical Technology (Biotechnology), National Institute of Pharmaceutical Education and Research, Sector-67, SAS Nagar, Punjab 160062, India*
[2] *Centre for Pharmaceutical Nanotechnology, Department of Pharmaceutics, National Institute of Pharmaceutical Education and Research, Sector-67, SAS Nagar, Punjab 160062, India*

Correspondence should be addressed to Uttam Chand Banerjee; ucbanerjee@niper.ac.in

Received 28 April 2013; Accepted 3 October 2013

Academic Editor: Maria Alice Zarur Coelho

Rapidly developing field of nanobiotechnology dealing with metallic nanoparticle (MNP) synthesis is primarily lacking control over size, shape, dispersity, yield, and reaction time. Present work describes an ecofriendly method for the synthesis of silver nanoparticles (AgNPs) by cell free extract (CFE) of *Saccharomyces boulardii*. Parameters such as culture age (stationary phase growth), cell mass concentration (400 mg/mL), temperature (35°C), and reaction time (4 h), have been optimized to exercise a control over the yield of nanoparticles and their properties. Nanoparticle (NP) formation was confirmed by UV-Vis spectroscopy, elemental composition by EDX (energy dispersive X-rays) analysis, and size and shape by transmission electron microscopy. Synthesized nanoparticles had the size range of 3–10 nm with high negative zeta potential (−31 mV) indicating excellent stability. Role of proteins/peptides in NP formation and their stability were also elucidated. Finally, anticancer activity of silver nanoparticles as compared to silver ions was determined on breast cancer cell lines.

1. Introduction

Classical physicochemical synthetic procedures of metal nanoparticles suffer from drawbacks such as polydispersity, low yield [1], and use of toxic reagents [2]. Traditional role of nanosilver as an antimicrobial agent [3] and an anti-inflammatory agent [4] is well known. Recently, nanosilver has found application in electrical batteries [5], as optical receptors in solar batteries [6], biolabelling [7], and in cancer treatment [8]. Considering such wide range of applications of AgNPs, there is a need to develop clean, nontoxic, and ecofriendly synthetic approach. Microorganisms (bacteria, fungi, yeast, etc.) are known to produce inorganic materials synthetic protocols for nanoparticle production that utilizes ecofriendly nanofactories. There are numerous reports available on the formation of various MNPs by microorganisms from their corresponding salts [9–12]. Microbial systems are mainly advantageous in terms of ecofriendliness. However, major drawbacks associated with these systems are longer reaction time, tedious purification steps, higher size of all nanoparticles, and poor understanding of mechanism. Microorganisms can synthesize nanoparticles both extracellularly and intracellularly, the former being advantageous as it minimizes the number of steps in downstream processing. The present work describes a method that utilized cell free extract of *S. boulardii* for the synthesis of silver nanoparticle in pure form. Furthermore, to gain control on the shape and size of the nanoparticle and to increase its yield, the effect of the physicochemical environment for CFE production has been checked and process parameters were optimized. Longer reaction time was shortened by concentrating CFE using freeze dryer. Finally, role of proteins and/or peptides in NP formation and their stabilization were established by inactivating the cellular machinery at various growth levels and by FTIR technique. Many metals including platinum [13], copper [14], and selenium [15], are being proven to be

useful as anticancer agents. The nano form of silver was also compared to its ionic form against breast cancer cell lines for its enhanced activity.

2. Materials and Methods

2.1. Chemicals. Silver nitrate (99.99%) was purchased from Sigma-Aldrich (Steinheim, Germany). Unless specified, different salts and media components were purchased from HiMedia (Mumbai, India).

2.2. Microorganism and Culture Conditions. The yeast *Saccharomyces boulardii*, a probiotic strain, was purchased from a local market. Seed culture was developed by inoculating a single colony of *S. boulardii* into growth medium (20 mL) containing peptone (3 g/L), yeast extract (3 g/L), and dextrose (10 g/L). The culture was incubated at 35°C for 24 h at 200 rpm after adjusting the pH to 6.5. Inoculum (2% v/v) was transferred to the production medium of the same composition and culture was grown for 48 h at 35°C and 200 rpm. After sufficient growth, cell mass was harvested by centrifugation at 10,000 ×g for 10 min. Cell mass was washed thrice with deionised water to remove remaining media components from cell surface and used for CFE preparation.

2.3. Preparation of Cell Free Extract (CFE). Harvested *S. boulardii* cells were resuspended in deionised water to obtain desired cell mass concentration. This cell suspension was incubated at 35°C for 36 h at 200 rpm. After 36 h, cell suspension was centrifuged at 10,000 ×g for 10 min and supernatant was collected. Cell free extract was also lyophilized to powder form and resuspended in minimum volume of deionised water. Silver nitrate was added and reaction was allowed to proceed in dark for specific period of time with periodic sampling.

2.4. Synthesis and Characterization of Silver Nanoparticles. Silver nitrate (1 mM) was added to cell free extract (10 mL) (prepared from cells harvested after 48 h of growth and having 100 mg/mL cell mass concentration) in a conical flask of 50 mL capacity. The reaction was allowed to proceed at 35°C (200 rpm) in the dark environment for 72 h. Two controls were used simultaneously (one having only silver nitrate in deionised water and other having only CFE without silver nitrate). The reaction mixture was periodically analyzed using U-3010 UV-Vis spectrophotometer (Hitachi) in the range of 200–800 nm unless the further increase in absorbance ceased. Synthesized Ag-nanoparticles were visualized by transmission electron microscopy (Hitachi, H-7500 instrument at a voltage of 80 kV). Silver nanoparticle film was formed on carbon coated copper grids and the micrograph of the sample was recorded. For the determination of particle potential, dynamic light scattering analysis was done using zeta sizer (Malvern Zeta Sizer, Nano-ZS). Biochemical nature of the capping agent present on surface of silver nanoparticles was determined using Fourier transform infrared spectroscope (FTIR). Energy-dispersive X-ray (EDX) spectra were obtained on a JEOL JEM-2010F microscope operated at 200 kV.

2.5. Bradford Assay for Protein Determination. The protein content was determined by Bradford assay, using BSA as a standard [16]. The absorbance was measured on MultiSkan Thermo 96-well plate reader at 595 nm. All the experiments were performed in triplicates on 96-well plates.

3. Optimization of Physicochemical Parameters for the Synthesis of Silver Nanoparticles

3.1. Cell Age and Its Concentration. To determine optimum cell age for the nanoparticle synthesis, yeast cells were harvested at different phases of their growth (log phase, early stationary phase, and late stationary phase). Harvested cells from different growth phases were then resuspended in deionised water and cell free extract was prepared as mentioned above. This cell free extract was used to synthesize silver nanoparticles in dark environment. After harvesting, wet cell mass was weighed correctly and then resuspended in the fixed volume of deionised water to give a specific concentration. Different concentrations of cells (25–500 mg/mL) were incubated in deionised water at 35°C, 200 rpm for 48 h followed by centrifugation at 10,000 ×g for 10 min. Upon addition of silver nitrate (final concentration 1 mM) to the cell free extract, reaction was carried out at 35°C, 200 rpm in dark environment.

3.2. Reaction Temperature. Effect of temperature on the nanoparticle synthesis was studied by incubating the cells in deionised water at various temperatures (20, 25, 30, 35, 40, and 45°C) for 48 h. Cell free extract was then collected by centrifugation at 10,000 ×g for 10 min. Silver nitrate was added to the cell free extract to a final concentration of 1 mM and reaction was allowed to proceed at the corresponding temperature and (200) rpm in dark environment.

3.3. Reaction pH. Hydrogen ion concentration of cell free extract was adjusted to acidic and basic values (pH range from 3 to 11) by acetic acid and sodium hydroxide, respectively. Reaction mixture containing CFE of various pH values and silver nitrate was incubated at 35°C for 48 h at 200 rpm in dark condition.

3.4. Reaction Time. Effect of reaction time was studied by incubating the reaction mixture at optimized condition up to 72 h. Samples were taken at a periodic interval and analyzed by UV-Vis spectrophotometer.

4. Use of Cellular Machinery in Nanoparticle Synthesis

Role of various cellular preparations was evaluated to have an insight into the process of nanoparticle biosynthesis. Initially, nanoparticle synthesis was carried out by resuspending whole cells in deionised water and using it as reaction mixture. The process required the disintegration of cells to recover nanoparticles, making downstream process difficult. To evaluate the involvement of cellular components in nanoparticle

synthesis, at the same time, cells after sufficient growth were heat-killed in growth medium by autoclaving, centrifuged out, and resuspended in deionised water. Separate set of experiments were carried out on the harvested cells (alive) that were resuspended in deionised water and heat-killed by boiling them for half an hour in water bath. To all the preparations, silver nitrate was added to a final concentration of 1 mM and reaction was allowed for 72 h (200 rpm) in dark conditions. It may also be mentioned that supernatant from microbial growth did not perform the reaction.

Cell free extract was developed at later stages with the purpose of making the reaction system extracellular. To establish the correlation between metabolic machineries of whole cells and CFE, further experiments were performed on cell free extract. Cell free extract was separated into three fractions. First fraction was boiled to denature proteins/enzymes. Second fraction was kept within dialysis membrane (10 KDa) and placed in a beaker containing silver salt solution. Third fraction was a control reaction containing cell free extract and silver nitrate. To all the fractions, silver nitrate solution (1 mM) was added and reaction was allowed to proceed for 72 h.

In another set of experiments, further hint about nature of enzyme was explored. Silver nanoparticle formation is a reduction process and might have involved a reducing enzyme. That reducing enzyme in most of the cases depends on the cofactors. To check whether protein (that could be enzyme also) involved in reduction process is dependent on cofactor, exogenous cofactor (NADH) was added to the reaction mixture.

5. Cytotoxicity Studies of Silver Nanoparticles

Cytotoxicity study was done by a method developed by Skehan et al. [17]. Briefly, MCF-7 cells were harvested in log phase using trypsin (0.05% trypsin, 0.02% EDTA, in PBS), counted using a haemocytometer and 1×10^4 cells/well in an aliquot of 100 μL were seeded in 96-wells cell culture plates. The cells were incubated for 24 h (at 37°C in an atmosphere of 5% CO_2 and 95% relative humidity in a CO_2 incubator) to adhere. Test materials (100 μL/well) were then added to the wells. The plates were further incubated for 24 h in the CO_2 incubator. The cells were then fixed by gently layering trichloroacetic acid (50 μL/well, 50% w/v) on top of the medium in all the wells and incubated at 4°C for 1 h. The plates were washed five times with distilled water and air-dried. Cell growth was measured by staining with sulforhodamine B dye (0.4% w/v in 1% acetic acid, 100 μL/well). The unbound dye was washed 3–5 times with 1% acetic acid and plates were air dried. The adsorbed dye was dissolved in Tris-buffer (100 μL/well, 0.01 M, pH 10.4) and plates were gently shaken for 10 min on a mechanical shaker. The optical density (OD) was recorded using a 96-well plate reader at 540 nm. Growth inhibition was calculated by the following formula:

$$\% \text{ Growth inhibition} = 100 - \left[\frac{OD_{\text{test sample}} - OD_{\text{blank}}}{OD_{\text{control}} - OD_{\text{blank}}}\right] \times 100. \quad (1)$$

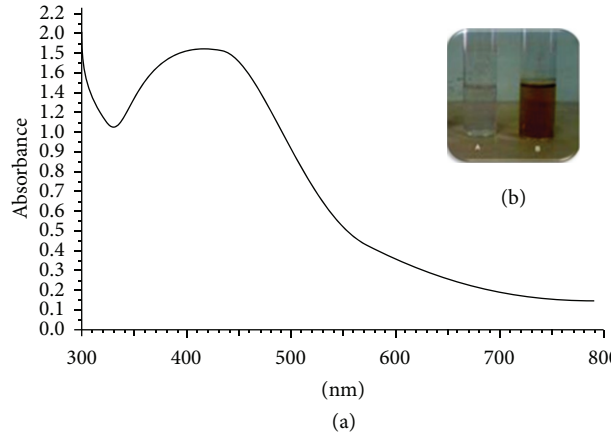

Figure 1: (a) UV-Vis spectrum of CFE in deionised water reacted with silver nitrate (1 mM) for 72 h. (b) Vials containing CFE of *S. boulardii* in deionised water without silver nitrate (Vial A) and with silver nitrate (1 mM) (Vial B) after 72 h incubation at 30°C, 200 rpm.

6. Results and Discussion

First step was to develop a catalyst system that can be used to synthesize stable nanoparticles in simple way while minimizing down streaming process. In an attempt to device a greener and less tedious methodology for the AgNPs formation, cell free extract was prepared. Factor(s) responsible for the reduction of metal salt may include but not limited to proteins, enzymes, and amino acid. Keeping in view these factors, cells were harvested from media and resuspended in demineralised water to prepare cell free extract. Formation of AgNPs was accompanied by colour change of the solution from colourless to dark brown which showed absorption in the visible range of electromagnetic radiation [12]. The formation of silver nanoparticles in the solution was confirmed by UV-Vis spectral analysis. Figure 1(a) shows UV-Vis spectrum of reaction mixture containing CFE and silver nitrate (1 mM) incubated for 72 h. Strong absorption at 420 nm confirms the formation of silver nanoparticles in solution. Parallel control experiments containing only CFE (without $AgNO_3$) and $AgNO_3$ solution (without CFE) did not show any absorption at ~420 nm. Figure 1(b) shows two vials, one containing only CFE of *S. boulardii* (Vial A) and another containing reaction mixture of CFE and silver nitrate (Vial B), both incubated for 72 h at 35°C (200 rpm). Colour of the solution in vial B changed from colourless to dark brown gradually, while vial A did not exhibit any colour change.

Figure 2(a) shows a representative TEM image of monodispersed AgNPs with size range of 3–10 nm. Previous investigators have reported the synthesis of Ag-nanoparticles having particle size of around 60 nm [18]. Dynamic light scattering analysis of the colloidal solution further confirmed monodispersity of the synthesized particles (PDI of 0.34). Zeta potential value of −31 mV on nanoparticles, indicates the presence of negatively charged molecules on the particles, which prevents them from agglomeration. Elemental composition of synthesized nanoparticle was determined by EDX spectra that showed strong signal of Ag^0 with high weight percentage of Ag (Figure 2(b)).

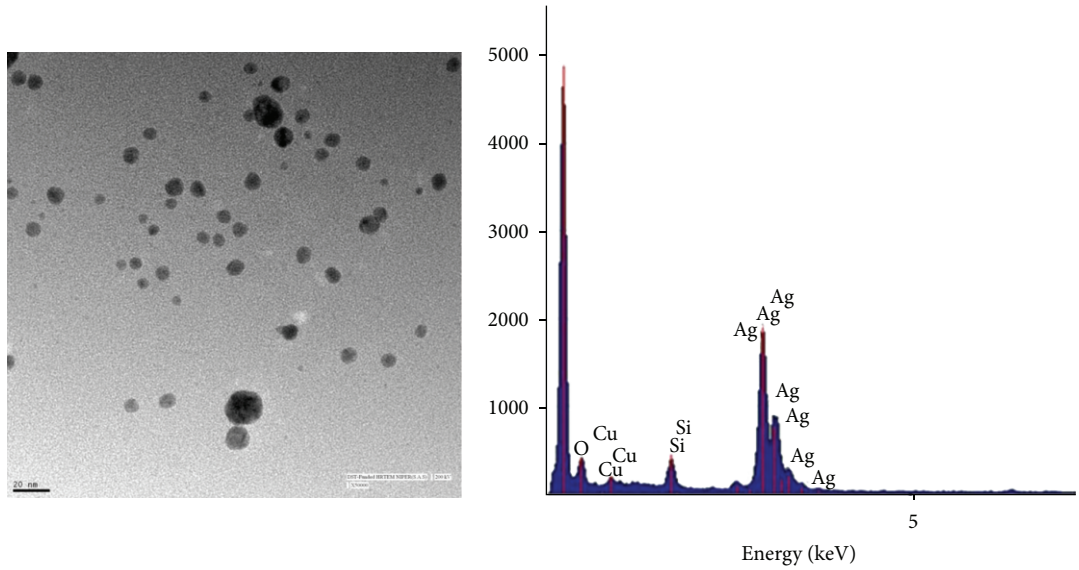

Figure 2: (a) TEM image and (b) EDX image of silver nanoparticles synthesised by CFE of *S. boulardii* in deionised water with silver nitrate (1 mM) after 12 h incubation at 37°C, 200 rpm.

FTIR analysis carried out on a drop-coated film of the silver nanoparticle that showed the presence of two bands of N–H and carbonyl at 3353 cm^{-1} and 1650 cm^{-1} due to the stretching vibrational frequency of amide bond, respectively. Bands at 1403 cm^{-1} are due to the side chain of amino acid such as CN stretch of amino group or carboxy group. Peak at 1049 cm^{-1} have aroused due to the aliphatic C–O stretching vibration (serine C–OH). All these observations indicate the involvement of proteins in the reduction and capping process. Previous reports have supported this fact where metal-protein interaction has been shown [19, 20]. Ahmad et al. [12] and Kalimuthu et al. [21] have reported the involvement of a nitrate reductase in a NADH dependent reduction of silver ion to metallic silver. *Fusarium oxysporum* is known to carryout a similar reduction through a nitrate dependent reductase which acts in shuttle with quinone [22].

Studies by Balaji et al. [23] have proved the role of carbonyl groups from amino acid residues and peptides of proteins to have strong affinity to Ag. This protein works by forming a protective coat on the nanoparticle surface preventing its aggregation and thus in stabilisation.

Preliminary results established CFE as a suitable replacement of whole cells for Ag-nanoparticle synthesis. Therefore, conditions affecting CFE generation were evaluated and various reaction parameters were optimized. Metabolic activities of the cells vary with its age and CFE prepared from these cells will vary in composition as well as in the corresponding activity. Figure 3(a) shows the varying effect on nanoparticle synthesis of CFE prepared from the cells harvested during different phases of growth (log phase, early stationary phase, and late stationary phase). CFE obtained from early stationary phase cells was the most efficient for nanoparticle synthesis. Furthermore, incubation period of 36 h gave better results as longer period of incubation of the cells at 40°C might have led to the denaturation of the proteins.

Silver ions beyond a certain limit can be toxic to proteins as they can cause precipitation. To prevent precipitation, ionic forms are transformed to nanoparticles by proteins. To determine maximum tolerable limit of CFE proteins to silver ions, different concentrations of silver nitrate were added. Figure 3(b) shows that no significant increase in absorption was there with the increase in silver nitrate concentration from 1 to 5 mM. That might be due to higher toxicity of silver ions at this concentration. Subsequent experiments were carried out with 1 mM salt concentration. Temperature can affect the rate as well as extent of protein/peptide release into the surrounding medium during CFE formation. Secondly, rate of reaction can be controlled by varying the reaction temperature. The effect of temperature on CFE formation was studied by incubating cell mass at different temperatures. Figure 3(c) shows the UV-Vis spectra of the Ag-nanoparticles formed with the CFE prepared at different temperatures. As the temperature of CFE preparation was increased the concentration of nanoparticles was found to increase. Optimum temperature for CFE formation was found to be 40°C beyond which there was again a fall in the absorbance of synthesized nanoparticles. Plausible explanation could be that at higher temperature the cells might have released more reducing agent due to thermal shock. Still at higher temperature (>40°C), protein denaturation might take place leading to fall in nanoparticle synthesis. Gericke and Pinches [24] also found similar effect of temperature for the Au-nanoparticle synthesis using *Verticillium luteoalbum* whole cells.

Nanoparticle formation starts following the process of crystallisation process which depends on factors like solubility of substrate and its supersaturation. Effect of pH on solubility of substrate is known and change in pH can affect

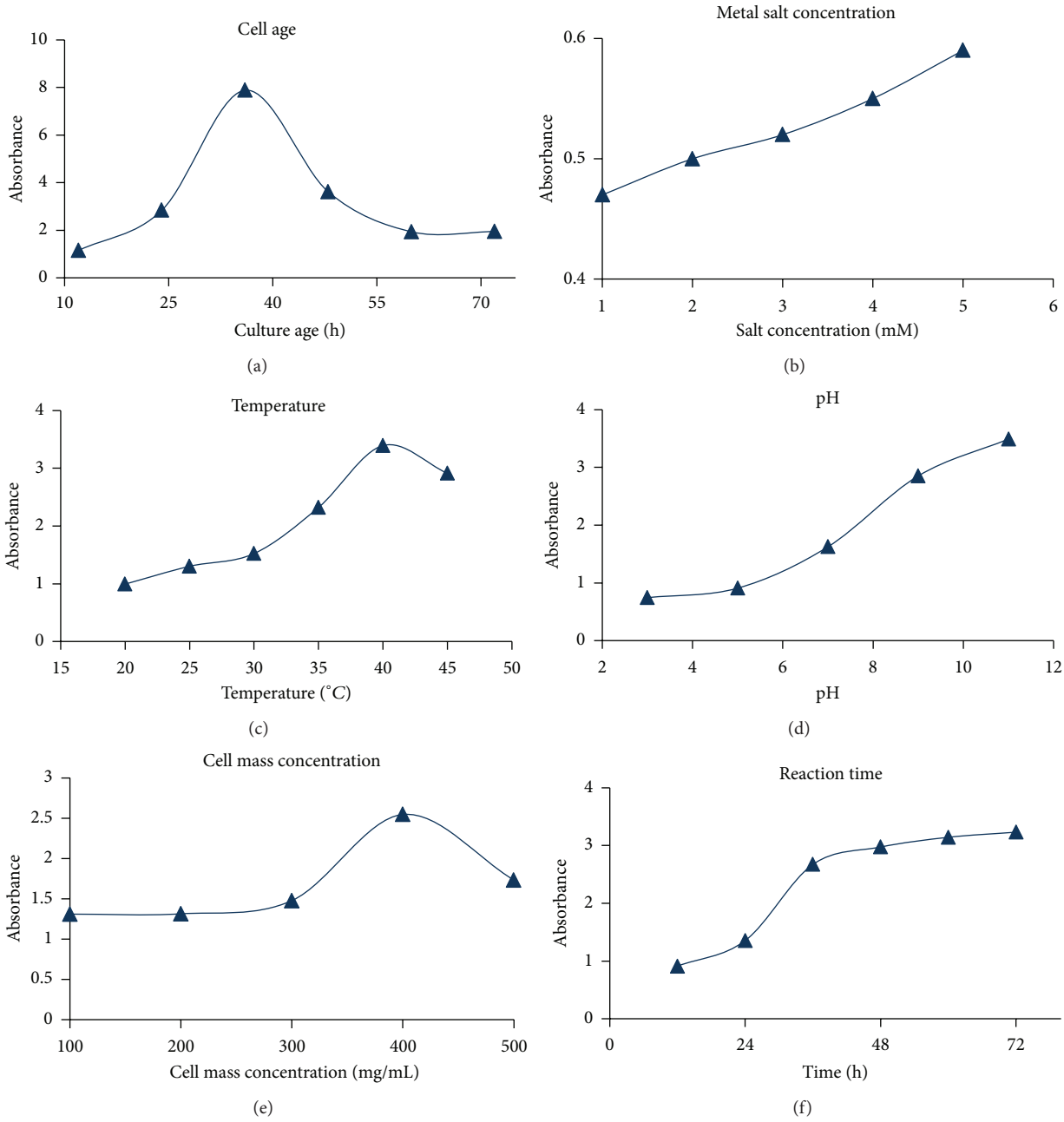

Figure 3: Optimisation of various physicochemical parameters for the synthesis of silver nanoparticles by cell free extract of *Saccharomyces boulardii*.

the nanoparticle synthesis as well as morphology [25]. It was observed in the present study that nanoparticle formation was higher at higher pH value. The increased synthesis of nanoparticles at higher pH is however nullified by the formation of aggregates at this pH. Optimum pH which showed significant yield without aggregation was selected to be 7 for further studies (Figure 3(d)). Concentration of reducing agent in CFE can be varied by varying the cell concentration used for preparation of CFE. Figure 3(e) summarizes the effect of CFE prepared using different cell mass concentrations on the nanoparticle formation. Average size of the particles decreased and yield increased with increase in reductant concentration in the CFE (Figure 3(e)). Smallest particle size was obtained with the CFE prepared from 400 mg/mL cell mass concentration. Also, the UV-Vis spectra showed the highest absorbance by nanoparticles formed by the CFE prepared from the increased amount of cell mass. Higher ratio of reducing agent to substrate accelerated the reduction of the Ag^{+} to Ag^{0} immediately followed by capping by the capping agents preventing from aggregation. Recent literature on metallic nanoparticle synthesis has demonstrated the use of whole cells for both

extracellular as well as intracellular nanoparticle formation [26, 27].

Time taken to complete nanoparticle synthesis is an important parameter from an industrial point of view. Moreover, aggregate formation of nanoparticles, a sign of instability, is also a problem when longer reaction time is desired. After optimization of the above mentioned parameters, it was found that nanoparticle synthesis was completed after 36 h as compared to initial 72 h of reaction in unoptimized conditions (Figure 3(f)).

Longer time taken to synthesize silver nanoparticle can be attributed to two factors. First is low redox potential of silver and second being dilute CFE. To overcome this problem, CFE was concentrated by lyophilisation technique. Lyophilisation of proteins can have deleterious effect on their properties and activity [28]. In the present case, however, it did not pose any such problem. CFE after concentration to powder form was resuspended in minimum volume of deionised water and subjected to reaction with silver nitrate as mentioned above. This step significantly reduced the reaction time from 36 h to 4 h with reaction that started immediately after addition of substrate.

To establish the role of cellular machinery in nanoparticle synthesis, yeast cells were subjected to heat treatment at various stages of growth. The cells were grown upto stationary phase and then killed and prepared for CFE. Heat-killed cells during growth phase (Figure 4(b)) were not able to produce AgNPs when treated with silver nitrate. This simple experimentation shows that nanoparticle synthesis essentially depends upon the active metabolites obtained from the native cells and not from the heat-killed cells. The results of Bradford assay showed the presence of protein in the cell free extract. It was assumed that small proteins/peptides are extracted out of cell due to osmotic shock during CFE formation. UV-Vis spectra of CFE (Figure 4(a)) showed a strong absorption at 280 nm which may be attributed to the aromatic residues (tyrosine and tryptophan) present in the protein or peptide.

The above assumption was strengthened by boiling a fraction of CFE and checking this fraction for its ability to synthesise AgNPs. This fraction did not synthesize nanoparticles and this can be attributed to denaturation of proteins present in CFE. Involvement of macromolecule like protein is further confirmed by placing a barrier (dialysis membrane, 10 KDa) between CFE and silver nitrate solution. Protein extract was placed in membrane which was dipped in a beaker containing silver nitrate solution. Beaker was kept in dark and after 72 h dark brown colour was observed in membrane but not in surrounding solution. This indicates that the size of macromolecule required for nanoparticle synthesis is greater than 10 KDa. Controlled reaction shows development of dark brown colour indicative of AgNPs formation.

Figure 4(c) shows the effect of cofactor on nanoparticle synthesis. Dark brown colour was developed in reaction mixture containing exogenously added cofactor, while colour intensity was less in flask without cofactor. Control containing only cofactor did not show any colour change. This proves

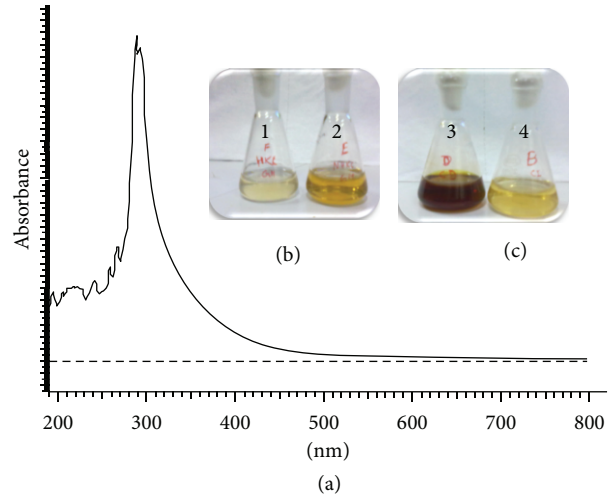

Figure 4: (a) UV-Vis spectra of cell free extract prepared from *Saccharomyces boulardii* in deionised water. (b) Colour comparison between reaction mixtures containing cells killed (1) in production media and control (2). (c) Colour comparison between reaction mixtures containing cofactors (3) and control (4).

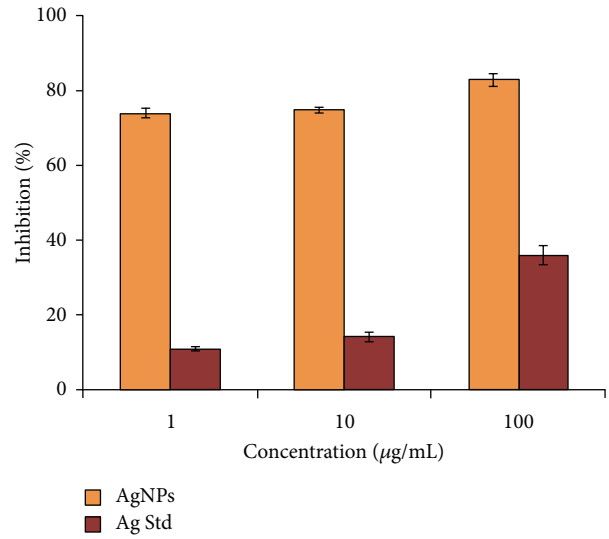

Figure 5: In vitro anticancer activities of silver nanoparticles synthesized by cell free extract of *S. boulardii*.

the dependence of possible enzyme on cofactor and that the reaction is a redox reaction.

Anticancer activity of silver nanoparticles was evaluated on MCF-7 cells in comparison to ionic silver salt (Figure 5). Silver nanoparticles at very low concentration showed very high activity on MCF-7 cells, showing almost 80% inhibition at this stage also. At higher concentration (10–100 μg/mL), no significant difference in inhibition of cancer cells was observed with silver nanoparticles. On the other hand, silver ions were able to achieve less than half of this even at 100 μg/mL of concentration. This indicates that the IC_{50} value for the silver nanoparticles synthesized by *S. boulardii* whole cells is less than 10 μg/mL.

7. Conclusion

There are many reports that describe methods making use of microbes for the synthesis of nanoparticles [29–32] as an alternative to cost-ineffective and toxic procedures [1, 2]. The present method describes the first time use of cell free extract of *S. boulardii* for the synthesis of silver nanoparticles. Resulted nanoparticles were smaller in size, uniform, monodispersed in nature, and were synthesised very rapidly. This method does not require tedious downstream processing and it may be scaled up to develop a viable technology for the Ag-nanoparticle synthesis. Preliminary studies confirm the role of protein in the synthesis and stabilisation of nanoparticles. Anticancer activity on early stage breast cancer cell lines gave very promising results and this application may be valuable for future biomedical research.

Conflict of Interests

None of the authors have a financial interest in any of the products, devices, or drugs mentioned in this paper.

Acknowledgments

Abhishek Kaler would like to thank the Department of Biotechnology, Government of India, for providing research fellowships. The author also gratefully acknowledges Dr. Jayeeta Bhaumik for critically going through the paper.

References

[1] K. Kowlgi, U. Lafont, M. Rappolt, and G. Koper, "Uniform metal nanoparticles produced at high yield in dense microemulsions," *Journal of Colloid and Interface Science*, vol. 372, no. 1, pp. 16–23, 2012.

[2] K. N. Thakkar, S. S. Mhatre, and R. Y. Parikh, "Biological synthesis of metallic nanoparticles," *Nanomedicine*, vol. 6, no. 2, pp. 257–262, 2010.

[3] I. Sondi and B. Salopek-Sondi, "Silver nanoparticles as antimicrobial agent: a case study on *E. coli* as a model for Gram-negative bacteria," *Journal of Colloid and Interface Science*, vol. 275, no. 1, pp. 177–182, 2004.

[4] P. L. Nadworny, J. Wang, E. E. Tredget, and R. E. Burrell, "Anti-inflammatory activity of nanocrystalline silver in a porcine contact dermatitis model," *Nanomedicine*, vol. 4, no. 3, pp. 241–251, 2008.

[5] T. Klaus-Joerger, R. Joerger, E. Olsson, and C. Granqvist, "Bacteria as workers in the living factory: metal-accumulating bacteria and their potential for materials science," *Trends in Biotechnology*, vol. 19, no. 1, pp. 15–20, 2001.

[6] S. Schultz, D. R. Smith, J. J. Mock, and D. A. Schultz, "Single-target molecule detection with nonbleaching multicolor optical immunolabels," *Proceedings of the National Academy of Sciences of the United States of America*, vol. 97, no. 3, pp. 996–1001, 2000.

[7] S. Xu, X. Ji, W. Xu et al., "Immunoassay using probe-labelling immunogold nanoparticles with silver staining enhancement via surface-enhanced Raman scattering," *Analyst*, vol. 129, no. 1, pp. 63–68, 2004.

[8] P. Gopinath, S. K. Gogoi, P. Sanpui, A. Paul, A. Chattopadhyay, and S. S. Ghosh, "Signaling gene cascade in silver nanoparticle induced apoptosis," *Colloids and Surfaces B*, vol. 77, no. 2, pp. 240–245, 2010.

[9] T. Klaus, R. Joerger, E. Olsson, and C. Granqvist, "Silver-based crystalline nanoparticles, microbially fabricated," *Proceedings of the National Academy of Sciences of the United States of America*, vol. 96, no. 24, pp. 13611–13614, 1999.

[10] B. Nair and T. Pradeep, "Coalescence of nanoclusters and formation of submicron crystallites assisted by lactobacillus strains," *Crystal Growth and Design*, vol. 2, no. 4, pp. 293–298, 2002.

[11] M. Kowshik, N. Deshmukh, W. Vogel, J. Urban, S. K. Kulkarni, and K. M. Paknikar, "Microbial synthesis of semiconductor CdS nanoparticles, their characterization, and their use in the fabrication of an ideal diode," *Biotechnology and Bioengineering*, vol. 78, no. 5, pp. 583–588, 2002.

[12] A. Ahmad, P. Mukherjee, S. Senapati et al., "Extracellular biosynthesis of silver nanoparticles using the fungus Fusarium oxysporum," *Colloids and Surfaces B*, vol. 28, no. 4, pp. 313–318, 2003.

[13] D. P. Gately and S. B. Howell, "Cellular accumulation of the anticancer agent cisplatin: a review," *British Journal of Cancer*, vol. 67, no. 6, pp. 1171–1176, 1993.

[14] A. De Vizcaya-Ruiz, A. Rivero-Muller, L. Ruiz-Ramirez et al., "Induction of apoptosis by a novel copper-based anticancer compound, casiopeina II, in L1210 murine leukaemia and CH1 human ovarian carcinoma cells," *Toxicology in Vitro*, vol. 14, no. 1, pp. 1–5, 2000.

[15] M. P. Rayman, "Selenium in cancer prevention: a review of the evidence and mechanism of action," *Proceedings of the Nutrition Society*, vol. 64, no. 4, pp. 527–542, 2005.

[16] S. Han, C. Auger, V. P. Appanna et al., "A blue native polyacrylamide gel electrophoretic technology to probe the functional proteomics mediating nitrogen homeostasis in *Pseudomonas fluorescens*," *Journal of Microbiological Methods*, vol. 90, no. 3, pp. 206–210, 2012.

[17] P. Skehan, R. Storeng, D. Scudiero et al., "New colorimetric cytotoxicity assay for anticancer-drug screening," *Journal of the National Cancer Institute*, vol. 82, no. 13, pp. 1107–1112, 1990.

[18] N. S. Shaligram, M. Bule, R. Bhambure et al., "Biosynthesis of silver nanoparticles using aqueous extract from the compactin producing fungal strain," *Process Biochemistry*, vol. 44, no. 8, pp. 939–943, 2009.

[19] A. Gole, C. Dash, V. Ramakrishnan et al., "Pepsin-gold colloid conjugates: preparation, characterization, and enzymatic activity," *Langmuir*, vol. 17, no. 5, pp. 1674–1679, 2001.

[20] S. Mandal, S. Phadtare, and M. Sastry, "Interfacing biology with nanoparticles," *Current Applied Physics*, vol. 5, no. 2, pp. 118–127, 2005.

[21] K. Kalimuthu, R. Suresh Babu, D. Venkataraman, M. Bilal, and S. Gurunathan, "Biosynthesis of silver nanocrystals by *Bacillus licheniformis*," *Colloids and Surfaces B*, vol. 65, no. 1, pp. 150–153, 2008.

[22] N. Durán, P. D. Marcato, O. L. Alves, G. I. H. De Souza, and E. Esposito, "Mechanistic aspects of biosynthesis of silver nanoparticles by several *Fusarium oxysporum* strains," *Journal of Nanobiotechnology*, vol. 3, pp. 8–14, 2005.

[23] D. S. Balaji, S. Basavaraja, R. Deshpande, D. B. Mahesh, B. K. Prabhakar, and A. Venkataraman, "Extracellular biosynthesis of functionalized silver nanoparticles by strains of *Cladosporium cladosporioides* fungus," *Colloids and Surfaces B*, vol. 68, no. 1, pp. 88–92, 2009.

[24] M. Gericke and A. Pinches, "Biological synthesis of metal nanoparticles," *Hydrometallurgy*, vol. 83, no. 1–4, pp. 132–140, 2006.

[25] C. Blanco-Andujar, D. Ortega, Q. A. Pankhurstab, and N. T. K. Thanh, "Elucidating the morphological and structural evolution of iron oxide nanoparticles formed by sodium carbonate in aqueous medium," *Journal of Materials Chemistry*, vol. 22, pp. 12498–12506, 2012.

[26] N. Vigneshwaran, A. A. Kathe, P. V. Varadarajan, R. P. Nachane, and R. H. Balasubramanya, "Biomimetics of silver nanoparticles by white rot fungus, *Phaenero-chaete chrysosporium*," *Colloids and Surfaces B*, vol. 53, no. 1, pp. 55–59, 2006.

[27] M. F. Lengke, M. E. Fleet, and G. Southam, "Morphology of gold nanoparticles synthesized by filamentous cyanobacteria from gold(I)-Thiosulfate and gold(III)-chloride complexes," *Langmuir*, vol. 22, no. 6, pp. 2780–2787, 2006.

[28] J. F. Carpenter, S. J. Prestrelski, and A. Dong, "Application of infrared spectroscopy to development of stable lyophilized protein formulations," *European Journal of Pharmaceutics and Biopharmaceutics*, vol. 45, no. 3, pp. 231–238, 1998.

[29] D. R. Lovley, J. F. Stolz, G. L. Nord Jr., and E. J. P. Phillips, "Anaerobic production of magnetite by a dissimilatory iron-reducing microorganism," *Nature*, vol. 330, no. 6145, pp. 252–254, 1987.

[30] S. Mann, "Molecular tectonics in biomineralization and biomimetic materials chemistry," *Nature*, vol. 365, no. 6446, pp. 499–505, 1993.

[31] D. Pum and U. B. Sleytr, "The application of bacterial S-layers in molecular nanotechnology," *Trends in Biotechnology*, vol. 17, no. 1, pp. 8–12, 1999.

[32] T. J. Beveridge and R. G. E. Murray, "Sites of metal deposition in the cell wall of Bacillus subtilis," *Journal of Bacteriology*, vol. 141, no. 2, pp. 876–887, 1980.

Hindawi Publishing Corporation
BioMed Research International
Volume 2013, Article ID 268349, 9 pages
http://dx.doi.org/10.1155/2013/268349

Research Article

Biological Pretreatment of Rubberwood with *Ceriporiopsis subvermispora* for Enzymatic Hydrolysis and Bioethanol Production

Forough Nazarpour,[1] Dzulkefly Kuang Abdullah,[2] Norhafizah Abdullah,[1,3] Nazila Motedayen,[1] and Reza Zamiri[4]

[1] *Institute of Bioscience, Universiti Putra Malaysia, 43400 Serdang, Selangor, Malaysia*
[2] *Department of Chemistry, Faculty of Science, Universiti Putra Malaysia, 43400 Serdang, Selangor, Malaysia*
[3] *Department of Chemical and Environmental Engineering, Faculty of Engineering, Universiti Putra Malaysia, 43400 Serdang, Selangor, Malaysia*
[4] *Department of Materials Engineering and Ceramic, CICECO, University of Aveiro, Campus Santiago, 3810-193 Aveiro, Portugal*

Correspondence should be addressed to Dzulkefly Kuang Abdullah; dzulkif@science.upm.edu.my and Norhafizah Abdullah; fizah@eng.upm.edu.my

Received 19 February 2013; Revised 16 July 2013; Accepted 23 August 2013

Academic Editor: Luciana Rocha Barros Gonçalves

Rubberwood (*Hevea brasiliensis*), a potential raw material for bioethanol production due to its high cellulose content, was used as a novel feedstock for enzymatic hydrolysis and bioethanol production using biological pretreatment. To improve ethanol production, rubberwood was pretreated with white rot fungus *Ceriporiopsis subvermispora* to increase fermentation efficiency. The effects of particle size of rubberwood (1 mm, 0.5 mm, and 0.25 mm) and pretreatment time on the biological pretreatment were first determined by chemical analysis and X-ray diffraction and their best condition obtained with 1 mm particle size and 90 days pretreatment. Further morphological study on rubberwood with 1 mm particle size pretreated by fungus was performed by FT-IR spectra analysis and SEM observation and the result indicated the ability of this fungus for pretreatment. A study on enzymatic hydrolysis resulted in an increased sugar yield of 27.67% as compared with untreated rubberwood (2.88%). The maximum ethanol concentration and yield were 17.9 g/L and 53% yield, respectively, after 120 hours. The results obtained demonstrate that rubberwood pretreated by *C. subvermispora* can be used as an alternative material for the enzymatic hydrolysis and bioethanol production.

1. Introduction

In recent years, rising gas prices and environmental concerns cause the driving force for developing alternative energy sources, especially fuel ethanol for automobiles [1]. Unlike fossil fuel, ethanol has the advantages of being renewable, cleaner having a burning, and producing no greenhouse gases [2]. Lignocellulosic biomass is an attractive option for the sustainable production of fuels [3]. Therefore, using lignocellulosic biomass as the feedstock reduces the costs of bioethanol production as a result of its widespread availability, sustainable production, and cheap availability [4]. Currently, rubber tree (*Hevea brasiliensis*) which is also known as *Hevea* wood is the most abundant lignocellulosic material in Malaysia which can be used as a potential raw material for bioethanol production due to its high cellulose content (53.01%) [5].

Lignocellulosic materials are composed mainly of cellulose, hemicellulose, and lignin. Pretreatment, as the first step towards conversion of lignocellulose to ethanol, removes lignin and hemicellulose, reduces cellulose crystallinity, and increases the porosity of materials [6]. In general, pretreatment can be classified into physical pretreatment physicochemical pretreatment, chemical pretreatment, and biological pretreatment [7]. However, physical and chemical pretreatment need high temperature treatment with acid

or alkali, which disrupts lignocellulose and also results in acidic or caustic hydrolysate and the production of inhibitory byproducts [8, 9]; therefore, such pretreatment methods increase the cost of processes with neutralization or washing step that results in the loss of sugars [6, 10]. Consequently, it is necessary to develop a benign alternative to harsh chemicals.

Biological pretreatment applies microorganisms especially fungi and their enzyme systems to delignify cellulosic feedstocks [11]. White rot fungi with high selectivity of lignin degradation over cellulose are important for successful microbial pretreatment. Most white rot fungi, such as *Phanerochaete chrysosporium*, simultaneously degrade holocellulose (cellulose and hemicellulose) and lignin, resulting in a low cellulose recovery [12, 13]. Some species preferentially degrade lignin and part of the hemicellulose, leaving a cellulose rich residue [13, 14]. *Ceriporiopsis subvermispora* is one of the most investigated white rot fungi for pretreatment because of its selectively for lignin biodegradation with very low cellulose loss [15].

In this research, we used a woody biomass (rubberwood) as an alternative material for the fungal pretreatment and bioethanol production. To date no such work has been reported. The objective of this study was to evaluate the effects of fungal pretreatment of rubberwood by *C. subvermispora* on enzymatic hydrolysis and ethanol production. The changes in lignin, cellulose, and hemicellulose after pretreatment, hydrolysis conversion efficiency, and ethanol yield from fermentation were measured to evaluate pretreatment effectiveness. The effects of particle size on degradation of rubberwood are also investigated.

2. Materials and Methods

2.1. Microorganism. *Ceriporiopsis subvermispora* FP-90031-Sp (ATCC 90467) was purchased from American Type Culture Collection (ATCC) and maintained as a frozen culture (−80°C) in 30% glycerol. The fungus was incubated on 2.4% potato dextrose agar (PDA) plates at 28°C for 7 days.

2.2. Biomass Preparation. The wood was chipped using the lab scale chipper. The chips then were transferred to a Pallman disc flaker and cut to smaller particle size. After flaking, they were ground to pass through 0.25, 0.5, and 1.00 mm screens, respectively, and approximately dried to 5% moisture content in an oven at 103 ± 2°C for 24 h.

2.3. Fungal Pretreatment with C. subvermispora. Seven grams of rubberwood with 0.25, 0.5, and 1 mm particle sizes was mixed with 12 mL distilled water to obtain an optimal moisture content of 75% [12], and this mixture was autoclaved at 121°C for 20 min and then cooled and aseptically inoculated with a plug (9 mm in diameter) from the plate culture to obtain the effect of fungus on the rubberwood. Parafilm was wrapped around flasks to act as a barrier against moisture loss and contamination. Small perforations were made to the film to avoid moisture condensation and allow ventilation of chambers. Fungal pretreatment was carried out in an incubator at 28°C under static conditions for 30, 60, and 90 days. A set of nonpretreated sterilized woods were used as controls. After pretreatment, the flasks were stored at 4°C for compositional analysis, enzymatic hydrolysis, and ethanol production. All tests were performed in triplicate [16].

2.4. Enzymatic Hydrolysis. Enzymatic hydrolysis was conducted following NREL laboratory analytical procedure LAP-008 [17]. Cellulase (Celluclast 1.5 L, produced by *Trichoderma reesei*) with activity of 70 FPU/mL, supplemented with β-glucosidase (Novozyme 188, produced by *Aspergillus niger*) with activity of 122 CBU/mL, was used. Enzymatic hydrolysis experiments were carried out in 250 mL bottles. Each bottle was loaded with 1% w/w effective cellulose content, 1% w/v yeast extract, 2% w/v peptone, and 0.05 M citrate buffer (pH 4.8) in a final working weight of 50 grams and autoclaved at 121°C for 15 min. After cooling, cellulase (25 FPU/g cellulose) was added and supplemented with β-glucosidase (60 CBU/g cellulose) to avoid inhibition due to cellobiose accumulation [5]. After hydrolyzing at 50°C for 168 h in an incubator shaker set at 150, hydrolysis was terminated by boiling in a water bath for exactly 5 min to inactivate cellulase before being chilled on ice. Hydrolyzed samples were centrifuged at 10,000 rpm for 5 min. The supernatants were recovered for reducing sugars analysis at least in triplicate.

2.5. Production of Bioethanol. Production of bioethanol was carried out by simultaneous saccharification and fermentation (SSF) following NREL LAP-008 procedure. The microorganism used for the fermentation was *Saccharomyces cerevisiae* D5A purchased from ATCC, USA.

The strain was maintained in glycerol vials at −80°C for use as a working stock. It was cultured on YPD plates containing yeast extract 10 g/L, peptone 20 g/L, dextrose 20 g/L, and agar 20 g/L. Plates were incubated at 37°C for 2 days. A loopful of yeast was taken from a single colony of YPD plate and used to inoculate 100 mL of YPD media containing 10 g/L yeast extract, 20 g/L peptone, and 50 g/L dextrose [18] in a 250 mL flask. The media were sterilized by filtration and the flasks were autoclaved without media at 121°C [19]. The flask was incubated for 10–14 h in an incubator shaker operating at 37°C and 130 rpm. The cells were harvested, washed with DI water twice by centrifugation (5000 rpm for 5 min), and used for inoculating SSF flasks [20]. SSF was then carried out in a 250 mL serum bottle containing 6% w/w cellulose, 1% w/v yeast extract, 2% w/v peptone, and 0.05 M citrate buffer (pH 4.8) in a final working weight of 100 grams. Bottles were sparged with nitrogen, sealed, and autoclaved at 121°C for 15 min. After cooling, medium was inoculated with *S. cerevisiae* D5A (10% v/v, starting OD. 0.5) and cellulase enzyme was injected at a dose of 25 FPU/g cellulose and supplemented with β-glucosidase at a dose of 60 CBU/g cellulose to avoid inhibition due to cellobiose accumulation [5]. The SSF was conducted at 37°C and 130 rpm for 7 days. Samples were taken after 0, 3, 24, 48, 72, 96, 120, 144, and 168 h, filtered, and stored at −20°C for ethanol and reducing sugar analysis. All assays were performed at least in triplicate. The ethanol produced was analyzed qualitatively using gas

chromatography. The ethanol yield (%) was calculated using the following equation:

$$\text{ethanol yield (\%)} = \frac{\text{g of ethanol in culture broth} \times 100}{\text{g of glucan in culture broth} \times 1.1 \times 0.511}. \quad (1)$$

2.6. Analysis Methods

2.6.1. Subexperiment 1: Analysis of Chemical Composition. The total solids content (also called the percent dry weight) was determined according to the Laboratory Analytical Procedure No. 001 (LAP-001) from the National Renewable Energy Laboratory (NREL) [21]. The extractives were removed from analyzed samples by Soxhlet extraction with acetone (6 h), according to the procedure adapted from TAPPI standard T 204 om-97. The percentage of acid-insoluble lignin was determined according to TAPPI procedure (T224 om-88). The holocellulose content was determined according to DIN 2403. The α-cellulose content of rubber was determined according to TAPPI 203 om-93. The percentage of hemicellulose was calculated by subtracting the percent α-cellulose from holocellulose. Dry mass loss was calculated as the percentage of total solids loss after pretreatment. Lignin degradation, cellulose loss, and hemicellulose loss were defined as the percentages of lignin, cellulose, and hemicellulose reduction.

2.6.2. Subexperiment 2: Determination of Reducing Sugar. Total reducing sugar was determined by the 3, 5-dinitrosalicylic acid (DNS) method using glucose as the standard [22]. The samples were analyzed using a spectrophotometer (Shimadzu, Columbia, MD, USA) at 540 nm. The absorbance readings were then converted into equivalent sugar concentration (mg/mL) using a standard glucose solution curve. Reducing sugar yield was calculated using the following equation:

$$\text{reducing sugar yield (\%)} = \frac{\text{reducing sugar produced} \times 0.9 \times 100}{\text{amount of H rubberwood}}, \quad (2)$$

where H are cellulose and hemicellulose.

2.6.3. Subexperiment 3: X-Ray Diffraction Analysis. The X-ray diffractograms were obtained with a Rigaku Geigeflex Diffractometer with Cu and Kα radiation at 30 kV and 30 mA. The diffraction intensity was measured between Bragg angles (2θ) of 5°–50° at the speed of 2°/min. The crystallinity index (CrI) was calculated using the intensities of crystalline region at $2\theta = 22.5^\circ$ and amorphous region $2\theta = 18^\circ$, respectively, using the following equation [23]:

$$\text{crystallinity index (CrI) \%} = \frac{I_{\text{crystalline}} - I_{\text{amorphous}}}{I_{\text{crystalline}}}, \quad (3)$$

where $I_{\text{crystalline}}$ is the intensity of crystalline region and $I_{\text{amorphous}}$ is the intensity of amorphous region.

2.6.4. Subexperiment 4: Fourier Transform Infrared Spectroscopy (FT-IR) Analysis. The FT-IR spectra of untreated and treated rubberwood were obtained by direct transmittance using the KBr pellet technique [24]. Spectra were recorded with a Perkin Elmer 1650 FT-IR spectrometer (Perkin Elmer, Waltham, MA, USA). The spectra (4000–500 cm^{-1}) were measured at a spectral resolution of 4 cm^{-1} and 64 scans per sample.

2.6.5. Subexperiment 5: Scanning Electron Microscopy (SEM). The morphologies of untreated and pretreated rubberwood were examined using scanning electron microscopy (SEM). Before analysis, samples were mounted on metal stubs by double tape and the surface was coated with gold to avoid charging. Images were taken at 15 kV by PHILLIPS XL30 ESEM.

2.6.6. Subexperiment 6: Gas Chromatography. The ethanol produced from the fermentation process was analyzed qualitatively after distillation. The qualitative analysis was carried out using gas chromatography Shimadzu GC-14B with a BP21 capillary column (30 m × 0.250 mm ID, 0.25 μm film) and GC-flame ionization detector (GC-FID). Initial and final oven temperatures were 40 and 130°C, detector temperature was 250°C, and injector temperature was 230°C.

2.6.7. Subexperiment 7: Statistical Analysis. All experiments (chemical compositions and sugar yield) were carried out in triplicate and the values are an average of the three values obtained within a 95% confidence level. The effects of biological pretreatment on lignin, hemicellulose, and cellulose reduction during biological pretreatments were analyzed using the Statistical Analysis Software (SAS) program (released 6.12, 1988.SAS Institute Inc., Cary, NC).

3. Results and Discussion

3.1. Effect of Particle Size on Degradation of Rubberwood by C. subvermispora

3.1.1. Analysis of Chemical Composition. Particle size of the substrate is important. It affects the performance of solid state fermentation [20]. Generally, reduced particle size provides larger surface area for microbial attack but leads to limitation in interparticle space availability and heat transfer. Compared to smaller particle size, bigger particles provide better aeration/respiration opportunities but result in lesser surface area. Hence, determination of particle size corresponding to optimum growth and enzyme production is necessary [25]. The effects of particle size (1 mm, 0.5 mm, and 0.250 mm) on degradation of rubberwood by *C. subvermispora* during 90

Table 1: Degradation of rubberwood pretreated by *C. subvermispora* at different particle sizes for 30, 60, and 90 days[1].

Particle size (mm)	Selectivity value[2]	Weight loss (%)		
		Lignin	Hemicellulose	Cellulose
0.25				
30	2.16[b]	13.10[c] (0.36)	17.80[c] (0.67)	6.06[a] (0.75)
60	2.46[b]	29.65[b] (0.31)	34.35[a,b] (0.36)	12.07[a] (0.29)
90	2.75[c]	34.89[c] (0.9)	38.76[b] (0.88)	12.69[a] (0.83)
0.50				
30	2.78[a,b]	15.13[b] (0.19)	19.75[b] (0.27)	5.44[a] (0.50)
60	2.75[b]	29.52[b] (0.23)	34.01[b] (0.46)	10.73[a,b] (0.92)
90	3.21[b]	38.78[b] (0.27)	39.91[b] (0.44)	12.08[a] (0.37)
1.00				
30	3.57[a]	16.65[a] (1.08)	25.13[a] (0.69)	4.66[a] (1.26)
60	3.95[a]	37.30[a] (1.31)	36.02[a] (1.48)	9.44[b] (1.42)
90	4.29[a]	45.06[a] (0.82)	42.08[a] (1.16)	10.50[b] (0.98)

[1]Standard deviations of three replicates in parentheses; letters on the right side of the data in the same column indicated significant levels ($P < 0.05$ ANOVA, $F(3, 6)$);[2] selectivity value = lignin loss/cellulose loss.

Table 2: Crystallinity index of untreated and treated rubberwood by *C. subvermispora* at different particle sizes for 30, 60, and 90 days.

Samples	CrI (%)		
	30 d	60 d	90 d
Untreated	43.12	43.12	43.12
0.25	52.66	58.25	60.77
0.50	47.66	59.68	62.32
1.00	52.37	65.84	66.71

days are shown in Table 1. As shown in Table 1, higher lignin degradation was obtained with 1 mm rubberwood (16.65%) than was obtained with 0.5 and 0.250 mm rubberwood (15.13% and 13.10%, resp.) after 30 days. Moreover, weight losses of hemicellulose were 25.13%, 19.75%, and 17.80%, respectively, with 1, 0.5, and 0.250 mm. However, there was no significant difference between the cellulose degradation of all particle sizes ($P > 0.05$).

For rubberwood with the particle sizes of 0.5 and 0.250 mm, substantially lower lignin degradation (29.52% and 29.65%, resp.) was observed compared to 1 mm particle size of rubberwood (37.30%) after 60 days. The hemicellulose degradation for 1 mm rubberwood particle size is 36.02% which is higher than 0.5 mm particle size, while no significant difference was seen in hemicellulose degradation for 0.250 mm with 1 mm and 0.5 mm. The lowest cellulose caused in 1 mm particle size of rubberwood.

Fungal pretreated rubberwood with all particle sizes lost significant ($P < 0.05$) lignin compared to untreated rubberwood after 90 days. The weight losses of lignin for 1.00, 0.50, and 0.25 mm were 45.06%, 38.78%, and 34.89%, respectively. Higher hemicellulose reduction was obtained with 1 mm particle size (42.08%) compared to 0.50 and 0.25 mm particle sizes (39.91% and 38.76%, resp.). The cellulose reduction obtained with 1 mm particle size (10.5%) was lower than those particle sizes.

Selectivity value, the lignin/cellulose loss ratio, was used to evaluate the selective lignin-degrading ability [26]. The selectivity values increased with increasing pretreatment time because *C. subvermispora* can effectively reduce recalcitrance of rubberwood with high selectivity of lignin degradation rate and minimal cellulose loss. The highest selectivity value of 4.29% with lignin degradation of 45.06% was obtained from 1 mm particle size of rubberwood after 90 days.

3.1.2. X-Ray Diffraction. X-ray diffraction is the best option to estimate the impacts of pretreatment on crystalline regions of cellulose. The crystallinity index (CrI), which is a measure of the amount of crystalline cellulose, was calculated according to Segal's empirical method [22]. The crystallinity data of untreated and fungal treated rubberwood at different particle sizes are shown in Table 2. The results show that there is a significant increase in the crystallinity between the pretreated and untreated wood. The CrI values of 1 mm, 0.5 mm, and 0.250 mm samples increased 23.59%, 19.20%, and 17.64%, respectively, compared with untreated wood during 90 days of pretreatment. The increase in the crystallinity is expected due to the degradation and modification of amorphous components as reported in previous studies [27, 28]. The amorphous part may include amorphous cellulose, hemicellulose, and lignin [28, 29]. Therefore, the CrI increase in pretreated samples indicates that the amorphous portion of the rubberwood was more removed than the crystalline portion and cellulose became more exposed after pretreatment. According to Table 1, the higher lignin and hemicellulose reduction and lower cellulose loss were obtained with 1 mm particle size compared to other particle sizes. The crystallinity data also indicated that samples with 1 mm particle size had higher CrI value which is consistent with the obtained results shown in Table 1. Based on the chemical analysis and X-ray diffraction results, we may conclude that 1 mm is the best considered size for the biological pretreatment. Hence,

rubberwood with 1 mm particle size was chosen for the rest of the study.

3.2. FT-IR Analysis

3.2.1. Undecayed Rubberwood. FT-IR spectroscopy was used to demonstrate the physical structures and functional groups of the lignocellulosic materials. FT-IR spectroscopy of undecayed rubberwood is shown in Figure 1. The absorbance peaks in the 3400–3300 cm^{-1} (1) region were attributed to the stretching of O–H groups, whereas those around 2900–2800 cm^{-1} (2) were due to the stretching of C–H [30]. The peak located at 1735 cm^{-1} (3) was assigned to the C=O stretching of the acetyl group in hemicellulose [31]. The peaks in the region between 1620 and 1650 cm^{-1} (4 and 5) for all samples were characterized by the absorbed water [32]. The absorbance at 1504 cm^{-1} (6) is attributed to aromatic skeletal vibrations in lignin [31]. The peaks located at 1428 and 1458 cm^{-1} (7 and 8) were assigned to the C–H deformation in lignin and carbohydrates [33]. The peaks observed in the range 1380–1320 cm^{-1} (9 and 10) in all samples were attributed to the bending vibration of C–H and C–O groups of the aromatic ring in polysaccharides [32]. The absorption located at 1234 cm^{-1} (11) is caused by O–H phenolic in lignin [34]. The absorbances at 1158 and 898 (12 and 14) cm^{-1} correspond to C–O–C vibration in cellulose and hemicellulose, and C–H deformation in cellulose, respectively [31]. The C–O–C pyranose ring skeletal vibrations occur in the region 1102 to 1024 cm^{-1} (13) [35]. The peaks below 898 cm^{-1} are of little importance in the characterization of cellulose.

3.2.2. Wood Decayed by C. subvermispora. FT-IR spectra of rubberwood (1 mm) exposed to *C. subvermispora* for 30, 60, and 90 days are shown in Figure 1. The intensities of carbohydrate bands at 1369 and 898 cm^{-1} were slightly decreased. The constant intensity of the carbohydrate band at 1158 cm^{-1} is remarkable. In particular, the effect of fungal attack on the wood is clearly noticeable by increasing intensity of the 1647 cm^{-1} band (conjugated carbonyl groups, mainly originating from lignin) and the significant decreasing intensities at 1593, 1504, and 1234 cm^{-1} with exposure time [36]. However, a significant decrease in the intensity of carbonyl absorption band at 1735 cm^{-1} also indicated the decay of xylan (hemicellulose) by *C. subvermispora*. From the FT-IR spectra analysis, it could be concluded that *C. subvermispora* improved the degradation of lignin but it should have little effect on degradation of carbohydrates which result from a selective lignin removal. These findings are in agreement with Ferraz et al. [37].

3.3. Scanning Electron Microscopy (SEM). The morphology of the untreated and pretreated rubberwood with 1 mm particle size by *C. subvermispora* was investigated using scanning electron microscopy (SEM) for 30, 60, and 90 days (Figures 2(a), 2(b), 2(c), and 2(d)). SEM images showed that lignocellulose in the untreated rubberwood had an intact surface structure (Figure 3(a)), while the pretreated rubberwood had

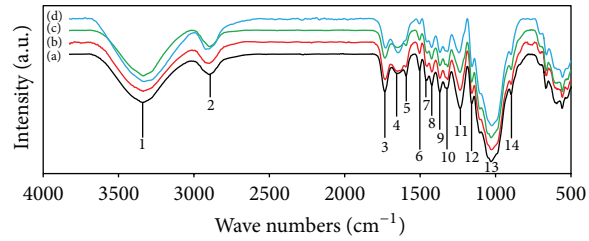

Figure 1: FT-IR spectra of rubberwood samples at various degrees of decay by *C. subvermispora*: (a) undecayed wood, (b) decayed for 30 d, (c) decayed for 60 d, and (d) decayed for 90 d.

a rugged and partially broken face which resulted from the removal of lignin and breaking of lignocelluloses networks during the pretreatment (marked circle in Figures 2(c) and 2(d)). As shown in Figure 2(b), rubberwood was quickly colonized by the fungus with the formation of abundant white mycelial mass on the wood chips after 30 days of pretreatment. The mycelial mass increased with biodegradation time, becoming whitish after 90 days of pretreatment (Figure 2(d)). SEM images also showed that in all treated samples, branched hyphae covered the surface of the wood chips. Mycelial mass increased during degradation. Hyphae penetrate the chips through the lumen and pit fiber wood cells (Figures 3(a) and 3(b)).

3.4. Enzymatic Hydrolysis. Lignin plays an important role in biomass recalcitrance to cellulolytic enzymes. It is generally well recognized that low lignin content results in high cellulose digestibility. Figure 4 shows the time courses of the production of reducing sugars using the untreated and fungal pretreated rubberwood for 0, 3, 24, 48, 72, 96, 120, 144, and 168 h as we have already published in our previous work [38]. As expected, the higher rate of enzymatic hydrolysis exhibited by pretreated samples was due to removal of the physical protective coat of cellulose and consequently the improved cellulose digestibility. Compared to pretreated samples, rubberwood without pretreatment was much more resistant to enzymatic hydrolysis, producing only 2.88% fermentable sugar yield after 168 h of hydrolysis. The reducing sugar yield from sample treated for 30 days was 17.23%. The reducing sugar yields increased with the cultivation time beyond 30 days, reaching 23.80% for samples pretreated for 60 days. Further increase was observed when the cultivation time was further extended to 90 days. The highest reducing sugar yield reached about 27.67% for samples pretreated for 90 days. These results show that the enzymatic hydrolysis yield of rubberwood is considerably affected by the cultivation time and the reducing sugar yield heavily depends on the extent of delignification and hemicellulose removal from the lignocellulosic materials [39]. This explains why sample pretreated by *C. subvermispora* resulted in high sugar yield (27.67%). It was reported that after 120 days of cultivation by a newly isolated fungus, *Echinodontium taxodii* 2538 on two native woods: *Chinese willow* (hard wood) and *China-fair* (soft wood), the enzymatic hydrolysis yield showed a significant increase (4.7-fold for hard wood and 3-fold for

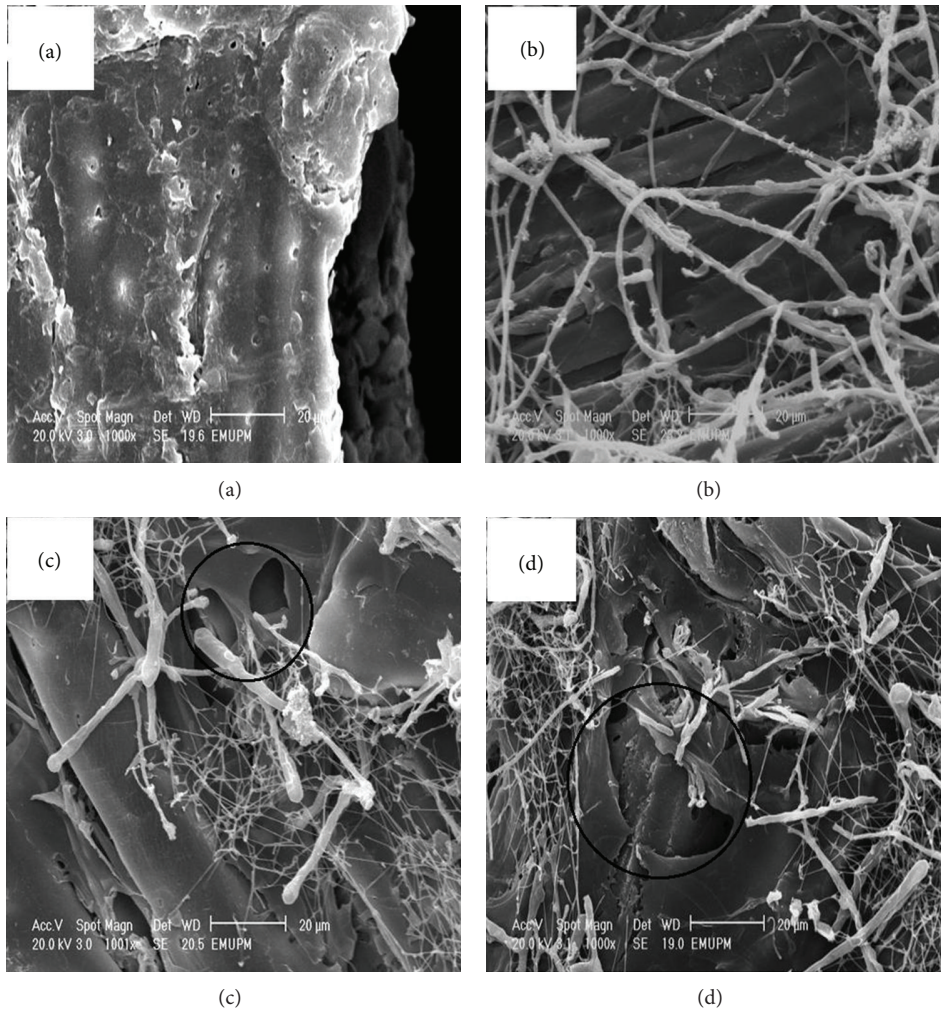

FIGURE 2: Scanning electron microscopy images of rubberwood pretreated with *C. subvermispora*. (a) Untreated rubberwood; (b) rubberwood pretreated with *C. subvermispora* for 30 d, (c) 60 d, and (d) 90 d.

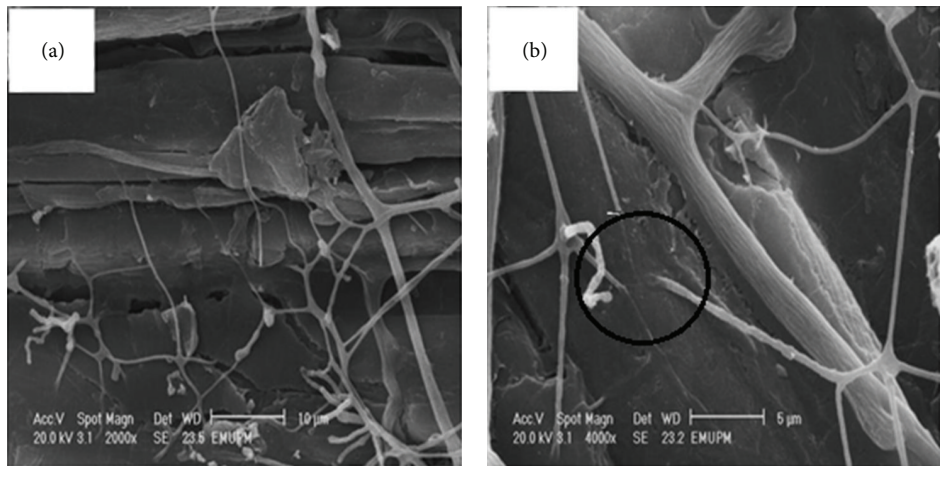

FIGURE 3: SEM images of pretreated rubberwood (a) showing hyphae penetration through cell walls; (b) same image at higher magnification.

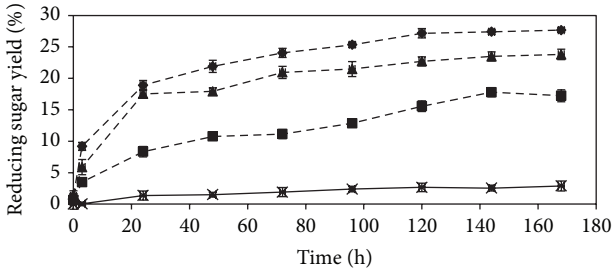

Figure 4: Time course of reducing sugar yield (%) during the hydrolysis of rubberwood. (×) untreated; (- - -) pretreated with *C. subvermispora*, for (■) 30, (▲) 60, and (♦) 90 days. Error bars represent standard error.

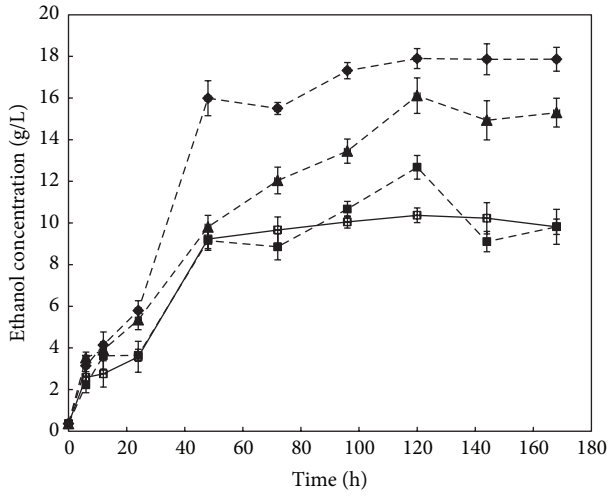

Figure 5: Time course of bioethanol concentration (g/L) of untreated and pretreated rubberwood by *C. subvermispora*. (□) untreated and (■) pretreated rubberwood after 30, (▲) 60, and (♦) 90 days. Error bars represent standard error.

soft wood) [26]. By contrast, pretreatment of rubberwood (hard wood) by *C. subvermispora* resulted in much higher enzymatic hydrolysis yields (9.6-fold) during a relatively short degradation period. Lee et al. [40] reported lower sugar yields (21.01%, 14.91%, and 15.03%) from soft wood *Pinus densiflora* pretreated with *Stereum hirsutum*, *Polyporus brumalis*, and *Ceriporia lacerate*, respectively, compared to rubberwood treated with *C. subvermispora* for 72 h at 50°C. However, the sugar yield obtained from wood treated with *C. subvermispora* (230.6 mg sugar/g rubberwood) in this study is comparable with that obtained by Zhang et al. (232.2 mg sugar/g bamboo) but in much shortened pretreatment time (90 days compared to 60–120 days by Zhang et al.) [41].

3.5. Production of Bioethanol. Bioethanol production was carried out by simultaneous saccharification and fermentation (SSF) process. The rubberwood samples pretreated with *C. subvermispora* for 30, 60, and 90 days were used in the bioethanol production. Untreated sample was used as control. The bioethanol produced by the fermentation process increased within the first 48 h of SSF and maximum

Table 3: Bioethanol yields (%) of untreated and pretreated rubberwood by *C. subvermispora* after 30, 60, and 90 days (samples 1, 2, and 3, resp.)[1].

Time (h)	Control	Sample 1	Sample 2	Sample 3
24	10.6 (1.2)	10.8 (2.4)	15.8 (0.9)	17.2 (0.6)
48	27.4 (0.8)	27.1 (1.9)	29.1 (1.3)	47.4 (1.4)
72	28.7 (2.1)	26.3 (1.7)	35.7 (2.5)	46.06 (2.3)
96	29.8 (1.7)	31.6 (0.7)	39.9 (3.1)	51.4 (2.8)
120	30.7 (2.3)	37.6 (1.5)	47.8 (2.2)	53.1 (3.5)
144	30.3 (1.4)	27.0 (2.6)	44.3 (3.7)	53.0 (2.9)

[1]Standard deviations of three replicates are in parentheses.

value was obtained after 120 h (Table 3 and Figure 5). After 120 h, the maximum bioethanol concentration and yield were 17.9 g/L and 53% yield, respectively. For fungal pretreated rubberwood for 30 and 60 days, the ethanol concentrations obtained were 12.7 g/L and 16.1 g/L, respectively. The bioethanol concentration and yield of untreated sample were 10.4 g/L and 30.7% after 120 h fermentation.

These results are comparable to that obtained from pretreated corn stover with *C. subvermispora,* where an overall ethanol yield of 57.80% was achieved [20]. Another report showed that a combination of *C. subvermispora* and ethanolysis pretreatment resulted in an overall ethanol yield of 62% [15]. This higher yield is expected due to additional ethanolysis treatment compared to this study using only *C. subvermispora* pretreatment. Bak et al. [9] reported that when fungal fermented rice straw with *Dichomitus squalens* was used as a substrate in SSF, the bioethanol yield was 54.2% after 24 h. Other works on production of ethanol from biomass treated with microorganism were 0.017 g of ethanol/g of corn stover after 144 h fermentation [42] and 0.004–0.027 g of ethanol/g of dry lignocelluloses after 48 h fermentation [43]. The bioethanol yields from these previously conducted studies are much lower than the yield obtained in this study (0.003–0.143 g of ethanol/g of dry rubberwood). The results of this work show that fungal pretreatment of rubberwood increased the enzymatic digestibility of cellulose that led to high bioethanol yield.

4. Conclusions

We may conclude that fungal pretreatment using *C. subvermispora* provides a cost-effective method for reducing the recalcitrance of rubberwood with high selectivity of lignin degradation rate and minimal cellulose loss for enzymatic hydrolysis and bioethanol production. The study showed that lignin degradation rate was significantly affected by the particle size of rubberwood and time of the pretreatment. XRD and chemical analysis of control and pretreated rubberwood with different particle sizes showed that rubberwood with the particle size of 1 mm was efficiently degraded due to providing better aeration/respiration opportunities compared to smaller particle sizes. FT-IR spectra analysis and SEM observations of control and pretreated rubberwood with 1 mm particle size showed equivalent results with

chemical analysis. The results of this work also revealed that rubberwood with high cellulose content can be successfully converted to bioethanol by the SSF process.

Acknowledgments

The authors wish to thank to the Laboratory of Industrial Biotechnology, Institute of Bioscience, Universiti Putra Malaysia for providing materials and facilities. Also we sincerely thank the staff of the Microscopy Unit at the Institute of Bioscience, Universiti Putra Malaysia for helpful assistance in the scanning electron microscopy assays. The author Reza Zamiri would like to express his personal thanks to FCT (Fundação para a Ciência e a Tecnologia) for post-doctoral research grant with reference number (SFRH/BPD/76185/2011).

References

[1] N. Mosier, C. Wyman, B. Dale et al., "Features of promising technologies for pretreatment of lignocellulosic biomass," *Bioresource Technology*, vol. 96, no. 6, pp. 673–686, 2005.

[2] M. Mete Altıntaş, K. Ö. Ülgen, B. Kırdar, Z. Ilsen Önsan, and S. G. Oliver, "Improvement of ethanol production from starch by recombinant yeast through manipulation of environmental factors," *Enzyme and Microbial Technology*, vol. 31, no. 5, pp. 640–647, 2002.

[3] R. K. Sukumaran, R. R. Singhania, G. M. Mathew, and A. Pandey, "Cellulase production using biomass feed stock and its application in lignocellulose saccharification for bio-ethanol production," *Renewable Energy*, vol. 34, no. 2, pp. 421–424, 2009.

[4] J. Shi, M. S. Chinn, and R. R. Sharma-Shivappa, "Microbial pretreatment of cotton stalks by solid state cultivation of *Phanerochaete chrysosporium*," *Bioresource Technology*, vol. 99, no. 14, pp. 6556–6564, 2008.

[5] A. M. Alhasan, D. Kuang, A. B. Mohammad, and R. R. Sharma-Shivappa, "Combined effect of nitric acid and sodium hydroxide pretreatments on enzymatic Saccharification of rubber wood (*Heavea brasiliensis*)," *International Journal of Chemical Technology*, vol. 2, no. 1, pp. 12–20, 2010.

[6] Y. Sun and J. Cheng, "Hydrolysis of lignocellulosic materials for ethanol production: a review," *Bioresource Technology*, vol. 83, no. 1, pp. 1–11, 2002.

[7] M. J. Taherzadeh and K. Karimi, "Pretreatment of lignocellulosic wastes to improve ethanol and biogas production: a review," *International Journal of Molecular Sciences*, vol. 9, no. 9, pp. 1621–1651, 2008.

[8] F. D. Haagensen, D. Joiner, P. Hedgepeth, E. Quattrini, and M. Torry-Smith, "Performance data of Novozymes new cellulase systems," in *Proceedings of the 30th Symposium on Biotechnology for Fuels and Chemicals*, New Orleans, LA, USA, 2008.

[9] J. S. Bak, M. D. Kim, I.-G. Choi, and K. H. Kim, "Biological pretreatment of rice straw by fermenting with Dichomitus squalens," *New Biotechnology*, vol. 27, no. 4, pp. 424–434, 2010.

[10] H. K. Murnen, V. Balan, S. P. S. Chundawat, B. Bals, L. D. C. Sousa, and B. E. Dale, "Optimization of ammonia fiber expansion (AFEX) pretreatment and enzymatic hydrolysis of Miscanthus x giganteus to fermentable sugars," *Biotechnology Progress*, vol. 23, no. 4, pp. 846–850, 2007.

[11] J. Shi, R. R. Sharma-Shivappa, M. Chinn, and N. Howell, "Effect of microbial pretreatment on enzymatic hydrolysis and fermentation of cotton stalks for ethanol production," *Biomass and Bioenergy*, vol. 33, no. 1, pp. 88–96, 2009.

[12] C. Wan and Y. Li, "Microbial pretreatment of corn stover with *Ceriporiopsis subvermispora* for enzymatic hydrolysis and ethanol production," *Bioresource Technology*, vol. 101, no. 16, pp. 6398–6403, 2010.

[13] K. E. L. Eriksson, R. A. Blanchette, and P. Ander, *Microbial and Enzymatic Degradation of Wood and Wood Components*, Springer, 1990.

[14] W. F. Anderson and D. E. Akin, "Structural and chemical properties of grass lignocelluloses related to conversion for biofuels," *Journal of Industrial Microbiology & Biotechnology*, vol. 35, no. 5, pp. 355–366, 2008.

[15] H. Itoh, M. Wada, Y. Honda, M. Kuwahara, and T. Watanabe, "Bioorganosolve pretreatments for simultaneous saccharification and fermentation of beech wood by ethanolysis and white rot fungi," *Journal of Biotechnology*, vol. 103, no. 3, pp. 273–280, 2003.

[16] H. Yu, G. Guo, X. Zhang, K. Yan, and C. Xu, "The effect of biological pretreatment with the selective white-rot fungus *Echinodontium taxodii* on enzymatic hydrolysis of softwoods and hardwoods," *Bioresource Technology*, vol. 100, no. 21, pp. 5170–5175, 2009.

[17] N. Dowe and J. McMillan, "SSF experimental protocols: lignocellulosic biomass hydrolysis and fermentation," Tech. Rep., National Renewable Energy Laboratory (NREL) Analytical Procedures, 2001.

[18] N. Dowe and J. McMillan, "SSF experimental protocols: lignocellulosic biomass hydrolysis and fermentation," Tech. Rep. LAP-008, Golden, NREL, 2001.

[19] B. A. Faga, M. R. Wilkins, and I. M. Banat, "Ethanol production through simultaneous saccharification and fermentation of switchgrass using Saccharomyces cerevisiae D5A and thermotolerant *Kluyveromyces marxianus* IMB strains," *Bioresource Technology*, vol. 101, no. 7, pp. 2273–2279, 2010.

[20] C. Wan and Y. Li, "Microbial pretreatment of corn stover with Ceriporiopsis subvermispora for enzymatic hydrolysis and ethanol production," *Bioresource Technology*, vol. 101, no. 16, pp. 6398–6403, 2010.

[21] T. Ehrman, "Standard method for determination of total solids in biomass," type 001, Laboratory Analytical Procedure, 1994.

[22] T. Ghose, "Measurement of cellulase activities," *Pure and Applied Chemistry*, vol. 59, no. 2, pp. 257–268, 1987.

[23] L. Segal, J. Creely, A. Martin, and C. Conrad, "An empirical method for estimating the degree of crystallinity of native cellulose using the X-ray diffractometer," *Textile Research Journal*, vol. 29, no. 10, pp. 786–794, 1959.

[24] R. Bodîrlău and C. Teacă, "Fourier transform infrared spectroscopy and thermal analysis of lignocellulose fillers treated with organic anhydrides," in *Proceedings of the 8th International Balkan Workshop on Applied Physics*, pp. 5–7, 2009.

[25] A. Pandey, "Solid-state fermentation," *Biochemical Engineering Journal*, vol. 13, no. 2-3, pp. 81–84, 2003.

[26] H. Yu, G. Guo, X. Zhang, K. Yan, and C. Xu, "The effect of biological pretreatment with the selective white-rot fungus *Echinodontium taxodii* on enzymatic hydrolysis of softwoods and hardwoods," *Bioresource Technology*, vol. 100, no. 21, pp. 5170–5175, 2009.

[27] K. Kasahara, H. Sasaki, N. Donkai, and T. Takagishi, "Modification of Tencel with treatment of ferric sodium tartrate complex solution," *Sen'i Gakkaishi*, vol. 60, no. 2, pp. 65–69, 2004.

[28] S. Kim and M. T. Holtzapple, "Effect of structural features on enzyme digestibility of corn stover," *Bioresource Technology*, vol. 97, no. 4, pp. 583–591, 2006.

[29] X.-B. Zhao, L. Wang, and D.-H. Liu, "Peracetic acid pretreatment of sugarcane bagasse for enzymatic hydrolysis: a continued work," *Journal of Chemical Technology and Biotechnology*, vol. 83, no. 6, pp. 950–956, 2008.

[30] H. P. S. A. Khalil, H. Ismail, H. D. Rozman, and M. N. Ahmad, "The effect of acetylation on interfacial shear strength between plant fibres and various matrices," *European Polymer Journal*, vol. 37, no. 5, pp. 1037–1045, 2001.

[31] K. K. Pandey and A. J. Pitman, "FTIR studies of the changes in wood chemistry following decay by brown-rot and white-rot fungi," *International Biodeterioration and Biodegradation*, vol. 52, no. 3, pp. 151–160, 2003.

[32] M. Le Troedec, D. Sedan, C. Peyratout et al., "Influence of various chemical treatments on the composition and structure of hemp fibres," *Composites A*, vol. 39, no. 3, pp. 514–522, 2008.

[33] C. Genestar and J. Palou, "SEM-FTIR spectroscopic evaluation of deterioration in an historic coffered ceiling," *Analytical and Bioanalytical Chemistry*, vol. 384, no. 4, pp. 987–993, 2006.

[34] R. Bodirlau, C. A. Teaca, and I. Spiridon, "Chemical modification of beech wood: effect on thermal stability," *BioResources*, vol. 3, no. 3, pp. 789–800, 2008.

[35] X. F. Sun, R. C. Sun, J. Tomkinson, and M. S. Baird, "Degradation of wheat straw lignin and hemicellulosic polymers by a totally chlorine-free method," *Polymer Degradation and Stability*, vol. 83, no. 1, pp. 47–57, 2004.

[36] O. Faix, J. Bremer, O. Schmidt, and S. J. Tatjana, "Monitoring of chemical changes in white-rot degraded beech wood by pyrolysis-gas chromatography and Fourier-transform infrared spectroscopy," *Journal of Analytical and Applied Pyrolysis*, vol. 21, no. 1-2, pp. 147–162, 1991.

[37] A. Ferraz, C. Parra, J. Freer, J. Baeza, and J. Rodríguez, "Characterization of white zones produced on Pinus radiata wood chips by *Ganoderma australe* and *Ceriporiopsis subvermispora*," *World Journal of Microbiology and Biotechnology*, vol. 16, no. 7, pp. 641–645, 2000.

[38] F. Nazarpour, D. K. Abdullah, N. Abdullah, and R. Zamiri, "Evaluation of biological pretreatment of rubberwood with white rot Fungi for enzymatic hydrolysis," *Materials*, vol. 6, no. 5, pp. 2059–2073, 2013.

[39] K. Öhgren, R. Bura, J. Saddler, and G. Zacchi, "Effect of hemicellulose and lignin removal on enzymatic hydrolysis of steam pretreated corn stover," *Bioresource Technology*, vol. 98, no. 13, pp. 2503–2510, 2007.

[40] J.-W. Lee, K.-S. Gwak, J.-Y. Park et al., "Biological pretreatment of softwood Pinus densiflora by three white rot fungi," *Journal of Microbiology*, vol. 45, no. 6, pp. 485–491, 2007.

[41] X. Zhang, C. Xu, and H. Wang, "Pretreatment of bamboo residues with *Coriolus versicolor* for enzymatic hydrolysis," *Journal of Bioscience and Bioengineering*, vol. 104, no. 2, pp. 149–151, 2007.

[42] P. Shrestha, M. Rasmussen, S. K. Khanal, A. L. Pometto III, and J. Van Leeuwen, "Solid-substrate fermentation of corn fiber by *Phanerochaete chrysosporium* and subsequent fermentation of hydrolysate into ethanol," *Journal of Agricultural and Food Chemistry*, vol. 56, no. 11, pp. 3918–3924, 2008.

[43] J. Shi, M. S. Chinn, and R. R. Sharma-Shivappa, "Microbial pretreatment of cotton stalks by solid state cultivation of *Phanerochaete chrysosporium*," *Bioresource Technology*, vol. 99, no. 14, pp. 6556–6564, 2008.

Hindawi Publishing Corporation
BioMed Research International
Volume 2013, Article ID 639725, 5 pages
http://dx.doi.org/10.1155/2013/639725

Research Article

Green Synthesis of Silver Nanoparticles Using *Pinus eldarica* Bark Extract

Siavash Iravani and Behzad Zolfaghari

Department of Pharmacognosy and Isfahan Pharmaceutical Sciences Research Center, School of Pharmacy and Pharmaceutical Sciences, Isfahan University of Medical Sciences, Isfahan 81744-176, Iran

Correspondence should be addressed to Siavash Iravani; siavashira@gmail.com

Received 24 April 2013; Accepted 6 August 2013

Academic Editor: Maria Alice Zarur Coelho

Recently, development of reliable experimental protocols for synthesis of metal nanoparticles with desired morphologies and sizes has become a major focus of researchers. Green synthesis of metal nanoparticles using organisms has emerged as a nontoxic and ecofriendly method for synthesis of metal nanoparticles. The objectives of this study were production of silver nanoparticles using *Pinus eldarica* bark extract and optimization of the biosynthesis process. The effects of quantity of extract, substrate concentration, temperature, and pH on the formation of silver nanoparticles are studied. TEM images showed that biosynthesized silver nanoparticles (approximately in the range of 10–40 nm) were predominantly spherical in shape. The preparation of nanostructured silver particles using *P. eldarica* bark extract provides an environmentally friendly option, as compared to currently available chemical and/or physical methods.

1. Introduction

In recent years, green synthesis of metal nanoparticles is an interesting issue of the nanoscience and nanobiotechnology. There is a growing attention to biosynthesis the metal nanoparticles using organisms. Among these organisms, plants seem to be the best candidate and they are suitable for large-scale biosynthesis of nanoparticles. Nanoparticles produced by plants are more stable, and the rate of synthesis is faster than that in the case of other organisms. Moreover, the nanoparticles are more various in shape and size in comparison with those produced by other organisms [1, 2].

Silver nanoparticles have drawn the attention of researchers because of their suitable applications in the fields of electronic, material science, and medicine [3, 4]. For instance, antimicrobial properties of silver nanoparticles caused the use of these nanometals in different fields of medicine, various industries, animal husbandry, packaging, accessories, cosmetics, health, and military. Silver nanoparticles show potential antimicrobial effects against infectious organisms such as *Escherichia coli*, *Bacillus subtilis*, *Vibrio cholerae*, *Pseudomonas aeruginosa*, *Syphilis typhus*, and *Staphylococcus aureus* [5, 6]. Moreover, these nanoparticles have drawn the attention of researchers because of their extensive applications in areas such as mechanics, optics, biomedical sciences, chemical industry, electronics, space industries, drug-gene delivery, energy science, catalysis [7, 8], optoelectronic devices [9, 10], photo-electrochemical applications [11], and nonlinear optical devices [12, 13].

Antioxidant action of phenolic compounds is due to their high tendency to chelate metals. These compounds consist of catechin, taxifolin, procyanidins of various chain lengths formed by catechin and epicatechin units, and phenolic acids. Phenolic compounds possess hydroxyl and carboxyl groups. These compounds may inactivate iron ions by chelating and additionally suppressing the superoxide-driven Fenton reaction, which is believed to be the most important source of reactive oxygen species (ROS). Therefore, plants with high content of phenolic compounds (e.g., Pinus species) are one of the best candidates for nanoparticle synthesis. Pine bark extract contains polyphenolic compounds which have considerable antioxidant activities. The objectives of this study were production of silver nanoparticles using *Pinus eldarica* bark extract and optimization of the biosynthesis process.

2. Materials and Methods

2.1. Plant Material. *Pinus eldarica* bark specimens were collected from a population growing in Isfahan (32°38′N 51°39′E, altitude, 1590 m) from Isfahan. The plant was identified by the Botany Department of the Faculty of Sciences at the University of Isfahan. The samples were collected between August and September 2010. The specimens were dried at room temperature, ground by using a conventional grinder, and stored at 4°C.

2.2. Plant Characteristics. *Pinus eldarica* (Pinaceae) is a medium-sized tree, reaching 12–15 m high. The bark is brownish gray or light gray, not flaking, and head broad-topped. The leaves are stiff, 6–9 cm long, and green. The cones are pedunculate, solitary or in pairs, and light reddish brown. Scales irregularly rhombic, glossy, smooth, the whitish-gray apophysis concave: seeds blackish, 6-7 mm long, the reddish-brown wing 18–28 mm long [14].

2.3. Biosynthesis and Characterization of Silver Nanoparticles. *P. eldarica* bark extract was used as a reducing agent for the development of silver nanoparticles. Fifty g of pine bark powders was added in 250 mL deionized water in 500 mL Erlenmeyer flask boiled for approximately 15 min. Whatman filter paper was used for the filtration of boiled materials to prepare the aqueous pine bark extract, which was used for metal nanoparticle synthesis. The reaction mixtures contained the following ingredients (final concentrations): $AgNO_3$ (1, 2, 4, and 6 mM) as the substrate, different quantities of *P. eldarica* bark extract, and phosphate buffer (pH = 3, 5, 7, 9, and 11). UV absorption of colloidal suspension (hydrosol) of silver nanoparticles was used as an easy and quick assay to check production of nanoparticles. Absorption spectra were measured on a Shimadzu (UVmini-1240, Japan) spectrophotometer. Transmission electron microscopy (TEM) analysis was performed on selected samples in order to investigate the process of formation of silver nanoparticles and study the size and shape of them. Micrographs were obtained using CM 200 FEG Phillips transmission electron microscope.

3. Results and Discussion

3.1. Visual Inspection. When *P. eldarica* bark extract was exposed to Ag^+ ions ($AgNO_3$, 1 mM), the color of the reaction mixture turned to yellowish brown and then to dark brown, which was in agreement with the previous studies, and was considered as the formation of silver nanoparticles [15, 16]. The appearance of dark brown seems to be due to excitation of surface plasmon resonance in the nanoparticles.

3.2. Monitoring the Production of Silver Nanoparticles. In order to study and optimize the production of nanoparticles, we needed an easy and cheap method to monitor the nanoparticles production. Most of the researchers have used the optical absorption of colloidal silver as an indicator of production of silver nanoparticles [1, 2, 17–22]. We examined the UV/Vis absorption spectrum of colloidal Ag to verify this. The λ_{max} was approximately 430 nm (Figure 1). By plotting UV/Vis absorption of the reaction mixture against time, time course of the reaction was obtained. During the reaction period, an increase in absorbance was observed in this wavelength, which can be due to the increase in production of colloidal silver nanoparticles [23, 24].

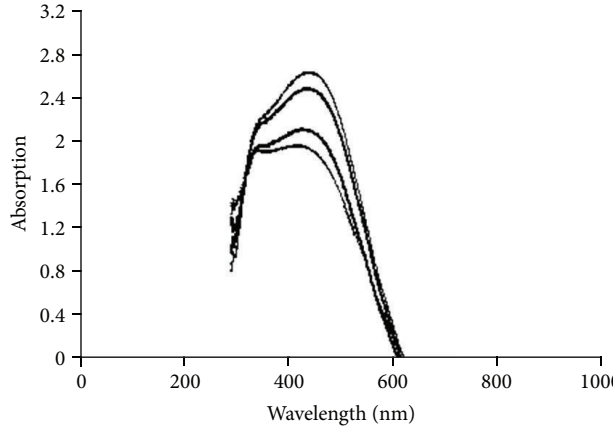

Figure 1: UV/Vis absorption spectrum of the produced colloidal silver. The spectrum was obtained at different time points after the start of $AgNO_3$ (1 mM) reduction.

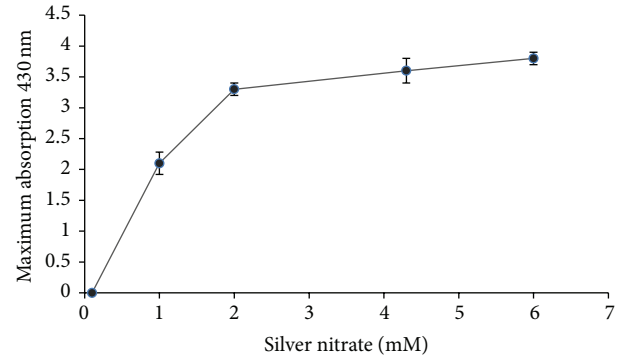

Figure 2: Effect of different concentrations of the substrate: absorption spectra of maximum production of silver nanoparticles against various concentrations of $AgNO_3$ (1, 2, 4, and 6 mM) were read and recorded (*n* value = 3).

The important challenges frequently encountered in the biosynthesis of nanoparticles are to control the shape and size of the particles as well as to achieve the monodispersity in solution phase. Several factors such as substrate concentration, electron donor, reaction or incubation time, pH, temperature, buffer strength, mixing speed, and light need to be optimized.

3.3. Effect of Substrate Concentration. One of the important measures to make the reaction more economical and efficient is finding the maximum concentration of substrate which could be converted to final product. The results obtained from time course of reaction indicated that by gradual increase in concentration of $AgNO_3$, the nanoparticle production was also increased (Figure 2).

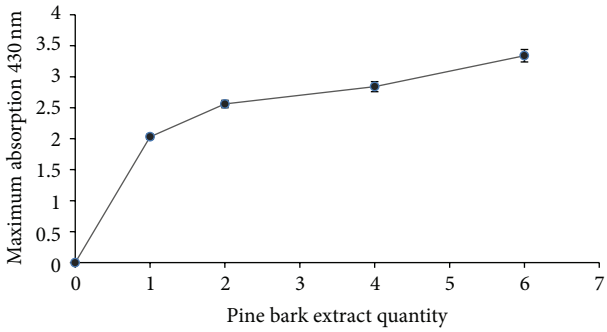

Figure 3: Effect of different quantities of *P. eldarica* bark extract: absorption spectra of maximum production of silver nanoparticles against various amounts of *P. eldarica* bark extract (×1, ×2, ×4, and ×6) were read and recorded (*n* value = 3).

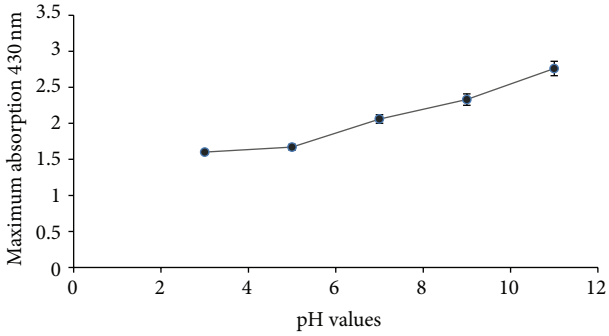

Figure 4: Effect of different pH on nanoparticle production: absorption spectra of maximum production of silver nanoparticles against 5 pH values of the reaction mixture were read and recorded (*n* value = 3).

3.4. Effect of Different Quantities of P. eldarica Bark Extract. The possibility of controlling the properties of nanoparticles by changing the composition of the reaction mixture has resulted in the use of different amount of biomass or cell extract in order to form nanoparticles with desired morphology and size. Different pine bark extract quantities were used for the synthesis of silver nanoparticles. The pine bark extract varied from 1, 2, 4, and 6 mL in 50 mL of 1 mM silver nitrate solution. As a result, larger quantities of bark extract lead to an increase in peak absorbance in UV/Vis spectrum. By increasing the extract concentrations, nanoparticle production was also increased, but this relationship was not linear (Figure 3). Moreover, decrease in particle size of Ag nanoparticles has been observed due to an increase in extract amount.

3.5. Effect of pH. The solution pH is a critical factor in controlling the size and morphology of nanoparticles and in the location of nanoparticle deposition [25–27]. The reduction of silver was performed at pH 3, 5, 7, 9, and 11 with *P. eldarica* bark extract. By increasing the pH of the reaction mixture, an increase in absorbance was observed, which can be due to the increase in production of colloidal silver nanoparticles and reduction rate (Figure 4). It seems that pH affects the amount of nanoparticle production and stability of

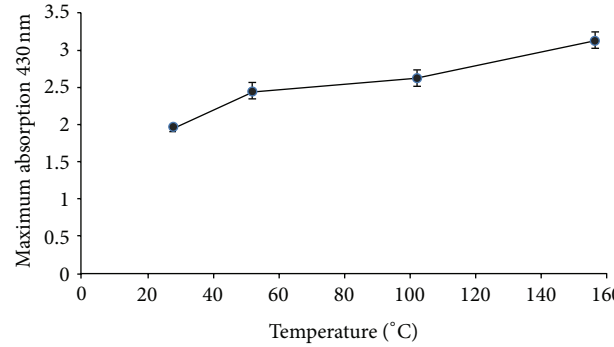

Figure 5: Effect of reaction temperature: absorption spectra of maximum production of silver nanoparticles against different reaction temperature were read and recorded (*n* value = 3).

them. Furthermore, pH influenced the rate of the reduction reaction. The reaction mixture turned brown when silver was reduced, and the reaction mixture coloring accelerated when increasing pH. Furthermore, the formation of large sized silver nanoparticles was observed at lower or acidic pH; while higher or alkaline pH highly dispersed, small sized nanoparticles tended to form. The results were in agreement with the previous studies. For instance, Gardea-Torresdey et al. [28] found that pH is an important factor in the biosynthesis of colloidal gold using alfalfa biomass and concluded that the size of nanoparticles varied with the change in pH. Mock et al. [29] also have reached similar conclusions and reported that pH is responsible for the formation of nanoparticles of various shapes and size as different plant extracts and even the extracts coming from different parts of the same plant may have different pH values which further need optimization for the efficient synthesis of nanoparticles. It has been reported by several researchers that larger nanoparticles formed at lower pH [2–4] as compared to higher pH. Moreover, Armendariz et al. [30] reported that the size of gold nanoparticle produced by *Avena sativa* was highly dependent on the pH value. At pH 2, large size nanoparticles (25–85 nm) were formed albeit in a small quantity, but at pH 3 and 4, smaller sized nanoparticles were formed in a large quantity. They speculated that at low pH (pH 2), the gold nanoparticles prefer to aggregate to form larger nanoparticles rather than to nucleate and form new nanoparticles. In contrast, at pH 3 and 4, more functional groups (carbonyl and hydroxyl) are available for gold binding; thus a higher number of Au (III) complexes would bind to the biomass at the same time. Dwivedi and Gopal [31] revealed that silver and gold nanoparticles are stable in a wider range of pH as they observed very small variation in the zeta potential values between pH 2 and 10 in their study using *Chenopodium album*. Veerasamy et al. [32], while working on mangosteen leaf extract, reported that at low pH, aggregation of silver nanoparticles is favoured over the nucleation. However, higher pH facilitates the nucleation and subsequent formation of large number of nanoparticles with smaller diameter.

3.6. Effect of Temperature. Temperature might be one of the crucial factors dominating the size and shape of

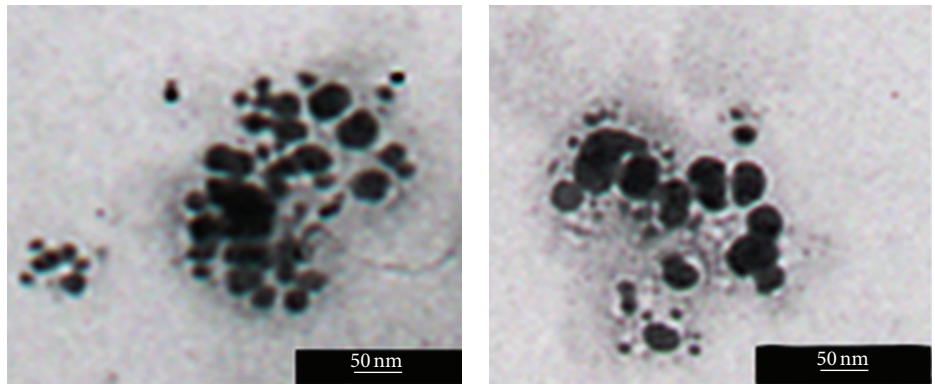

Figure 6: TEM micrographs recorded from the drop-coated film of the silver nanoparticles synthesized by treating the silver nitrate solution with *P. eldarica* bark extract.

nanoparticles. In order to investigate the effect of temperature, the reaction mixture was heated at different temperatures (25°C, 50°C, 100°C, and 150°C). Samples were collected from the reaction mixture, and surface plasmon resonance-spectra were taken. By increasing reaction temperature, an increase in absorbance was observed, which can be due to the increase in production of colloidal silver nanoparticles and reduction rate (Figure 5). Moreover, when the reaction temperature was increased from 25 to 150°C, the size of silver nanoparticles became smaller which resulted into sharpness of plasmon resonance band of them.

3.7. TEM Analysis of Produced Silver Nanoparticles. Figure 6 shows TEM images recorded from the drop-coated film of the silver nanoparticles synthesized by treating the silver nitrate solution with the pine bark extract. Silver nanoparticles, mainly spherical assemblies, were obtained by room-temperature synthesis. Biosynthesized silver nanoparticles (approximately in the range of 10–40 nm) were predominantly spherical in shape. The reduction and growth of silver nuclei using pine bark extract as a green process present a reliable and economic method, taking advantages of an efficient bioresource.

4. Conclusions

In conclusion, silver nanoparticles were successfully produced using *P. eldarica* bark extract. Characterization by UV-visible and TEM techniques confirmed the reduction of silver ions to silver nanoparticles. The preparation of nanostructured silver particles using *P. eldarica* bark extract provides an environmentally friendly option, as compared to currently available chemical and/or physical methods.

Various chemical, physical and biological synthetic methods have been developed to obtain metal nanoparticles of various shapes and sizes, including laser ablation, gamma irradiation, electron irradiation, chemical reduction, photochemical methods, microwave processing, and biological synthetic methods. The organisms used in biological synthesis of nanoparticles vary from simple prokaryotic bacterial cells to complex eukaryotes. Plants are able to reduce the metal ions faster than fungi or bacteria. Furthermore, in order to use an easy and safe green method in scaleup and industrial production of well-dispersed metal nanoparticles, plant extract is better than plant biomass or living plant in the rate of production. Problems experienced in biological synthesis of metal nanoparticles are stability and aggregation of nanoparticles, control of crystal growth, morphology, size, and size distribution. Moreover, separation of produced nanoparticles for further applications is still an important issue.

Acknowledgment

This study was part of the project of Faculty of Pharmacy and Pharmaceutical Sciences, Isfahan University of Medical Sciences.

References

[1] S. Iravani, "Green synthesis of metal nanoparticles using plants," *Green Chemistry*, vol. 13, no. 10, pp. 2638–2650, 2011.

[2] H. Korbekandi, S. Iravani, and S. Abbasi, "Production of nanoparticles using organisms production of nanoparticles using organisms," *Critical Reviews in Biotechnology*, vol. 29, no. 4, pp. 279–306, 2009.

[3] S. Kotthaus, B. H. Günther, R. Haug, and H. Schäfer, "Study of isotropically conductive bondings filled with aggregates of nano-sized Ag-particles," *IEEE Transactions on Components Packaging and Manufacturing Technology A*, vol. 20, no. 1, pp. 15–20, 1997.

[4] T. Klaus-Joerger, R. Joerger, E. Olsson, and C. Granqvist, "Bacteria as workers in the living factory: metal-accumulating bacteria and their potential for materials science," *Trends in Biotechnology*, vol. 19, no. 1, pp. 15–20, 2001.

[5] K. Cho, J. Park, T. Osaka, and S. Park, "The study of antimicrobial activity and preservative effects of nanosilver ingredient," *Electrochimica Acta*, vol. 51, no. 5, pp. 956–960, 2005.

[6] N. Durán, P. D. Marcato, G. I. H. de Souza, O. L. Alves, and E. Esposito, "Antibacterial effect of silver nanoparticles produced by fungal process on textile fabrics and their effluent treatment," *Journal of Biomedical Nanotechnology*, vol. 3, no. 2, pp. 203–208, 2007.

[7] G. Schmid, "Large clusters and colloids. Metals in the embryonic state," *Chemical Reviews*, vol. 92, no. 8, pp. 1709–1727, 1992.

[8] A. J. Hoffman, G. Mills, H. Yee, and M. R. Hoffmann, "Q-sized CdS: synthesis, characterization, and efficiency of photoinitiation of polymerization of several vinylic monomers," *Journal of Physical Chemistry*, vol. 96, no. 13, pp. 5546–5552, 1992.

[9] V. L. Colvin, M. C. Schlamp, and A. P. Alivisatos, "Light-emitting diodes made from cadmium selenide nanocrystals and a semiconducting polymer," *Nature*, vol. 370, no. 6488, pp. 354–357, 1994.

[10] Y. Wang and N. Herron, "Nanometer-sized semiconductor clusters: materials synthesis, quantum size effects, and photophysical properties," *Journal of Physical Chemistry*, vol. 95, no. 2, pp. 525–532, 1991.

[11] H. S. Mansur, F. Grieser, M. S. Marychurch, S. Biggs, R. S. Urquhart, and D. N. Furlong, "Photoelectrochemical properties of "Q-state" CdS particles in arachidic acid Langmuir-Blodgett films," *Journal of the Chemical Society, Faraday Transactions*, vol. 91, no. 4, pp. 665–672, 1995.

[12] Y. Wang, "Nonlinear optical properties of nanometer sized semi-conductor clusters," *Accounts of Chemical Research*, vol. 24, pp. 133–139, 1991.

[13] A. D. Yoffe, "Low-dimensional systems: quantum size effects and electronic properties of semiconductor microcrystallites (zero-dimensional systems) and some quasi-two-dimensional systems," *Advances in Physics*, vol. 42, no. 2, pp. 173–266, 1993.

[14] A. Parsa, "flora of Iran. sponsord by ministry of science & higher," *Education of Iran, Tehran*, vol. 1, pp. 448–449, 1978.

[15] D. S. Balaji, S. Basavaraja, R. Deshpande, D. B. Mahesh, B. K. Prabhakar, and A. Venkataraman, "Extracellular biosynthesis of functionalized silver nanoparticles by strains of *Cladosporium cladosporioides* fungus," *Colloids and Surfaces B*, vol. 68, no. 1, pp. 88–92, 2009.

[16] P. Mukherjee, A. Ahmad, D. Mandal et al., "Fungus-mediated synthesis of silver nanoparticles and their immobilization in the mycelial matrix: a novel biological approach to nanoparticle synthesis," *Nano Letters*, vol. 1, no. 10, pp. 515–519, 2001.

[17] B. Nair and T. Pradeep, "Coalescence of nanoclusters and formation of submicron crystallites assisted by *Lactobacillus* strains," *Crystal Growth and Design*, vol. 2, no. 4, pp. 293–298, 2002.

[18] S. S. Shankar, A. Absar, and S. Murali, "Geranium leaf assisted biosynthesis of silver nanoparticles," *Biotechnology Progress*, vol. 19, no. 6, pp. 1627–1631, 2003.

[19] S. P. Chandran, M. Chaudhary, R. Pasricha, A. Ahmad, and M. Sastry, "Synthesis of gold nanotriangles and silver nanoparticles using Aloe vera plant extract," *Biotechnology Progress*, vol. 22, no. 2, pp. 577–583, 2006.

[20] A. Ahmad, S. Senapati, M. I. Khan et al., "Intracellular synthesis of gold nanoparticles by a novel alkalotolerant actinomycete, *Rhodococcus* species," *Nanotechnology*, vol. 14, no. 7, pp. 824–828, 2003.

[21] R. W. Sun, R. Chen, N. P.-Y. Chung, C. Ho, C. S. Lin, and C. Che, "Silver nanoparticles fabricated in Hepes buffer exhibit cytoprotective activities toward HIV-1 infected cells," *Chemical Communications*, vol. 40, pp. 5059–5061, 2005.

[22] L. Sintubin, W. de Windt, J. Dick et al., "Lactic acid bacteria as reducing and capping agent for the fast and efficient production of silver nanoparticles," *Applied Microbiology and Biotechnology*, vol. 84, no. 4, pp. 741–749, 2009.

[23] A. Ahmad, P. Mukherjee, D. Mandal et al., "Enzyme mediated extracellular synthesis of CdS nanoparticles by the fungus, *Fusarium oxysporum*," *Journal of the American Chemical Society*, vol. 124, no. 41, pp. 12108–12109, 2002.

[24] S. Basavaraja, S. D. Balaji, A. Lagashetty, A. H. Rajasab, and A. Venkataraman, "Extracellular biosynthesis of silver nanoparticles using the fungus *Fusarium semitectum*," *Materials Research Bulletin*, vol. 43, no. 5, pp. 1164–1170, 2008.

[25] Y. Konishi, K. Ohno, N. Saitoh et al., "Bioreductive deposition of platinum nanoparticles on the bacterium Shewanella algae," *Journal of Biotechnology*, vol. 128, no. 3, pp. 648–653, 2007.

[26] Y. Konishi, T. Tsukiyama, K. Ohno, N. Saitoh, T. Nomura, and S. Nagamine, "Intracellular recovery of gold by microbial reduction of AuCl 4-ions using the anaerobic bacterium Shewanella algae," *Hydrometallurgy*, vol. 81, no. 1, pp. 24–29, 2006.

[27] Y. Konishi, T. Tsukiyama, T. Tachimi, N. Saitoh, T. Nomura, and S. Nagamine, "Microbial deposition of gold nanoparticles by the metal-reducing bacterium *Shewanella algae*," *Electrochimica Acta*, vol. 53, no. 1, pp. 186–192, 2007.

[28] J. L. Gardea-Torresdey, K. J. Tiemann, G. Gamez, K. Dokken, S. Tehuacanero, and M. José-Yacamán, "Gold nanoparticles obtained by bio-precipitation from gold(III) solutions," *Journal of Nanoparticle Research*, vol. 1, no. 3, pp. 397–404, 1999.

[29] J. J. Mock, M. Barbic, D. R. Smith, D. A. Schultz, and S. Schultz, "Shape effects in plasmon resonance of individual colloidal silver nanoparticles," *Journal of Chemical Physics*, vol. 116, no. 15, pp. 6755–6759, 2002.

[30] V. Armendariz, I. Herrera, J. R. Peralta-Videa et al., "Size controlled gold nanoparticle formation by *Avena sativa* biomass: use of plants in nanobiotechnology," *Journal of Nanoparticle Research*, vol. 6, no. 4, pp. 377–382, 2004.

[31] A. D. Dwivedi and K. Gopal, "Biosynthesis of silver and gold nanoparticles using *Chenopodium album* leaf extract," *Colloids and Surfaces A*, vol. 369, no. 1–3, pp. 27–33, 2010.

[32] R. Veerasamy, T. Z. Xin, S. Gunasagaran et al., "Biosynthesis of silver nanoparticles using mangosteen leaf extract and evaluation of their antimicrobial activities," *Journal of Saudi Chemical Society*, vol. 15, no. 2, pp. 113–120, 2011.

Hindawi Publishing Corporation
BioMed Research International
Volume 2013, Article ID 287638, 9 pages
http://dx.doi.org/10.1155/2013/287638

Research Article

Biosynthesis, Antimicrobial and Cytotoxic Effect of Silver Nanoparticles Using a Novel *Nocardiopsis* sp. MBRC-1

Panchanathan Manivasagan,[1] Jayachandran Venkatesan,[2] Kalimuthu Senthilkumar,[2] Kannan Sivakumar,[3] and Se-Kwon Kim[1,2]

[1] *Marine Biotechnology Laboratory, Department of Chemistry and Marine Bioprocess Research Center, Pukyong National University, Busan 608-737, Republic of Korea*
[2] *Department of Chemistry and Marine Bioprocess Research Center, Pukyong National University, Busan 608-737, Republic of Korea*
[3] *Centre of Advanced Study in Marine Biology, Faculty of Marine Sciences, Annamalai University, Parangipettai, Tamil Nadu 608 502, India*

Correspondence should be addressed to Se-Kwon Kim; sknkim@pknu.ac.kr

Received 4 May 2013; Revised 18 June 2013; Accepted 20 June 2013

Academic Editor: Maria Alice Zarur Coelho

The biosynthesis of nanoparticles has been proposed as a cost effective environmental friendly alternative to chemical and physical methods. Microbial synthesis of nanoparticles is under exploration due to wide biomedical applications, research interest in nanotechnology and microbial biotechnology. In the present study, an ecofriendly process for the synthesis of nanoparticles using a novel *Nocardiopsis* sp. MBRC-1 has been attempted. We used culture supernatant of *Nocardiopsis* sp. MBRC-1 for the simple and cost effective green synthesis of silver nanoparticles. The reduction of silver ions occurred when silver nitrate solution was treated with the *Nocardiopsis* sp. MBRC-1 culture supernatant at room temperature. The nanoparticles were characterized by UV-visible, TEM, FE-SEM, EDX, FTIR, and XRD spectroscopy. The nanoparticles exhibited an absorption peak around 420 nm, a characteristic surface plasmon resonance band of silver nanoparticles. They were spherical in shape with an average particle size of 45 ± 0.15 nm. The EDX analysis showed the presence of elemental silver signal in the synthesized nanoparticles. The FTIR analysis revealed that the protein component in the form of enzyme nitrate reductase produced by the isolate in the culture supernatant may be responsible for reduction and as capping agents. The XRD spectrum showed the characteristic Bragg peaks of 1 2 3, 2 0 4, 0 4 3, 1 4 4, and 3 1 1 facets of the face centered cubic silver nanoparticles and confirms that these nanoparticles are crystalline in nature. The prepared silver nanoparticles exhibited strong antimicrobial activity against bacteria and fungi. Cytotoxicity of biosynthesized AgNPs against in vitro human cervical cancer cell line (HeLa) showed a dose-response activity. IC_{50} value was found to be 200 μg/mL of AgNPs against HeLa cancer cells. Further studies are needed to elucidate the toxicity and the mechanism involved with antimicrobial and anticancer activity of the synthesized AgNPs as nanomedicine.

1. Introduction

Nanotechnology is emerging as a rapidly growing field with its application in science and technology [1]. Noble metal nanoparticles such as gold, silver, and platinum are widely applied in medicinal applications. Marine actinobacteria are high Guanine+Cytosine content Gram-positive bacteria with an unparalleled ability to produce diverse secondary metabolites, such as antibiotics, immunosuppressors, and many other biologically active compounds [2]. Exploitation of marine actinobacteria in nanotechnology has recently received considerable attention [3, 4]. Nanotechnology holds promising application in biosensing, drug delivery, and cancer therapy [5–7]. The expensive and extensive use of toxic solvents and hazardous reducing agents in chemical procedures to synthesize nanoparticles has augmented the necessity in view of ecofriendly and green chemistry approach. Hence, a well established nontoxic and ecofriendly potent

methodology for the synthesis of nanoparticles has mounted to a level of supreme importance [8–11]. An alternative approach for the synthesis of metal nanoparticles is to apply biomaterials such as plants, microorganisms encompassing groups such as bacteria, fungi, and actinobacteria as nanofactories [12–14]. Emerging multidrug resistant (MDR) bacteria has raised a demand for the urgent need to identify novel antimicrobial agents. It was reported that silver had been used as antimicrobial agents since ancient times [3]. With the advancements in nanotechnology, AgNPs have found its significant applications as antimicrobial agents, in fields of microelectronics, catalysis, and biomolecular detection [15–17]. Although the antibacterial activity of AgNPs has been proved in the recent years, the actual mechanism of action is not yet clear. They may inactivate microorganisms by interacting with their enzymes, proteins, or DNA to inhibit cell proliferation [18]. It is also evident that the increased antimicrobial activity of AgNPs may be attributed to its special characteristics of small size and high surface area to volume ratio [19]. The advantage of adapting biosynthesis of AgNPs is the simplicity of extracellular synthesis and downstream processing [20, 21].

Nanoparticles have a wide range of applications, as in combating microbes [22], biolabelling [23], and in the treatment of cancer [24]. The antibacterial activity of silver species is known since ancient times [25] and it has been demonstrated that, at low concentrations, silver is nontoxic to human cells [26]. It has also been reported that Ag^+ ions uncouple the respiratory chain from oxidative phosphorylation or collapse the proton-motive force across the cytoplasmic membrane [27]. The interaction of Ag^+ with bacteria is directly related to the size and shape of the nanoparticles [26, 28].

Sastry et al. [29] reported on the biosynthesis of metal nanoparticles using the mycelial extract of fungi and actinobacteria [29]. In addition, the time required for completion of the reaction using both bacteria and fungi ranges between approximately 24 hrs and 120 hrs, whereas maximum synthesis of AgNPs can be achieved after 24 hrs of incubation. Moreover, metal accumulation is dependent on the growth phase of the cells [30]. Sadhasivam et al. [3] reported on the extracellular biosynthesis of NPs by *Streptomyces hygroscopicus* and antimicrobial activity against medically important pathogenic micro-organisms [3]. Sivalingam et al. [31] reported on the biosynthesis of bactericidal silver nanoparticles (AgNPs) using a novel *Streptomyces* sp. BDUKAS10, an isolated mangrove sediment [31]. Though the mechanism of silver resistance offered by bacteria using the silver binding protein is well documented, their extraction and purification need to be elucidated further for large-scale production. However, only a few studies have examined the components of marine actinobacteria that mediated the reduction of silver ions into AgNPs. In this study, we examined and characterized the extracellular biosynthesis of AgNPs using a novel *Nocardiopsis* sp. MBRC-1, which is a very important micro-organism to the production of several antibiotics and enzymes of commercial value. To the best of our knowledge, this marine actinobacterium (*Nocardiopsis* sp. MBRC-1) has never been used for nanoparticles biosynthesis.

2. Materials and Methods

2.1. Chemicals. All analytical reagents and media components were purchased from Sigma-Aldrich (St. Louis, USA).

2.2. Microbial Synthesis of AgNPs. The *Nocardiopsis* sp. MBRC-1 strain was isolated from the marine sediment samples from the Busan coast (Lat 35°09′ N; Long 129°07′ E), South Korea. Their partial 16S rRNA gene sequences were deposited in GenBank under the accession number KC179785. For the synthesis of silver nanoparticles, the active *Nocardiopsis* sp. MBRC-1 culture was freshly inoculated on sterile starch casein medium and the flasks were incubated at 25–28°C and 180 rpm for 96 hrs (pH 7.0). After the incubation period was complete, the culture was centrifuged at 5000 rpm for 30 min and the supernatant was used for the biosynthesis of AgNPs. Deionized water was used as a solvent in the synthesis of AgNPs. The collected supernatant (pH 7.0) was added separately to the reaction vessel containing silver nitrate at a concentration of 10^{-3} M (1% (v/v)) and incubated on an orbital shaker (dark condition) for 96 hrs at 30°C. The reaction was carried out in the dark after the addition of the $AgNO_3$, and color change appeared transparent. It confirmed the synthesis of AgNPs. The formation of the AgNPs was monitored by UV-vis spectroscopy using Shimadzu (Model No-UV 1800) double beam UV-vis spectrophotometer [3]. All the experiments were carried out in triplicate and average values have been reported.

2.3. Characterization of AgNPs. The synthesized AgNPs were freeze dried, powdered, and used for XRD analysis. The spectra were evaluated using an X-ray diffractometer (PHILIPS X'Pert-MPD diffractometer, The Netherlands) and Cu-Kα radiation 1.5405 Å over an angular range of 5 to 80°, a step size of 0.02, a scan speed of $4^\circ\,m^{-1}$ at a 40 kV voltage, and a 30 mA current. The dried powder was diluted with potassium bromide in the ratio of 1 : 100 and recorded the Fourier transform infrared spectroscopy (FTIR) (Perkin Elmer Inc., USA) and spectrum GX spectrometry within the range of 400 to 4000 cm^{-1}. Synthesized AgNPs were mounted on specimen stubs with double-sided adhesive tape coated with platinum in a sputter coater and examined under field emission scanning electron microscopy (FE-SEM) (JSM-6700, JEOL, Japan). For transmission electron microscopy (TEM) imaging, a drop of aqueous solution containing the AgNPs was placed on carbon coated copper grids and dried under an infrared lamp (JEM 1010 JEOL, Japan) (AC voltage −80.0 kV). In addition, the presence of silver metals in the sample was analyzed by energy dispersive X-ray analysis (EDX) combined with FE-SEM. Finally, the size distribution of the nanoparticles was evaluated using dynamic light scattering measurements conducted with a Malvern Zetasizer ZS compact scattering spectrometer (Malvern Instruments Ltd., Malvern, UK).

2.4. Particle-Size Distribution of AgNPs. Particle-size distribution analysis was carried out after treatment of a 1 mM solution of $AgNO_3$ with the culture supernatant of *Nocardiopsis* sp. MBRC-1 at room temperature for 98 hrs. The organism

was grown in starch casein broth under incubation at 30°C for 98 hrs. After the incubation period, the culture was centrifuged at 10,000 rpm and the supernatant was used to reduce the $AgNO_3$ solution. For the DLS measurements, the supernatant thus obtained was a clear brown homogenous suspension of AgNPs diluted 10-fold for all experiments involving measurement of DLS. The solutions were then filtered through syringe membrane filters with pores less than 0.4 μm, then centrifuged at 5000 rpm for 30 min.

2.5. Antimicrobial Activity of the AgNPs. The antimicrobial activity of the microbiologically synthesized AgNPs against pathogenic organisms such as bacteria (*Escherichia coli*, *Bacillus subtilis*, *Enterococcus hirae*, *Pseudomonas aeruginosa*, *Shigella flexneri* and *Staphylococcus aureus*) and fungi (*Aspergillus niger, A. brasiliensis, A. fumigates* and *Candida albicans*) was measured using the well-diffusion method [26]. Pure cultures of bacteria and fungi were grown in Mueller-Hinton broth (Sigma, USA) for bacteria and Sabouraud-broth for fungi at 35°C and 30°C, respectively, on a rotary shaker at 180 rpm. Wells that were 6 mm in diameter were made on the Mueller-Hinton agar and Sabouraud agar plates using a gel puncture and each well was inoculated with individual cultures. The AgNPs in various concentrations (10, 20, 30, 40, and 50 μg/mL) were loaded in each well. The positive and negative controls were also maintained, and the plates (triplicates) were incubated at 35°C and 30°C for 24 and 48 hrs. Simultaneously, the synergistic effects of different commercial antibiotics (Amoxicillin and Nystatin, Sigma, USA) with AgNPs against multidrug resistant pathogens were also checked in well diffusion method. After incubation, the susceptibility pattern of the test organisms was determined by measuring the diameter of the zone of inhibition for well diffusion method.

2.6. Determination of Minimum Inhibitory Concentration. The synthesized silver nanoparticles were tested (triplicates) for minimum inhibitory concentration by microtiter broth dilution method [32]. Muller-Hinton broth was used as diluents for bacterial strains and Sabouraud broth for fungal species. About 10^6 CFU/mL cells were inoculated, and the final volume in each microtiter plate well was 0.1 mL. After incubation for 24 h, at 35°C for bacterial strains and 30°C for fungal strains, the microtiter plates were read at 450 nm using TRIAD multimode reader prior to and after incubation to determine the minimum inhibitory concentration (MIC) values. The MIC is defined as the lowest concentration of compound, which inhibited 90% of the growth when compared with that of the growth control.

2.7. Cell Culture. Human cervical cancer cell line (HeLa) was cultured in Dulbecco's Modified Eagle Medium (DMEM). Culture media were supplemented with 10% fetal bovine serum (FBS) and 1% antibiotic and antimycotic (Penicillin-Streptomycin cocktail) solution. The cells were grown in a humidified atmosphere containing 5% CO_2 at 37°C and subcultured by detaching with trypsin-EDTA solution at about 70–80% confluent.

2.8. Cytotoxic Activity. Cell viability was evaluated by the MTT colorimetric technique. Human HeLa cancer cell lines (5000 cells/well) were seeded in 96 well tissue culture plates. Stock solutions of nanoparticles (5 mg/mL) were prepared in sterile distilled water and diluted to the required concentrations (50, 100, 150, 200, and 250 μg/mL) using the cell culture medium. Appropriate concentrations of AgNPs stock solution were added to the cultures to obtain respective concentration of AgNPs and incubated for 24 hrs at 37°C. Nontreated cells were used as control. After 24 hrs, cells were washed with PBS and then 100 μL of the yellow tetrazolium MTT solution (3-(4,5-dimethylthiazolyl-2)-2,5-diphenyltetrazolium bromide) without phenol red (0.5 mg/mL in phosphate buffer solution) was added to each well. The plates were incubated for 3-4 hrs at 37°C, for reduction of MTT by metabolically active cells, in part by the action of dehydrogenase enzymes, to generate reducing equivalents such as NADH and NADPH. For solubilization of the MTT crystals, 100 μL of DMSO was added to the wells. The plates were placed on a shaker for 15 min to complete solubilization of crystals, and then the optical density of each well was determined. The quantity of formazan product as measured by the amount of 545 nm absorbance is directly proportional to the number of living cells in culture. Each experiment was done in triplicate. The relative cell viability (%) related to control wells containing cell culture medium without nanoparticles as a vehicle was calculated as follows: Percentage of cell viability (%) = Sample absorbance/control absorbance × 100.

2.9. Cytomorphological Changes in HeLa Cells by AgNPs. HeLa cells (1×10^5 cells/well) were seeded in a 6 well plate for 24 hrs. After 24 hrs, they were treated with 100 and 200 μg/mL of synthesized AgNPs and incubated for 24 hrs at 37°C in 5% CO_2 atmosphere. After the incubation, the cells were washed twice with PBS, and morphological changes in the cells were visualized and photographed under phase contrast microscope (CTR 6000; Leica, Wetzlar, Germany).

2.10. Statistical Analysis. The grouped data were statistically evaluated using ANOVA with SPSS/14 software. Values are presented as the mean ± SD of the three replicates of each experiment.

3. Results and Discussion

3.1. Isolation and Identification of Marine Actinobacteria. A marine actinobacterium MBRC-1 strain was isolated from the marine sediment samples from the Busan coast, South Korea, and was used for the synthesis of silver nanoparticles. The marine actinobacterium MBRC-1 shows that the presence of *meso*-diaminopimelic acid as the amino acid in the cell wall and arabinose and galactose as whole cell sugars and the absence of characteristic glycine in their cell credibly categorized the cell wall of this strain belonged to the cell wall type-IV [33]. This isolate was identified as *Nocardiopsis* sp. MBRC-1 based on the morphological, physiological, and biochemical characteristics, and it was confirmed by the 16S rDNA sequencing

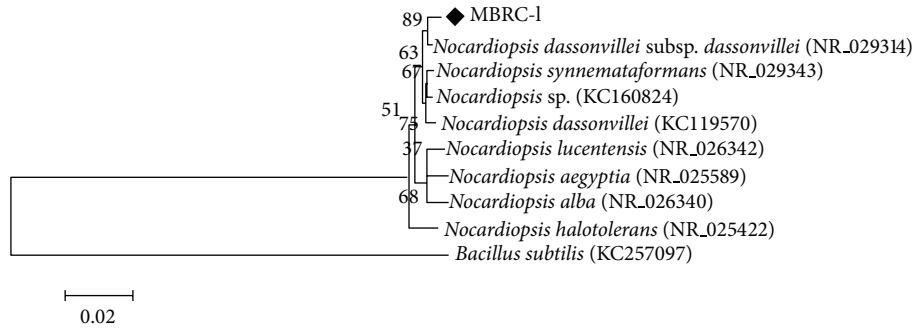

Figure 1: Phylogenetic tree of the 16S rDNA sequence of strain *Nocardiopsis* sp. MBRC-1 and related strains.

(Figure 1). The sequence was submitted to GenBank in NCBI (http://www.ncbi.nlm.nih.gov/nuccore/443501390/) with the accession number KC179785.

3.2. UV-Vis Analysis of AgNPs. In this study, AgNPs were successfully synthesized in the culture supernatant of *Nocardiopsis* sp. MBRC-1. Interestingly, the culture supernatant incubated with the silver nitrate mediated the biosynthesizing of AgNPs within 24 hrs of incubation. During the experiment, the pH of the sample was adjusted to 7.0. The appearance of a yellowish brown color in the silver nitrate treated flask indicated the formation of silver nanoparticles, whereas no color change was observed in either the culture supernatant without silver nitrate or the silver nitrate control experiments. Notably, the intensity of the brown color increased dramatically up to 24 hrs and was maintained throughout the experiment. This may have been due to the excitation of surface plasmon resonance (SPR) and the reduction of $AgNO_3$. In the UV-visible spectrum, a strong and broad peak was observed between 420 nm, indicating the presence of AgNPs. This may have occurred due to the reduction of metal ions by secondary metabolites present in the cells. The 24, 48, 72, and 96 hrs peaks indicate the absorption spectra of biosynthesized AgNPs at different incubation times (Figure 2). Numerous reports have discussed the biosynthesis of silver nanoparticles [3, 31, 34], but to the best of knowledge, this was the first report on biosynthesis of silver nanoparticles using a novel *Nocardiopsis* sp. MBRC-1.

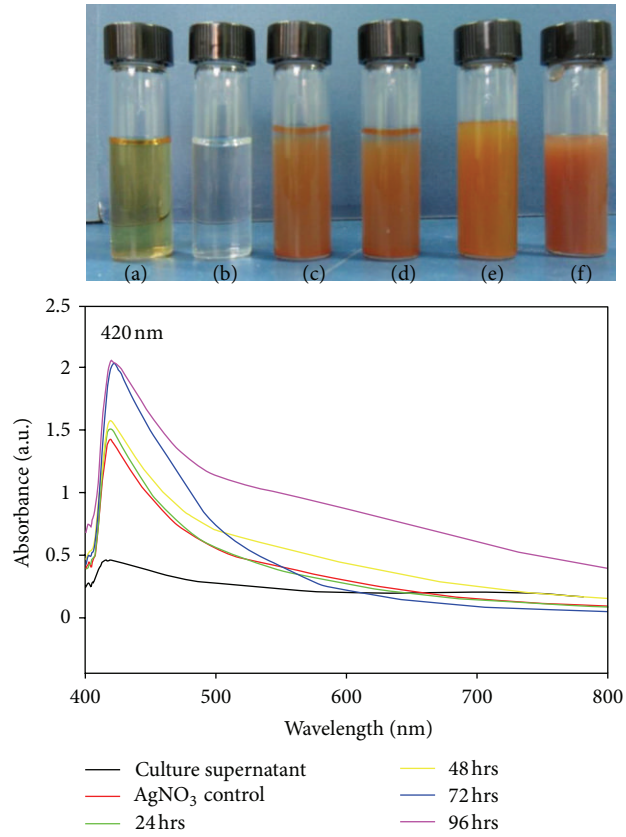

Figure 2: UV-Vis spectra of AgNPs synthesized using cell free supernatant of *Nocardiopsis* sp. MBRC-1. (a) Culture supernatant; (b) $AgNO_3$ control; ((c)–(f)) correspond to the $AgNO_3$ treated with culture supernatant incubated for 24, 48, 72, and 96 hrs, respectively.

3.3. FTIR Analysis of AgNPs. FTIR spectrum analysis of AgNPs showed intense absorption bands at 3440, 2923, 2853, 1655, 1460, and 685 cm^{-1}. The intense broad absorbance at 3440 cm^{-1} (O–H stretch) is the characteristic of the H-bonded functional group in alcohols and phenolic compounds. The band at 2923 and 2853 cm^{-1} (C–H stretch) can be assigned to the alkanes group. The intense medium absorbance at 1655 cm^{-1} (–C=C– stretch) is the characteristic of the alkenes group. The intense medium absorbance at 1460 cm^{-1} (C–H bend) is the characteristic of the alkanes group. The intense broad absorbance at 685 cm^{-1} (–C=C–H: C–H bend) is the characteristic of the alkynes group. A previous report reveals that the alcohols, phenolic, alkynes, and alkanes groups have a strong ability to interact with nanoparticles [31, 35, 36].

3.4. XRD Analysis of AgNPs. The XRD pattern of the silver nitrate-treated sample (Figure 3) corresponds to that of silver nanoparticles. The XRD pattern shows five intense peaks in the whole spectrum of 2θ values ranging from 30 to 80. It is important to know the exact nature of the silver particles formed and this can be deduced from the XRD

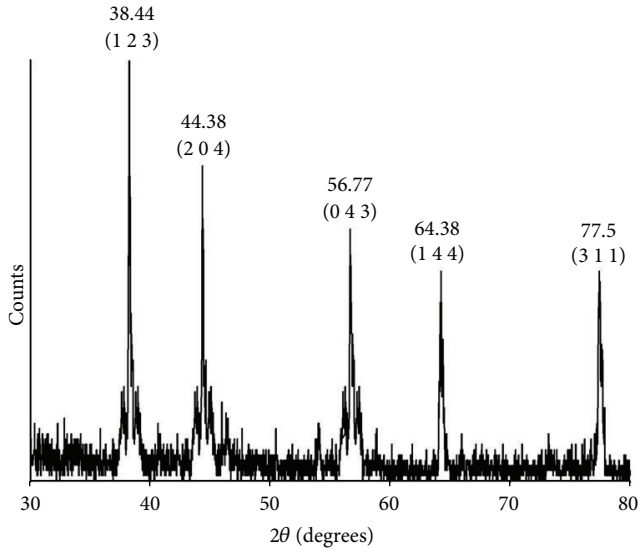

Figure 3: X-ray diffraction pattern of the AgNPs obtained from *Nocardiopsis* sp. MBRC-1.

spectrum of the sample. XRD spectra of pure nanoparticles silver structures and pure silver nitrate have been published by the Joint Committee on Powder Diffraction Standards (file no. 04-0783). A comparison of our XRD spectrum with the standard confirmed that the silver particles formed in our experiments were in the form of nanoparticles, as evidenced by the peaks at 2θ values of 38.44°, 44.38°, 56.77°, 64.38°, and 77.50°, corresponding to 1 2 3, 2 0 4, 0 4 3, 1 4 4, and 3 1 1 planes for silver, respectively. The full width at half maximum (FWHM) values measured for 1 2 3, 2 0 4, 0 4 3, 1 4 4, and 3 1 1 planes of reflection was used with the Debye-Scherrer equation to calculate the size of the nanoparticles. The particle sizes obtained from XRD line broadening agreed well with those obtained from SEM. From these, the average particle size was found to be around 45 ± 0.05 nm.

3.5. FE-SEM Analysis of AgNPs. FE-SEM determinations of the above-mentioned sample showed the formation of nanoparticles, which were confirmed to be of silver by EDX. As shown in Figures 4(a) and 4(b), well-dispersed nanoparticles could be seen in the samples treated with silver nitrate. EDX analysis also showed a peak in the silver region, confirming the formation of silver nanoparticles (Figure 4(c)). The optical absorption peak is observed approximately at 3 keV, which is typical for the absorption of metallic silver nanoparticles due to surface Plasmon resonance [37]. In addition, other peaks for Cl and O were observed which are possibly due to emissions from proteins or enzymes present in the culture supernatant [30].

3.6. TEM Analysis of AgNPs. The TEM image analysis (Figures 5(a) and 5(b)) revealed that silver nanoparticles were spherical in shape. The micrograph showed NPs with variable shape; most of them present in spherical in nature. The TEM micrograph also confirmed the size of NPs, which

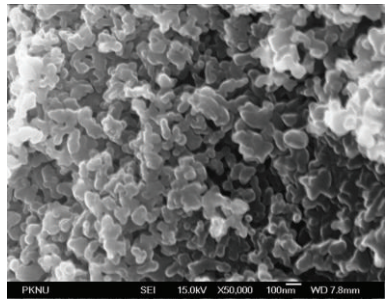

(a)

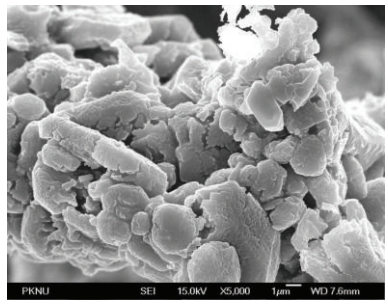

(b)

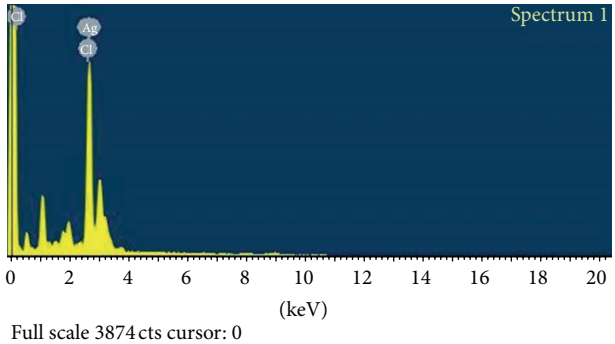

(c)

Figure 4: ((a) and (b)) FE-SEM images of AgNPs synthesized by *Nocardiopsis* sp. MBRC-1. (a) 100 nm scale, (b) 1 μm scale, and (c) EDX analysis of AgNPs synthesized by *Nocardiopsis* sp. MBRC-1.

were in the range of 30–90 nm with an average particle size of 45 ± 0.15 nm. Majority of the AgNPs were aggregates with only a few of them showing scattering of varying sizes as observed under TEM. The particle size distribution histogram plot constructed from the TEM micrograph is shown in Figure 5(c). Synthesis of AgNPs by treating $AgNO_3$ solution with the culture supernatant of *K. pneumonia* (belonging to the family Enterobacteriaceae) has also been reported, in which the particles range in size from 28.2 to 122 nm and possess an average size of 52.5 nm [14]. A study on synthesis of AgNPs using *Morganella* sp. (belonging to the family *Enterobacteriaceae*) reported spherical nanoparticles of ~20 nm size [38].

3.7. Antimicrobial Activity of the AgNPs. In this study, the antimicrobial activity of AgNPs using a novel biosynthetic method was evaluated. In this analysis, the AgNPs displayed

Table 1: Antimicrobial activity of the AgNPs against various pathogenic micro-organisms. The data is presented as the mean ± value standard deviation of three replicates.

Micro-organisms	Zone of inhibition (mm in diameter)					
	10 μg/mL	20 μg/mL	30 μg/mL	40 μg/mL	50 μg/mL	Antibiotics 30 μg/mL
Bacteria						Amoxicillin
Escherichia coli ATCC 10536	7.5 ± 0.35	15.2 ± 0.31	18.8 ± 0.30	23.3 ± 0.20	27.3 ± 0.15	19.3 ± 0.10
Bacillus subtilis ATCC 6633	11.2 ± 0.35	19.4 ± 0.25	22.5 ± 0.10	28.1 ± 0.20	33.2 ± 0.20	23.8 ± 0.25
Enterococcus hirae ATCC 10541	6.3 ± 0.20	13.3 ± 0.14	17.2 ± 0.15	21.8 ± 0.30	25.4 ± 0.25	19.5 ± 0.10
Pseudomonas aeruginosa ATCC 27853	9.1 ± 0.15	17.7 ± 0.30	19.4 ± 0.20	23.6 ± 0.35	28.3 ± 0.20	21.3 ± 0.30
Shigella flexneri ATCC 12022	5.2 ± 0.20	11.2 ± 0.21	15.4 ± 0.15	19.3 ± 0.25	22.5 ± 0.10	17.5 ± 0.30
Staphylococcus aureus ATCC 6538	7.8 ± 0.25	15.1 ± 0.32	19.1 ± 0.20	24.2 ± 0.20	27.1 ± 0.15	21.3 ± 0.10
Fungi						Nystatin
Aspergillus niger ATCC 1015	6.7 ± 0.32	13.6 ± 0.22	17.3 ± 0.25	21.4 ± 0.20	25.3 ± 0.15	18.1 ± 0.10
A. brasiliensis ATCC 16404	4.8 ± 0.25	10.2 ± 0.15	14.6 ± 0.20	19.4 ± 0.10	23.4 ± 0.15	15.8 ± 0.30
A. fumigates ATCC 1022	7.2 ± 0.35	15.4 ± 0.22	19.3 ± 0.20	24.3 ± 0.10	26.3 ± 0.30	21.4 ± 0.15
Candida albicans ATCC 10231	9.5 ± 0.20	18.1 ± 0.21	22.4 ± 0.25	25.2 ± 0.25	28.4 ± 0.25	24.5 ± 0.20

Table 2: Minimum inhibitory concentration of the AgNPs against various bacterial and fungal strains. The data is presented as the mean ± value standard deviation of three replicates.

Micro-organisms	Minimum inhibitory concentration	
	AgNPs (μg/mL)	Antibiotics (μg/mL)
Bacteria		Amoxicillin
Escherichia coli ATCC 10536	13	11
Bacillus subtilis ATCC 6633	7	6
Enterococcus hirae ATCC 10541	16	14
Pseudomonas aeruginosa ATCC 27853	10	9
Shigella flexneri ATCC 12022	18	15
Staphylococcus aureus ATCC 6538	14	12
Fungi		Nystatin
Aspergillus niger ATCC 1015	16	14
A. brasiliensis ATCC 16404	18	16
A. fumigates ATCC 1022	13	12
Candida albicans ATCC 10231	10	7

antimicrobial activity against a range of different pathogenic microorganisms (Table 1). The mean of three replicates of the diameter of the zone of inhibition (30 μg/mL) for each microorganism was determined to be about 18.8 ± 0.30, 22.5 ± 0.10, 17.2 ± 0.15, 19.4 ± 0.20, 15.4 ± 0.15, 19.1 ± 0.20, 17.3 ± 0.25, 14.6 ± 0.20, 19.3 ± 0.20, and 22.4 ± 0.25 mm, respectively, for *Escherichia coli, Bacillus subtilis*, *Enterococcus hirae*, *Pseudomonas aeruginosa*, *Shigella flexneri*, *Staphylococcus aureus*, *Aspergillus niger*, *A. brasiliensis*, *A. fumigates*, and *Candida albicans*. The highest antimicrobial activity was observed against *Bacillus subtilis*, *Pseudomonas aeruginosa*, and *Candida albicans*. These findings are in agreement with previous studies that examined the antimicrobial activity of AgNPs against *Bacillus subtilis* and *Candida albicans* [3]. The antimicrobial activity of silver nanoparticles was reported to be due to the penetration into the bacteria, damage of cell membrane, and release of cell contents [39]. Another possibility suggested that [40, 41] was the release of silver ions from the nanoparticles, which may contribute to the bactericidal properties of silver nanoparticles.

3.8. Determination of Minimum Inhibitory Concentration. Minimum inhibitory concentration of AgNPs (Table 2) was evaluated against various pathogenic bacteria and fungi. The silver nanoparticles exhibited lowest minimum inhibitory concentration (MIC) against *Bacillus subtilis* at 7 μg/mL, *Bacillus subtilis* 10 μg/mL, and *Candida albicans* at 10 μg/mL, suggesting the broad spectrum nature of their minimum inhibitory concentration. Kumar and Mamidyala [35] reported the minimum inhibitory concentration of AgNPs against Gram-positive, Gram-negative, and different *Candida* species at concentrations ranging between 4 and 32 μg/mL.

3.9. Cytotoxic Activity. The *in vitro* potential cytotoxic activity of AgNPs against cervical cancer cell lines HeLa. The use of synthetic AgNPs, there are only a few studies to determine that the cytotoxic effects of biologically synthesized AgNPs. MTT assay was used to assess the effect of AgNPs on the cytotoxicity of cancer cells. This study to evaluate the marine sediment samples isolated species *Nocardiopsis* sp. MBRC-1 derived AgNPs cytotoxicity against HeLa cancer cell lines. AgNPs inhibit the viability of the HeLa cancer cell lines in dose dependent manner. The IC_{50} value of biosynthesized AgNPs against HeLa cells at 200 μg/mL concentrations (Figure 6(a)). Previously, synthesized AgNPs inducing cytotoxicity were discussed by Sriram et al. [42] and Safaepour et al. [43].

3.10. Cytomorphological Changes of HeLa Cells Induced by AgNPs. The morphological examinations of the HeLa cancer cells were observed and photographed using phase contrast microscope. The morphological alteration was observed in

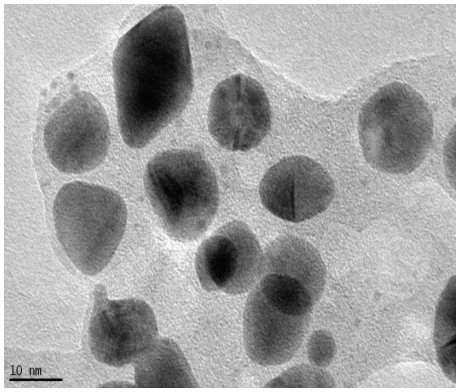

(a)

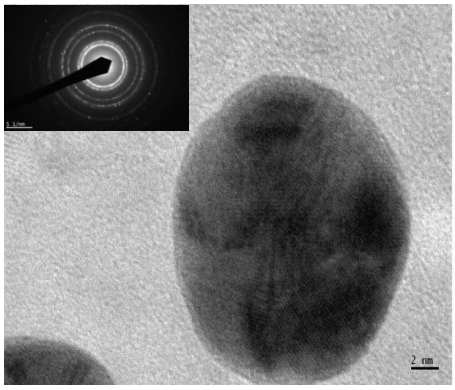

(b)

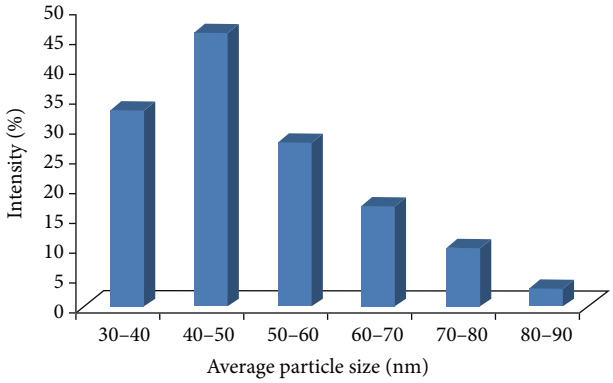

(c)

Figure 5: HR-TEM images of AgNPs formed by *Nocardiopsis* sp. MBRC-1. (a) 10 nm scale, (b) 2 nm scale and selected area diffraction pattern. (c) Particle-size distribution under unoptimized conditions. The particle-size distribution revealed that the particles ranging from 30 to 90 nm had the maximum intensity, and thereafter the intensity was reduced. The average particle size was found to be 45 ± 0.15 nm.

control and AgNPs treated HeLa cancer cells. The HeLa cells were treated with AgNPs at 100 and 200 μg/mL concentrations for 24 hrs showing that significant morphological changes, which are characteristic features of apoptotic cells, such as loss of membrane integrity, cell shrinkage, and reduced cell density (Figures 6(b) and 6(c)).

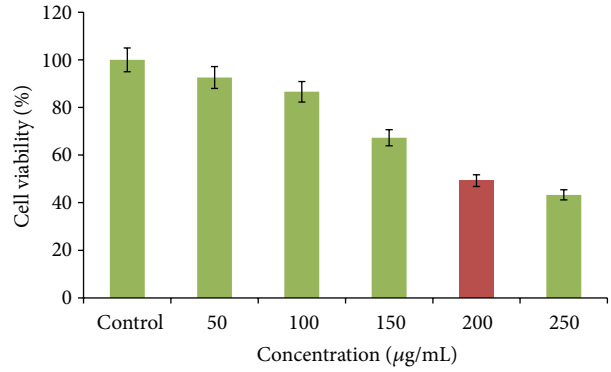

(a)

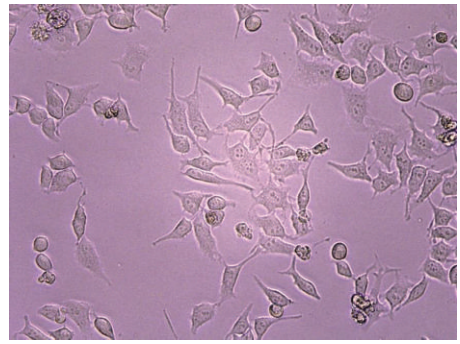

(b)

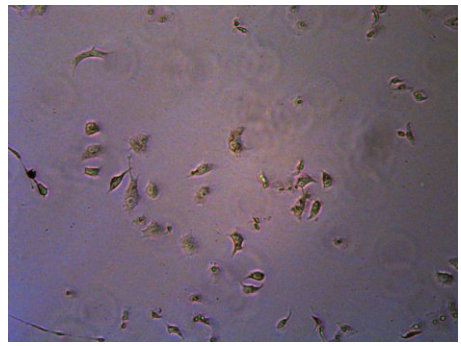

(c)

Figure 6: (a) MTT assay results confirming the *in vitro* cytotoxicity of AgNPs against HeLa cell lines. ((b) and (c)) Morphology of control and AgNPs treated HeLa cell lines (10x magnification). (b) Control. (c) IC_{50} concentration (200 μg/mL).

4. Conclusions

In conclusion, silver nanoparticles are synthesized by the biomass of the marine actinobacterium, *Nocardiopsis* sp. MBRC-1. Marine actinobacteria are easy to handle and can be manipulated genetically without much difficulty. Considering these advantages, a bacterial system could prove to be an excellent alternative for synthesis of AgNPs. *Nocardiopsis* sp. MBRC-1 can be a good candidate for the synthesis of the AgNPs using silver nitrate of average size 45 ± 0.15 nm. *Nocardiopsis* sp. MBRC-1 genetics and enzymatic activities, sophisticated molecular breeding can produce strains and biotechnological processes, which could eliminate

many types of contaminants in an economical, efficient, and simple process and environmentally friendly manner. The biosynthesized silver nanoparticles showed excellent antimicrobial activity and possessed considerable cytotoxic effect against *in vitro* HeLa cancer cell lines. IC_{50} value was found to be 200 μg/mL of AgNPs against HeLa cell lines. The data represented in our study contribute to a novel and unexplored area of nanomaterials as alternative medicine. Furthermore, the biosynthesized AgNPs displayed a pronounced antimicrobial and cytotoxicity activity against clinical pathogenic microorganisms and HeLa cancer cell lines. Taken together, the data collected in this study suggests that it would be important to understand the mode of action of the biosynthesized nanoparticles prior to their use in nanomedicine applications.

Acknowledgment

This research was supported by a grant from Marine Bioprocess Research Center of the Marine Biotechnology Program funded by the Ministry of Oceans and Fisheries, Republic of Korea. One of the authors Kannan Sivakumar expresses his thanks to the Director, Centre of Advanced Study in Marine Biology, Faculty of Marine Sciences and Annamalai University authorities for facilities and encouragement.

References

[1] M. A. Albrecht, C. W. Evans, and C. L. Raston, "Green chemistry and the health implications of nanoparticles," *Green Chemistry*, vol. 8, no. 5, pp. 417–432, 2006.

[2] K. F. Chater, "Genetics of differentiation in Streptomyces," *Annual Review of Microbiology*, vol. 47, pp. 685–713, 1993.

[3] S. Sadhasivam, P. Shanmugam, and K. Yun, "Biosynthesis of silver nanoparticles by *Streptomyces hygroscopicus* and antimicrobial activity against medically important pathogenic microorganisms," *Colloids and Surfaces B*, vol. 81, no. 1, pp. 358–362, 2010.

[4] S. Sadhasivam, P. Shanmugam, M. Veerapandian, R. Subbiah, and K. Yun, "Biogenic synthesis of multidimensional gold nanoparticles assisted by *Streptomyces hygroscopicus* and its electrochemical and antibacterial properties," *BioMetals*, vol. 25, no. 2, pp. 351–360, 2011.

[5] K. A. Willets and R. P. Van Duyne, "Localized surface plasmon resonance spectroscopy and sensing," *Annual Review of Physical Chemistry*, vol. 58, pp. 267–297, 2007.

[6] D. I. Gittins, D. Bethell, D. J. Schiffrin, and R. J. Nichols, "A nanometre-scale electronic switch consisting of a metal cluster and redox-addressable groups," *Nature*, vol. 408, no. 6808, pp. 67–69, 2000.

[7] P. K. Jain, I. H. ElSayed, and M. A. El-Sayed, "Au nanoparticles target cancer," *Nano Today*, vol. 2, no. 1, pp. 18–29, 2007.

[8] D. Yu, "Formation of colloidal silver nanoparticles stabilized by Na^+-poly(γ-glutamic acid)-silver nitrate complex via chemical reduction process," *Colloids and Surfaces B*, vol. 59, no. 2, pp. 171–178, 2007.

[9] K. Mallick, M. J. Witcomb, and M. S. Scurrell, "Self-assembly of silver nanoparticles in a polymer solvent: Formation of a nanochain through nanoscale soldering," *Materials Chemistry and Physics*, vol. 90, no. 2-3, pp. 221–224, 2005.

[10] Y.-C. Liu and L.-H. Lin, "New pathway for the synthesis of ultrafine silver nanoparticles from bulk silver substrates in aqueous solutions by sonoelectrochemical methods," *Electrochemistry Communications*, vol. 6, no. 11, pp. 1163–1168, 2004.

[11] A. B. Smetana, K. J. Klabunde, and C. M. Sorensen, "Synthesis of spherical silver nanoparticles by digestive ripening, stabilization with various agents, and their 3-D and 2-D superlattice formation," *Journal of Colloid and Interface Science*, vol. 284, no. 2, pp. 521–526, 2005.

[12] M. Kowshik, S. Ashtaputre, S. Kharrazi et al., "Extracellular synthesis of silver nanoparticles by a silver-tolerant yeast strain MKY3," *Nanotechnology*, vol. 14, no. 1, pp. 95–100, 2003.

[13] S. Senapati, A. Ahmad, M. I. Khan, M. Sastry, and R. Kumar, "Extracellular biosynthesis of bimetallic Au–Ag alloy nanoparticles," *Small*, vol. 1, no. 5, pp. 517–520, 2005.

[14] A. R. Shahverdi, S. Minaeian, H. R. Shahverdi, H. Jamalifar, and A. Nohi, "Rapid synthesis of silver nanoparticles using culture supernatants of Enterobacteria: a novel biological approach," *Process Biochemistry*, vol. 42, no. 5, pp. 919–923, 2007.

[15] M. Liong, B. France, K. A. Bradley, and J. I. Zink, "Antimicrobial activity of silver nanocrystals encapsulated in mesoporous silica nanoparticles," *Advanced Materials*, vol. 21, no. 17, pp. 1684–1689, 2009.

[16] K.-H. Cho, J.-E. Park, T. Osaka, and S.-G. Park, "The study of antimicrobial activity and preservative effects of nanosilver ingredient," *Electrochimica Acta*, vol. 51, no. 5, pp. 956–960, 2005.

[17] H. Wei, C. Chen, B. Han, and E. Wang, "Enzyme colorimetric assay using unmodified silver nanoparticles," *Analytical Chemistry*, vol. 80, no. 18, pp. 7051–7055, 2008.

[18] A. K. Singh, M. Talat, D. P. Singh, and O. N. Srivastava, "Biosynthesis of gold and silver nanoparticles by natural precursor clove and their functionalization with amine group," *Journal of Nanoparticle Research*, vol. 12, no. 5, pp. 1667–1675, 2010.

[19] A. R. Shahverdi, A. Fakhimi, H. R. Shahverdi, and S. Minaian, "Synthesis and effect of silver nanoparticles on the antibacterial activity of different antibiotics against *Staphylococcus aureus* and *Escherichia coli*," *Nanomedicine*, vol. 3, no. 2, pp. 168–171, 2007.

[20] A. Ingle, M. Rai, A. Gade, and M. Bawaskar, "Fusarium solani: a novel biological agent for the extracellular synthesis of silver nanoparticles," *Journal of Nanoparticle Research*, vol. 11, no. 8, pp. 2079–2085, 2009.

[21] H. Bai, B. Yang, C. Chai, G. Yang, W. Jia, and Z. Yi, "Green synthesis of silver nanoparticles using *Rhodobacter sphaeroides*," *World Journal of Microbiology and Biotechnology*, vol. 27, no. 11, pp. 2723–2728, 2011.

[22] N. Durán, P. D. Marcato, O. L. Alves, G. I. H. De Souza, and E. Esposito, "Mechanistic aspects of biosynthesis of silver nanoparticles by several *Fusarium oxysporum* strains," *Journal of Nanobiotechnology*, vol. 3, article 8, 2005.

[23] T. Klaus, R. Joerger, E. Olsson, and C. Granqvist, "Silver-based crystalline nanoparticles, microbially fabricated," *Proceedings of the National Academy of Sciences of the United States of America*, vol. 96, no. 24, pp. 13611–13614, 1999.

[24] S. Arora, J. Jain, J. M. Rajwade, and K. M. Paknikar, "Cellular responses induced by silver nanoparticles: *in vitro* studies," *Toxicology Letters*, vol. 179, no. 2, pp. 93–100, 2008.

[25] S. Gurunathan, K. Kalishwaralal, R. Vaidyanathan et al., "Biosynthesis, purification and characterization of silver nanoparticles using *Escherichia coli*," *Colloids and Surfaces B*, vol. 74, no. 1, pp. 328–335, 2009.

[26] S. Pal, Y. K. Tak, and J. M. Song, "Does the antibacterial activity of silver nanoparticles depend on the shape of the nanoparticle? A study of the gram-negative bacterium *Escherichia coli*," *Applied and Environmental Microbiology*, vol. 73, no. 6, pp. 1712–1720, 2007.

[27] K. B. Holt and A. J. Bard, "Interaction of silver(I) ions with the respiratory chain of *Escherichia coli*: an electrochemical and scanning electrochemical microscopy study of the antimicrobial mechanism of micromolar Ag^+," *Biochemistry*, vol. 44, no. 39, pp. 13214–13223, 2005.

[28] J. R. Morones, J. L. Elechiguerra, A. Camacho et al., "The bactericidal effect of silver nanoparticles," *Nanotechnology*, vol. 16, no. 10, pp. 2346–2353, 2005.

[29] M. Sastry, A. Ahmad, M. Islam Khan, and R. Kumar, "Biosynthesis of metal nanoparticles using fungi and actinomycete," *Current Science*, vol. 85, no. 2, pp. 162–170, 2003.

[30] P. Mukherjee, A. Ahmad, D. Mandal et al., "Fungus-mediated synthesis of silver nanoparticles and their immobilization in the mycelial matrix: a novel biological approach to nanoparticle synthesis," *Nano Letters*, vol. 1, no. 10, pp. 515–519, 2001.

[31] P. Sivalingam, J. J. Antony, D. Siva, S. Achiraman, and K. Anbarasu, "Mangrove *Streptomyces* sp. BDUKAS10 as nanofactory for fabrication of bactericidal silver nanoparticles," *Colloids and Surfaces A*, vol. 98, pp. 12–17, 2012.

[32] S. D. Sarker, L. Nahar, and Y. Kumarasamy, "Microtitre plate-based antibacterial assay incorporating resazurin as an indicator of cell growth, and its application in the *in vitro* antibacterial screening of phytochemicals," *Methods*, vol. 42, no. 4, pp. 321–324, 2007.

[33] M. P. Lechevalier and H. Lechevalier, "Chemical composition as a criterion in the classification of aerobic actinomycetes," *International Journal of Systematic Bacteriology*, vol. 20, no. 4, pp. 435–443, 1970.

[34] A. V. Kirthi, A. A. Rahuman, C. Jayaseelan et al., "Novel approach to synthesis silver nanoparticles using plant pathogenic fungi, *Puccinia graminis*," *Materials Letters*, vol. 81, pp. 61–72, 2013.

[35] C. G. Kumar and S. K. Mamidyala, "Extracellular synthesis of silver nanoparticles using culture supernatant of *Pseudomonas aeruginosa*," *Colloids and Surfaces B*, vol. 84, no. 2, pp. 462–466, 2011.

[36] C. Krishnaraj, E. G. Jagan, S. Rajasekar, P. Selvakumar, P. T. Kalaichelvan, and N. Mohan, "Synthesis of silver nanoparticles using *Acalypha indica* leaf extracts and its antibacterial activity against water borne pathogens," *Colloids and Surfaces B*, vol. 76, no. 1, pp. 50–56, 2010.

[37] P. Magudapathy, P. Gangopadhyay, B. K. Panigrahi, K. G. M. Nair, and S. Dhara, "Electrical transport studies of Ag nanoclusters embedded in glass matrix," *Physica B: Condensed Matter*, vol. 299, no. 1-2, pp. 142–146, 2001.

[38] K. Kalishwaralal, V. Deepak, S. Ramkumarpandian, H. Nellaiah, and G. Sangiliyandi, "Extracellular biosynthesis of silver nanoparticles by the culture supernatant of *Bacillus licheniformis*," *Materials Letters*, vol. 62, no. 29, pp. 4411–4413, 2008.

[39] A. Panáček, L. Kvítek, R. Prucek et al., "Silver colloid nanoparticles: synthesis, characterization, and their antibacterial activity," *Journal of Physical Chemistry B*, vol. 110, no. 33, pp. 16248–16253, 2006.

[40] K.J. Kim, W. S. Sung, B. K. Suh et al., "Antifungal activity and mode of action of silver nano-particles on *Candida albicans*," *BioMetals*, vol. 22, no. 2, pp. 235–242, 2009.

[41] W.-R. Li, X.-B. Xie, Q.-S. Shi, H.-Y. Zeng, Y. Ou-Yang, and Y.-B. Chen, "Antibacterial activity and mechanism of silver nanoparticles on *Escherichia coli*," *Applied Microbiology and Biotechnology*, vol. 85, no. 4, pp. 1115–1122, 2010.

[42] M. I. Sriram, S. B. M. Kanth, K. Kalishwaralal, and S. Gurunathan, "Antitumor activity of silver nanoparticles in Dalton's lymphoma ascites tumor model," *International Journal of Nanomedicine*, vol. 5, no. 1, pp. 753–762, 2010.

[43] M. Safaepour, A. R. Shahverdi, H. R. Shahverdi, M. R. Khorramizadeh, and A. R. Gohari, "Green synthesis of small silver nanoparticles using geraniol and its cytotoxicity against Fibrosarcoma-Wehi 164," *Avicenna Journal of Medical Biotechnology*, vol. 1, no. 2, pp. 111–115, 2009.